AFFDL-TR-78-110
VOLUME II

LEVEL II

AD A066560

COMPOSITE FORWARD FUSELAGE SYSTEMS INTEGRATION

VOLUME II

General Dynamics
Fort Worth Division
Fort Worth, Texas 76101

DDC FILE COPY

September 1978

Final Report for April 1977—May 1978

APPROVED FOR PUBLIC RELEASE:
DISTRIBUTION UNLIMITED

AIR FORCE FLIGHT DYNAMICS LABORATORY
AIR FORCE WRIGHT AERONAUTICAL LABORATORIES
AIR FORCE SYSTEMS COMMAND
WRIGHT-PATTERSON AIR FORCE BASE, OHIO

632.11F

NOTICE

When Government drawings, specifications, or other data are used for any purpose other than in connection with a definitely related Government procurement operation, the United States Government thereby incurs no responsibility nor any obligation furnished, or in any way supplied the said drawing, specifications, or other data, is not to be regarded by implication or otherwise as in any manner licensing the holder or any other person or corporation, or conveying any rights or permission to manufacture, use, or sell any patented invention that may in any way be related thereto.

This technical report has been reviewed and is approved for publication.

Gene Shumaker

GENE SHUMAKER
Project Engineer
Advanced Composites ADP Office

Havard A. Wood

HAVARD A. WOOD
Program Manager
Advanced Composites ADP Office

FOR THE COMMANDER

Ralph L. Kuster Jr.

RALPH L. KUSTER, COL. USAF
Chief
Structures Division
AF Flight Dynamics Laboratory

Copies of this report should not be returned unless return is required by security consideration, contractual obligations, or notice on a specific document.

AIR FORCE/56780/8 March 1979 — 200

Unclassified

SECURITY CLASSIFICATION OF THIS PAGE (When Data Entered)

REPORT DOCUMENTATION PAGE

READ INSTRUCTIONS BEFORE COMPLETING FORM

1. REPORT NUMBER: AFFDL-TR-78-110- Volume II
2. GOVT ACCESSION NO
3. RECIPIENT'S CATALOG NUMBER
4. TITLE (and Subtitle): Composite Forward Fuselage Systems Integration, Volume II.
5. TYPE OF REPORT & PERIOD COVERED: Final Report, April 1977 – May 1978
6. PERFORMING ORG. REPORT NUMBER
7. AUTHOR(s): B. J. Wallace, B. J. C. Burrows, R. T. Zeitler, A. J. Ledwig, K. G. Wiles
8. CONTRACT OR GRANT NUMBER(s): F33615-76-C-5439
9. PERFORMING ORGANIZATION NAME AND ADDRESS: General Dynamics Corporation, Fort Worth Division, P. O. Box 748, Fort Worth, Texas 76101
10. PROGRAM ELEMENT, PROJECT, TASK AREA & WORK UNIT NUMBERS: 69CW-01-19
11. CONTROLLING OFFICE NAME AND ADDRESS: Air Force Flight Dynamics Laboratory (FBC), Advanced Composite Structures (ADP), Wright-Patterson AFB, Ohio 45433
12. REPORT DATE: September 1978
13. NUMBER OF PAGES: 137
14. MONITORING AGENCY NAME & ADDRESS (if different from Controlling Office): 12 139
15. SECURITY CLASS. (of this report): Unclassified

15a. DECLASSIFICATION DOWNGRADING SCHEDULE

16. DISTRIBUTION STATEMENT (of this Report)

This document has been approved for public release and sale; its distribution is unlimited.

17. DISTRIBUTION STATEMENT (of the abstract entered in Block 20, if different from Report)

18. SUPPLEMENTARY NOTES

19. KEY WORDS (Continue on reverse side if necessary and identify by block number)

Composites, Electromagnetic Compatibility, Effects of Lightning.

20. ABSTRACT (Continue on reverse side if necessary and identify by block number)

The Composite Forward Fuselage Systems Integration program has performed the development necessary to guide the integration of avionic and electrical systems into composite aircraft structure. This volume of the report presents one phase of the program; it presents that phase in which the induced effects of lightning are identified and modeled.

DD FORM 1473, 1 JAN 73 — EDITION OF 1 NOV 65 IS OBSOLETE

Unclassified

SECURITY CLASSIFICATION OF THIS PAGE (When Data Entered)

402 191

JB

FOREWORD

The development reported herein was performed under Contract F33615-76-C-5439 under the sponsorship of the Air Force Flight Dynamics Laboratory, Advanced Composites ADP, Wright-Patterson AFB, Ohio. Mr. Gene Shumaker, AFFDL/FBC, was the Air Force Project Engineer.

The contractor was General Dynamics' Fort Worth Division. Mr. R. H. Roberts was the Program Manager, and Mr. B. J. Wallace served as Deputy Program Manager and Principal Investigator for the Electromagnetic Compatibility Development. Other key personnel contributing to the program included:

P. F. Carrier	-	System Design
J. L. Hudson	-	Structural Design
A. J. Ledwig	-	Lightning Strike Test
B. R. Smith	-	Structural Analysis
F. Spelce	-	Manufacturing Development
R. E. Stephens	-	Electrical & Installation
K. G. Wiles	-	Electromagnetic Effects
R. T. Zeitler	-	Electromagnetic Effects

In addition, Mr. B. J. C. Burrows of Culham Laboratory, UKAEA Research Group, United Kingdom, made significant contributions to the series of tests concerning the induced effects of lightning strikes.

The Defense Division, Lincoln Facility, of the Brunswick Corporation also contributed, from their own resources, in the area of reducing composite part fabrication cost via filament winding. This effort was directed by Mr. B. W. Quinlan with Mr. R. E. Curran serving as the Principal Investigator.

The development reported herein was performed during the period of April 1977 to May 1978.

This final report is divided into two volumes. Volume I (limited distribution) defines the program, presents test data except for the induced effects of lightning strike test, and presents design guidelines. Volume II (unlimited distribution) presents the induced effects of lightning strike test and data.

TABLE OF CONTENTS

PRECEDING PAGE BLANK

TABLE OF CONTENTS
(Continued)

LIST OF ILLUSTRATIONS

LIST OF ILLUSTRATIONS
(Continued)

LIST OF ILLUSTRATIONS
(Continued)

LIST OF ILLUSTRATIONS
(Continued)

LIST OF ILLUSTRATIONS
(Continued)

LIST OF TABLES

SECTION 1

SUMMARY

This document, Volume II, reports the phase of the contract which studied the effects of atomspheric lightning on aircraft avionic systems installed in graphite/epoxy aircraft structure. The work draws heavily from testing technology developed by a recognized authority in the field, Culham Laboratory of UKAEA. In fact, the test configuration, instrumentation techniques, and test parameters were established by Mr. B. J. C. Burrows of Culham Laboratory. This work however, extends previous testing and, in the opinion of the authors, represents a significant contribution to the technology of lightning-effect evaluation.

There were a number of salient features of this program which, the authors believe, have led to advancements in lightning studies technology. These include:

1) A simplified test configuration.

2) The evaluation of low and high frequency effects.

3) The measurement of basic coupling mechanisms.

4) Simplified models and theory with demonstrated accuracy.

The useful product of the program is, of course, the models and theory which allow general-case lightning environments to be analized as threat voltages, currents, and fields acting upon the avionics. The primary thrust of this report is therefore to develop and support these models with hard data.

The significant conclusion resulting from this work is that the threat of external lightning can be handled with design considerations which neither compromise the efficiency of the composite airframe or impose escalating hardness requirements on the avionics. In fact, in many instances no special design considerations are necessary. A demonstration test consisted of F-111 vintage avionics installed, in a typical manner, in a YF-16 graphite epoxy forward fuselage. The structure was pulsed with a 125 kA peak/32 kA/us rise time strike while the systems were operating. No failures or perturbations occurred.

SECTION 2

PROGRAM INTENT

The intent of this program was to determine and explain the induced effects resulting from a lightning strike to the graphite/epoxy (Gr/Ep) forward fuselage illustrated in Figure 1. To meet this intent, a number of considerations had to be addressed. Primarily, we had to be able to simulate an actual lightning strike with the best methods available and we had to be assured the measured data represented lightning effects and not instrumentation or test set-up effects.

Since the very basis for this test was emulation of an actual strike, in both magnitude and rise time, we begin our discussions with the requirements and how to simulate a lightning strike. Next, we discuss the test configuration and test apparatus, provide data on the waveform used in the test, and finally the instrumentation techniques employed.

The last two sections discuss the testing along with predicted and measured data and finally the generalizations necessary for effective predictions.

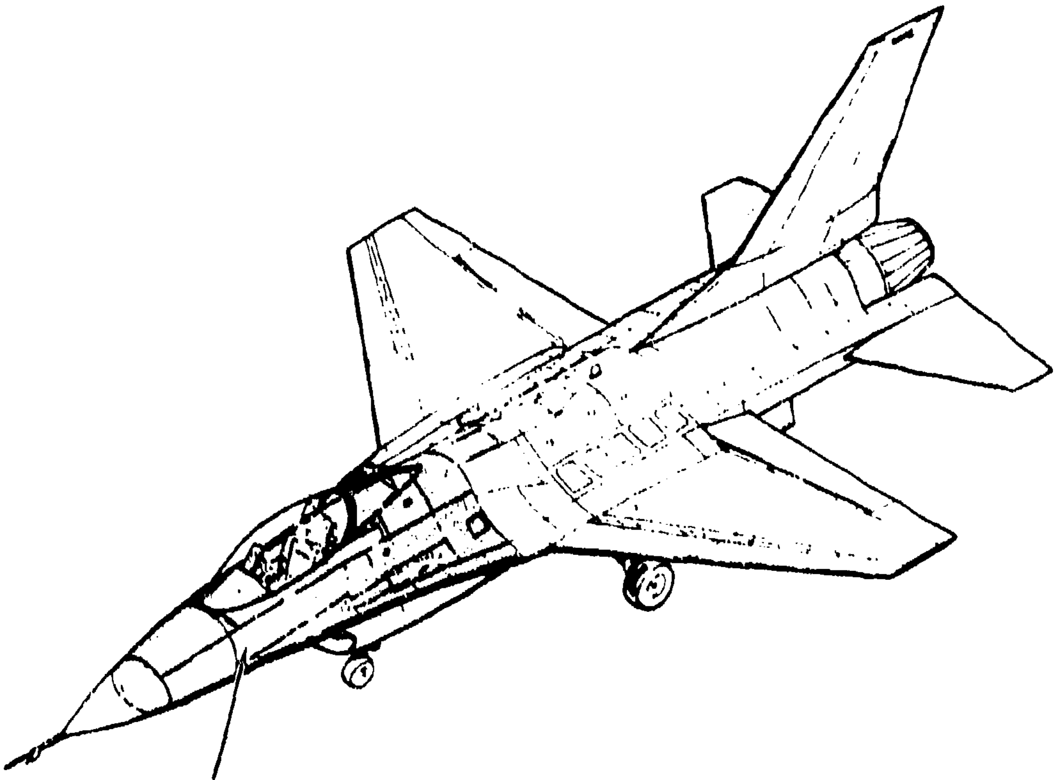

Figure 1   Composite Forward Fuselage Lightning Test Article

SECTION 3

REQUIREMENTS AND SIMULATION METHODS

As previously stated, our singular intent was to provide lightning test data which is relatable to an actual strike. This section outlines our thinking and the considerations for the test configuration and the type of tests that were performed.

3.1 CURRENT EXPOSURE LEVEL BY ZONES

In the natural lightning strike situation, fuselage could experience strikes swept back from a front attachment point onto the fuselage surface itself, i.e., a Zone 2A strike. This condition is of more interest to studies of structural damage to the graphite/epoxy surface than to induced voltage studies. In general, the worst case for induced voltages would occur during the return stroke of a lightning strike where the current peak amplitude and di/dt would be the largest. A forward fuselage will conduct this current through its total length when the aircraft radome becomes the primary lightning attachment point (Zone 1A as defined in reference 1). Reference 9 has predicted that approximately 75% of all lightning strikes to the F-16 will initially attach in this area. For these reasons, we simulated a Zone 1A strike by applying current pulses to the foremost part of the composite fuselage (assumes a radome attachment) and conducted it along the entire fuselage length to the aft-most section (assumes a lightning exit point at the aircraft tail). Entrance or exit in terms of polarity is of no significance; the point of the description is to explain that the test configuration provides for an entrance point at one end and an exit or return point at the other.

3.2 CURRENT PULSE PARAMETERS AND SCALING REQUIREMENTS

Very severe lightning current pulses have been measured with maximum amplitudes around 140kA and maximum rates of change, di/dt, of 100kA/us. Both values correspond to strikes whose values would be exceeded only 2% of the time or a 2% severity. Complete duplication of maximum rate of change and amplitude was not possible in our laboratory nor is complete duplication a necessity. The problem we attacked was to make the amplitude and rise time realistic. Reality was judged on the basis of whether test pulse parameters were comparable to parameters of an actual strike, and consequently whether the signal (induced voltages expected) to noise (systematic noise, spurious responses, etc.) ratio was great enough such that results could be scaled to a severe strike.

The smaller the scaling factor between the test pulse and real pulse, the more reliable the scaled up value. Scaling factors of around five are considered satisfactory, therefore, the current pulse parameters should be approximately 30 kA peak current and 20 kA/us rate of rise. 30 kA is the 53% severity value for the negative ground flash return stroke, and 20 kA/us is the 23% severity level for return stroke and 82% for restrikes (Reference 2). Choice of scaling parameter (I or di/dt) is addressed in Section 3.4.

The recommendation of Reference 3, which described work on a Hawker Hunter all-metal fuselage at high current and high di/dt, stated that a high signal-to-noise ratio and high repeatability were best attained with a single stage capacitor bank operating at a low voltage and producing the highest practical current. The highest current at the lowest voltage requires a minimum inductance test configuration. Thus, the low inductance multibroad conductor system used in Reference 3 was adopted for this test.

At this point, requirements and configuration have begun to form. The generator is a single capacitor capable of accepting a charging voltage sufficient to produce approximately 30 kA peak with a 20 kA/us rate of rise. The fuselage and return conductors (load assembly) is configured as a multi-conductor, low inductance assembly so that the operating voltage available on one capacitor produces maximum current amplitude and maximum rate of rise.

3.3 FUSELAGE CURRENT DISTRIBUTION

In simulating a lightning strike passing along and through the fuselage, one of the key requirements was maintenance of fuselage current distribution such as would exist in free space. Maintenance of the required current distribution is primarily a function of a return conductor configuration. This subsection discusses the current distribution by frequency bands along with requirements placed on the return conductors to maintain "free space" distribution.

3.3.1 Low Frequency (LF) Current Distribution (Below 1 MHz)

During a natural strike, the aircraft is remote from ground, or any other object, and the lightning current passes into and out of the complete aircraft via very long arcs. The return path for the current is remote and distributed and comprises the displacement current flowing as the cloud-to-ground or cloud-to-cloud capacitance is discharged by the flash. Current flow through the fuselage in this condition produces the "free space" field through the aircraft and the geometry of the magnetic and electric fields are not distorted by the presence of nearby return current paths. The current distribution on the aircraft in free space is such that the aircraft is the center of a nesting series of magnetic field lines which conform to the fuselage cross-section close in, and are approximately circular beyond a few fuselage radii as illustrated in Figure 2(a).

To achieve a good simulation of lightning, it is important only that the free space field of Figure 2(a) is duplicated close to the fuselage. Close-in, the field lines follow the fuselage shape. Since field lines are lines of constant flux, there are more lines per area (high density) at projections, like the strakes or cockpit sill, and less lines per area (low density) on the flat or concave surfaces. Surface current density for the fast changing current pulses is inversely proportional to the distance from the fuselage surface to the first field line. Since the magnatizing force H, is equal to the surface current density, J, in amperes per meter, then $B = \mu_0 J$, and B is inversely proportional to the distance from the fuselage surface of the first field line.

The portion of the free space field close to the aircraft can be duplicated by enclosing the fuselage in a complete return conductor exactly on one of the field lines of Figure 2(a), as in Figure 2(b). Now, very small fields exist outside the return conductor, as in a coaxial cable, but the field within is identical to the free space field.

The current return conductor shown in Figure 2(b) could be either a solid sheet or many individual, closely spaced, thin wires. The latter method was used in Reference 4. Neither this nor the complete sheet system is very convenient, however, being either costly to make or causing access difficulties. A useful working system which provides adequate simulation consists of a sectional current return around the fuselage circumference consisting of two, three or more conductors; the greater number providing the best simulation.

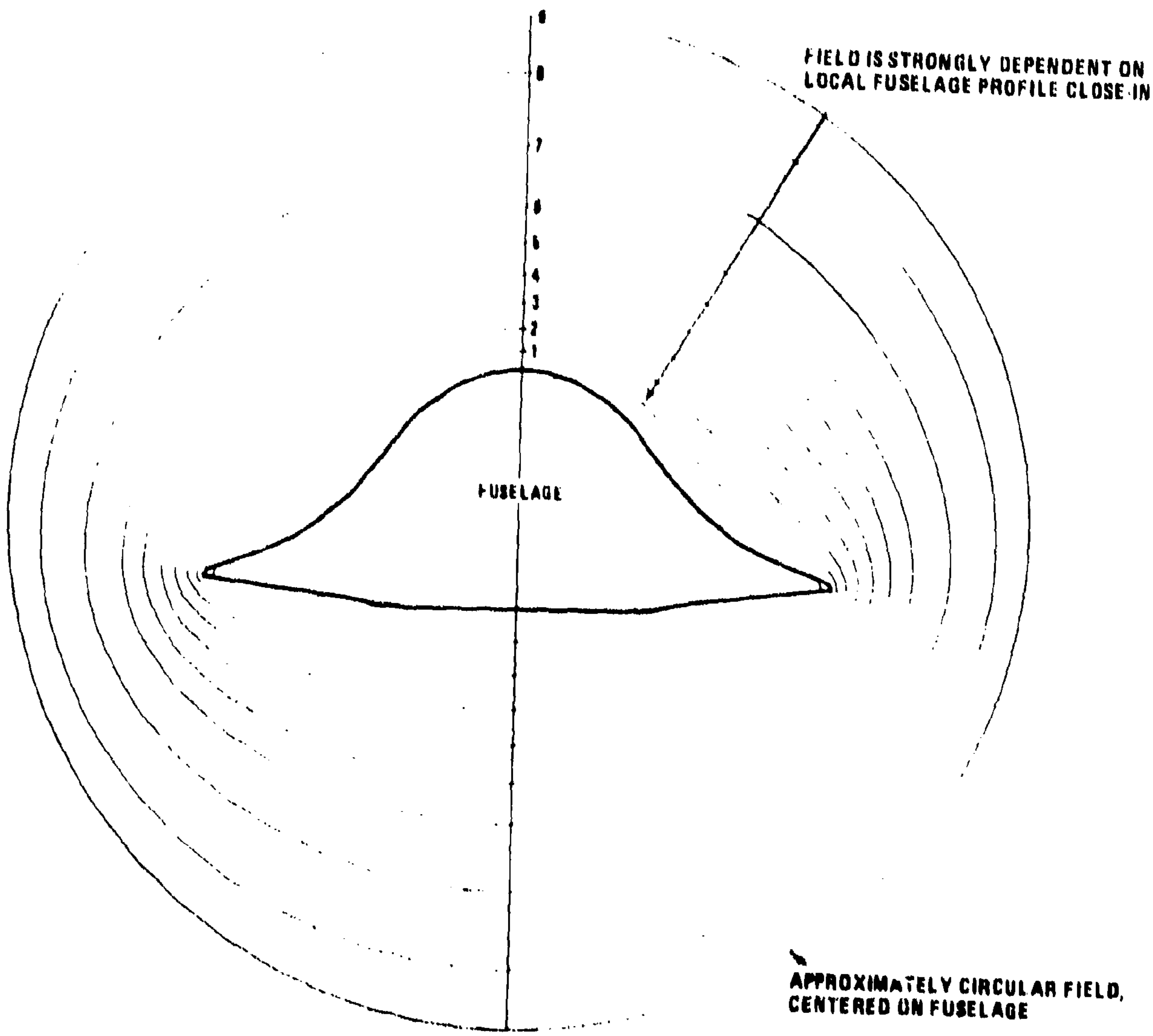

Figure 2(a) Free Space Magnetic Field Configuration For Metal Fuselage

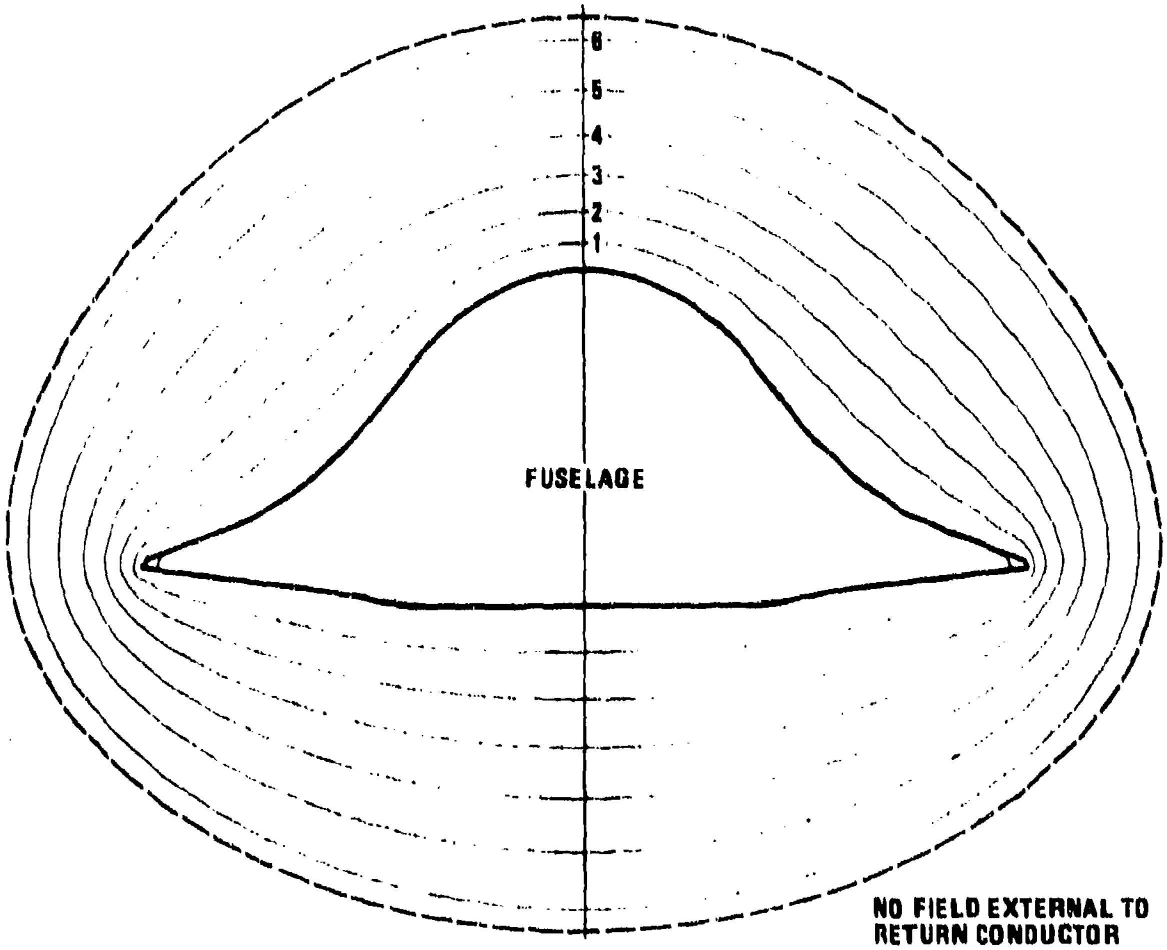

RETURN CONDUCTOR ON FIELD LINE 6 OF Fig. 2A

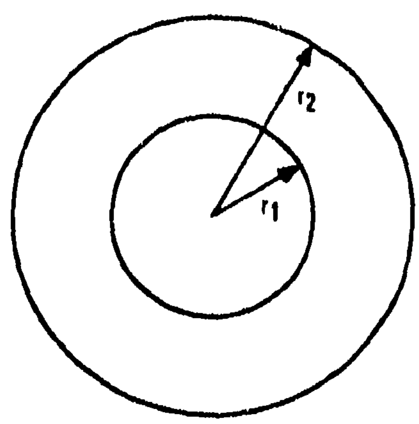

CIRCULAR EQUIVALENT (c.f. Coaxial Cable)

Figure 2(b) Free Space Field of Figure 2(a) Retained by Return Conductor Placed on a Field Line

Figure 2(c) shows the three conductor system used for this test which follows the technique described in Reference 3. Two conductors alone do not normally give an adequate simulation of the free space field unless they are fairly distant - say five or more fuselage radii. A two-conductor system has the additional disadvantage of high inductance (the inductance of the fuselage and return conductors), whereas the systems shown in Figures 2(b) and 2(c), the full coaxial, and quasi-coaxial test systems both have the bonus of a very low inductance when relatively close spacing is used. The low inductance is a necessity for our test configuration for the reasons cited in subsection 3.2.

The three-conductor system of Figure 2(c) provides a close enough approximation of the free space field close to the fuselage, and, therefore, the current distribution around the periphery of the fuselage will be simulated, as long as the three conductors are correctly placed. This applies equally to a graphite or graphite/metal fuselage. Theoretically in a graphite fuselage, the current distribution corresponds more to the free space condition since current sharing tends to be more resistively controlled in graphite and hence less dependent on return conductor number, size, and position.

The biggest difference in the current distribution of the Gr/Ep forward fuselage from that of a production airplane is caused by the absence of the inlet which starts at Station 161 and runs aft. Over its length, the inlet tends to "screen" the underside of the fuselage and reduce the current density there by a large factor.

The tendency toward current redistribution around the fuselage (i.e., for current to forsake the Gr/Ep in favor of metal, Sec.6) occurs with the low frequency components of the lightning pulse, which peak around 50 kHz. The same pulse on an all metal aircraft does not suffer current redistribution since current is inductively shared around the fuselage and the current is a skin effect current only. (Reference page 130, appendix)

3.3.2 High Frequency (HF) Current Distribution (Above 1 MHz)

Much higher frequencies can be theoretically predicted to occur on an aircraft in a natural lightning strike situation and are observed in lightning simulation tests on large components. Ideally, the test rig duplicates the predicted "free space" HF currents where possible, and the design of the test rig and current return system is also considered from this aspect.

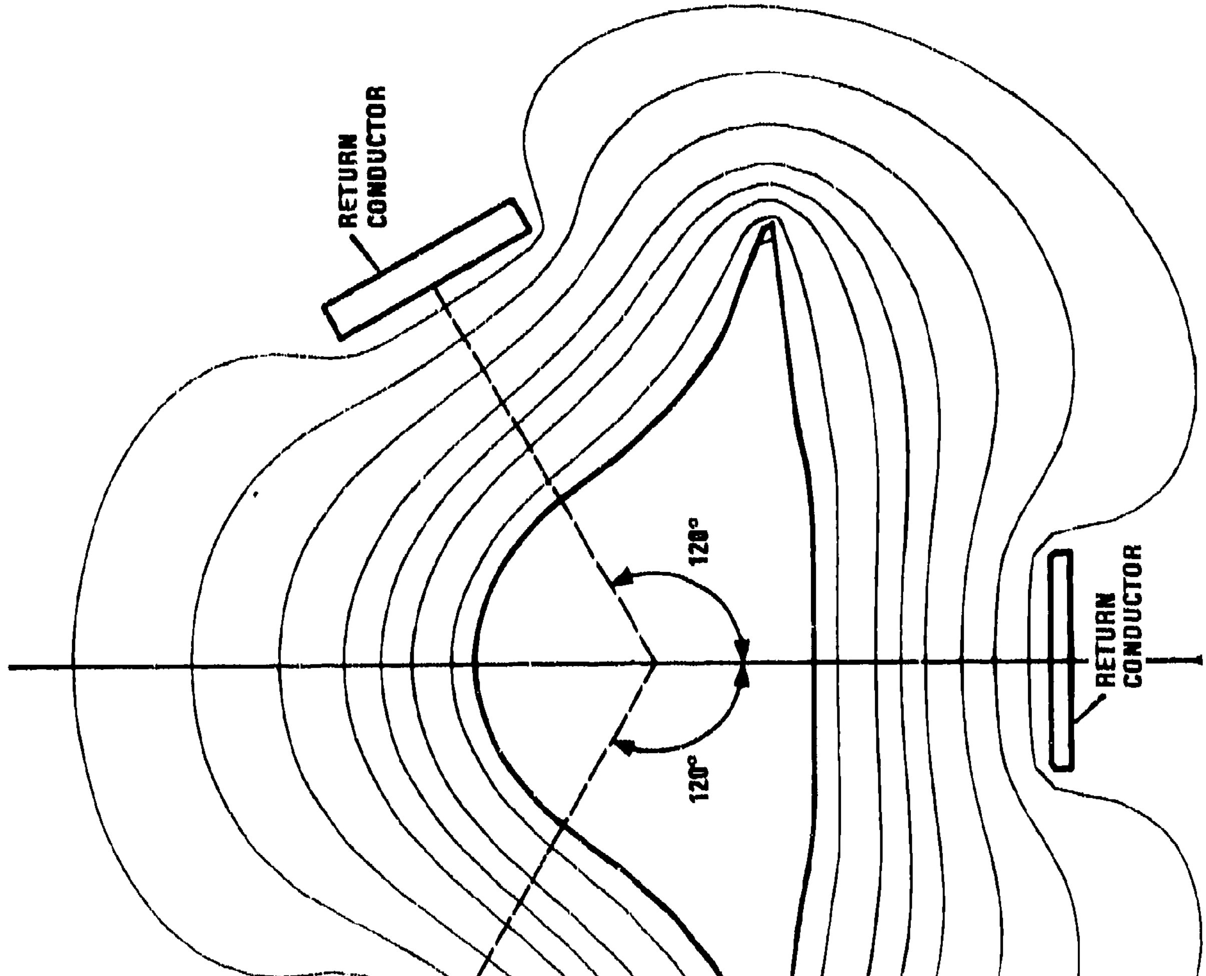

Figure 2(c) Quasi Coaxial 3-Conductor Return Current System

The HF currents have a similar circumferential pattern as the LF currents in a metal fuselage, but have the additional complication of a longitudinal variation since the HF currents are associated with standing waves on the fuselage excited by the transients of the lightning. Airframe resonances have been predicted and observed in NEMP investigations of spacecraft, missiles and aircraft (Reference 5). Figure 3 illustrates the mechanism for lightning attachment, where the fuselage is represented by a simple cylinder. A considerable impedance mismatch occurs at the two attachment points, since the arc channel radius is ~ 0.5 mm compared with an aircraft radius of 0.5 to 1.5m. The standing wave pattern shown is the principal mode which corresponds to a frequency f_1 whose wavelength is twice the aircraft length - (i.e., the $\lambda/2$ mode)

$$f_1 = \frac{c}{2\ell} \text{ Hz} \qquad \begin{aligned} c &= \text{velocity of EM waves} \\ &= 3 \times 10^8 \text{ m/s} \\ \ell &= \text{aircraft length in meters.} \end{aligned}$$

Thus, for an 11m aircraft total length, f_1 is 300/22 MHz = 14MHz. This mode has a current maximum at the middle, point A, and a voltage maximum at the end, point B. Higher modes occur at $2f_1$, $3f_1$, etc., on the simple cylinder and on an aircraft, and the aircraft case is further complicated by wing modes and fuselage/wing modes.

The fuselage we tested is slightly shorter than half the total length of the full F-16 fuselage and when the return conductors are assembled, the choice exists to connect them to the fuselage at the front or back. Clearly a current maximum must occur at the connection point in Figure 4, point A. In this case, the resonance is a quarter wave line resonance, as might be assumed from transmission line theory, but it is the same frequency f_1 as the $\lambda/2$ mode for a full length fuselage and the current and voltage anti-nodes occur as in figure 3. For this configuration, the fields are now largely contained between the conductors of the load assembly and do not appreciably radiate into space as for the isolated "aircraft" of Figure 3, and the Q of the system is therefore higher. The "quarter wave line" load assembly suppresses $2f_1$, $4f_1$, etc. but f_1,$3f_1$ -- may be observed.[1]

Thus, the structures shown in Figure 2(c) and Figure 4 produce a simulation of LF and HF circumferential and longitudinal current distribution expected on an aircraft in free space except that the quarter wave line inhibits $2f_1$, $4f_1$, etc. and wing-

1 Our test data showed a significant amount of high frequency components at 14 and 46 MHz. See Sections 5 and 8.

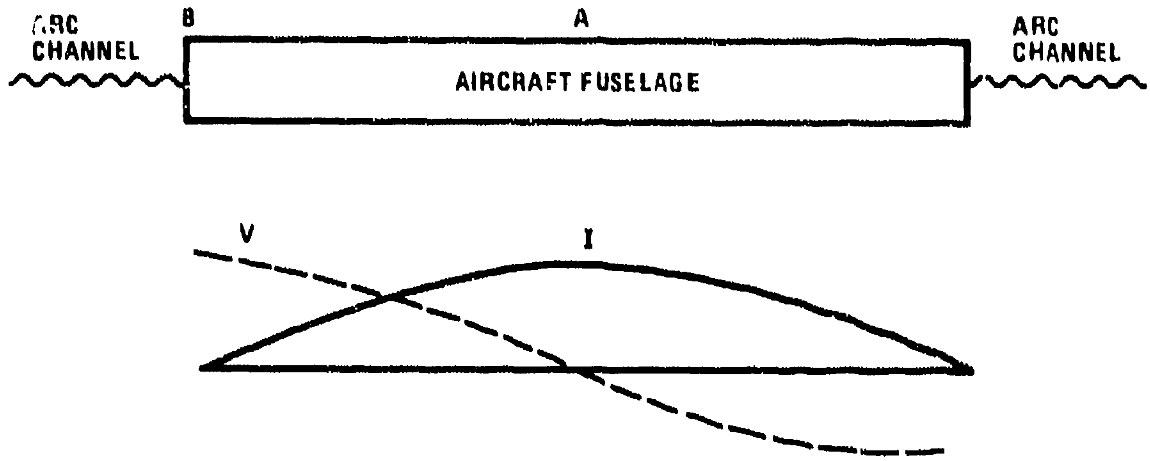

Figure 3 Standing Wave Pattern at First Fuselage Resonance, f_1 ($\lambda/2$ mode)

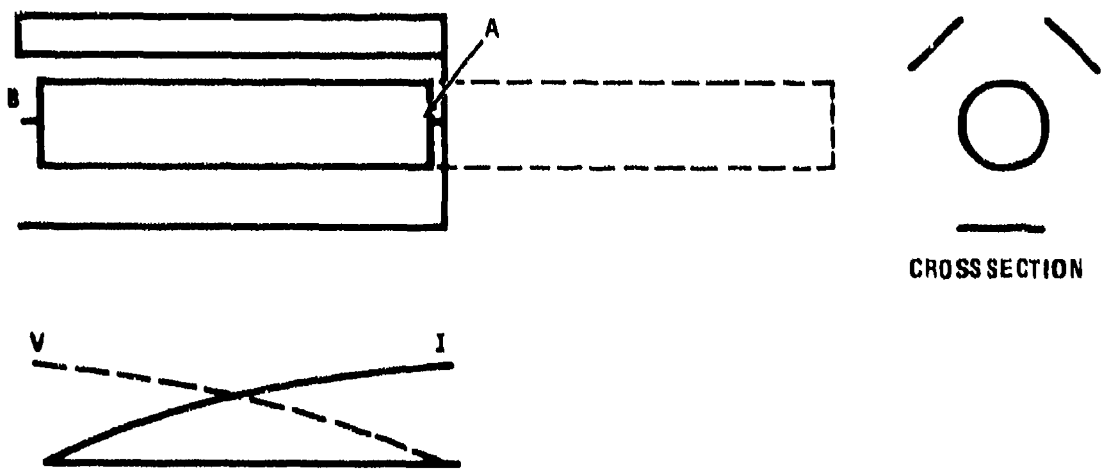

Figure 4 Standing Wave Pattern for One Half Fuselage with Return Conductors (Natural Resonance is at $\lambda/4$ mode = f_1 in Figure 3)

fuselage modes are not represented. To excite the f_1, $3f_1$, etc., modes, a mismatch must occur at the capacitor bank/load assembly junction.

3.4 CHOICE OF PARAMETERS FOR SCALING

Much previously reported work has shown that voltages induced into avionic interfaces are generated by two main mechanisms:

a) Rate of change of fields ($\frac{dB}{dt}$ or $\frac{dE}{dt}$); for aperture coupling and other direct coupling processes where interface conductors are influenced directly by the external fields, or;

b) Resistively generated voltages which are proportional to the current amplitude and which occur along the enclosed structures. This could be called "internal" coupling. Resistive-type voltages also occur in loops within enclosed bays by induction from flux which has diffused through a resistive material. Although such a process is theoretically a $\frac{d\phi_D}{dt}$ induction, the ϕ_D is a diffusion flux and <u>not</u> the same flux which occurs externally or in apertures. For clarity in this report, this process is called resistive/diffusion coupling and invariably has the amplitude and spectrum characteristic of resistive voltages, with only minor differences. This is an important distinction since resistive/diffusion coupling is an important feature of induced voltage within graphite, and metal/graphite airframes.

The two coupling methods induce voltages having distinctly different characteristics due to the difference of the excitation spectrum. The spectrum of I applicable to resistive coupling and the dI/dt applicable to aperture and direct coupling are shown in Figure 5 for the unipolar simulation pulse used in tests detailed later.

The characteristic dI/dt spectrum with its predominance of HF energy is observed externally, in the cockpit and within other apertures.

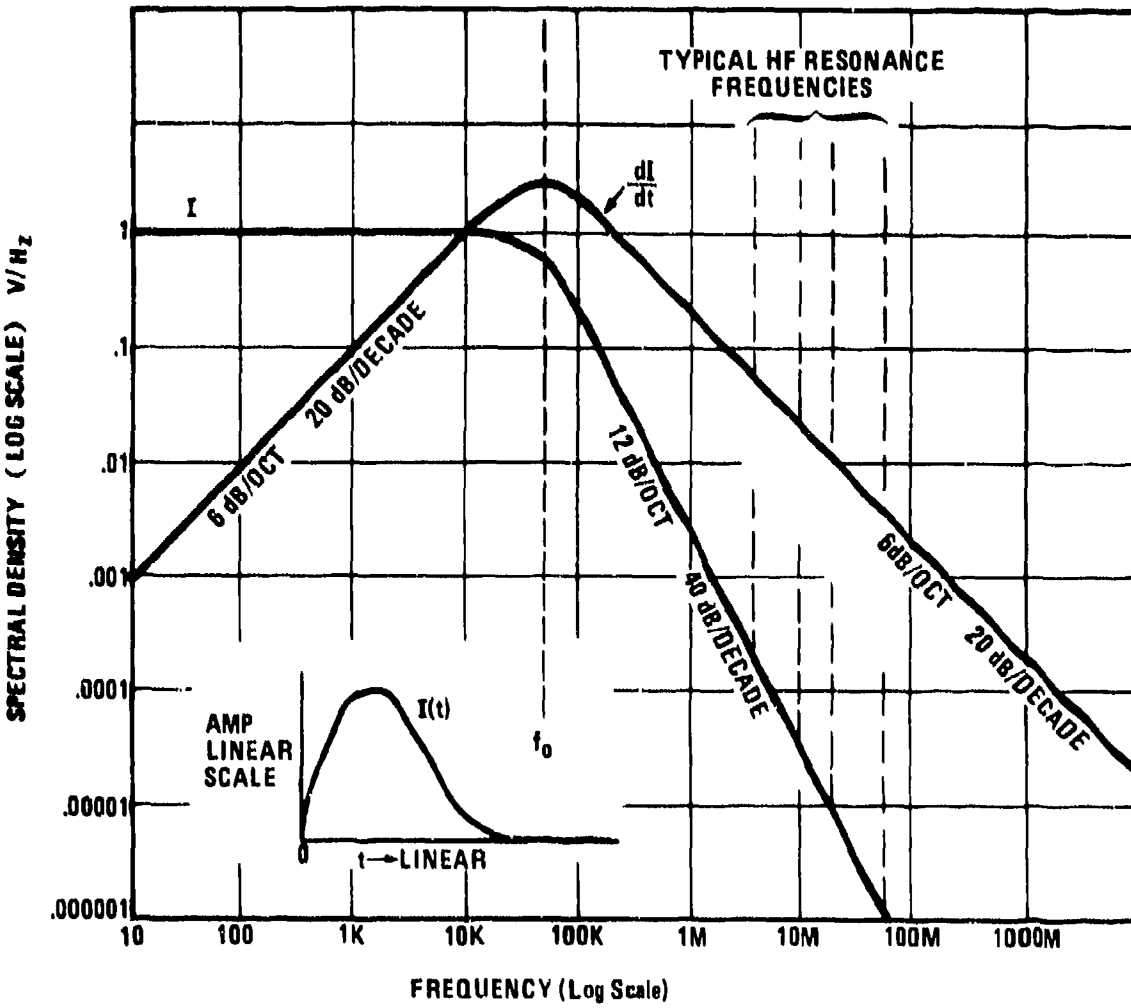

Figure 5 Theoretical and Practical Spectra of I and $\frac{dI}{dt}$ for Current Pulse (shown inset). Practical Spectra Have the Additional Effect of HF Resonances

Likewise, voltages having the characteristic spectrum of the current pulse, a predominantly low frequency spectrum, are observed within compartments having a graphite outer skin.

Test data in Section 7 demonstrates the application of I scaling to resistive voltages and di/dt scaling for aperture voltages.

External electric field induced voltages (dE/dt) also occur in the cockpit, etc. and have a predominantly HF spectrum but the graphite shields these electric fields from the enclosed equipment bay.

Another class of coupling is demonstrated in the test data in Section 7 and deals with (dE/dt) HF effects inside enclosures.

SECTION IV

TEST CONFIGURATION DESIGN AND DESCRIPTION

The considerations in the design of the test system may be summarized as follows:

1) A low inductance system is desirable for achieving high I and di/dt of the order suggested in Section 3.2, while simulating the LF free space field configuration as described in Section 3.3.1.

2) The return conductors should be connected to the fuselage in such a manner as to produce the HF longitudinal current distribution described in Section 3.3.2. This requires the return conductors to be connected to the rear of the forward fuselage section.

3) The capacitor bank shall be compact and introduce minimum extra inductance and should be a one stage system for consistency and repeatability.

4) There must be an impedance mismatch between the capacitor bank/waveshaping resistor and the load assembly in order to encourage the quarter wave line resonance (See Section 3.3.2.).

5) A waveshaping resistor should be designed to have minimum inductance, and should be readily shorted for "ring"discharges, with least disturbance of the total circuit inductance.

6) System grounding is required for safety, for the bank charging current, to route power into the fuselage for powering-up electronics and for routing hard-wired instrumentation back to the screen room, but the grounding position shall be chosen to minimize bank-to-ground and load assembly-to-ground currents. One end of the fuselage is preferred for the grounding point, preferably at the fuselage rear where avionic power reference was located.

7) The charging supply for the bank and the trigger feed to the switch (an electrically triggered field distortion gap was available) should not introduce spurious resonances, nor form ground loops via the power supply unit in conjunction with the main system grounding point.

Since satisfying most of the above requirements is dependent on the parameters of the load assembly, the load assembly design and description will be given first. From this data, approximate current and current rate-of-change values are calculated. Following these calculations we have described the design of the impulse generator, and finally total configuration.

4.1 DESIGN AND DESCRIPTION OF LOAD ASSEMBLY

The load assembly comprises the forward fuselage mounted horizontally on a wooden stand, the instrumentation break-out box at the back (—.7m projection), the current transformer mounting and the three-24" wide return conductors. The returns are illustrated in Figure 2(c) and are shown in the photograph in Figure 6. The return conductors are 8mm thick, .6 meter wide aluminum sheets fastened to a wooden frame. Insulation presents no problem because of the low voltages involved, the grounding point position, and the short pulse duration, therefore, return conductors were supported by a simple wooden frame.

In the configuration shown (three conductor return), the inductance is only 20% more than that of a full coaxial system. For a full coaxial system, if $r_2 = 2r_1$, the inductance per meter, L', is given by

$$L' = \frac{\mu_0}{2\pi} \log_e \left(\frac{r_2}{r_1}\right) \qquad \mu\mathrm{H/m}$$

$$= 0.2 \log_e 2 \qquad \mu\mathrm{H/m} \qquad (1)$$

and therefore the inductance of the configuration is approximately 0.14 μH/m.

The circumferential positions of the return conductors were obtained from POTENT[1] (Reference 6) calculations. The spacing of

[1]POTENT is a 2-dimensional field mapping program for electrostatic and magnetic field problems. Calculations are performed on a 50X50 mesh, and for the magnetic case, tabulations at each mesh point provide values of magnetic flux, Hx, Hy, and |H|. Arbitrary geometry can be specified and the program allows variable mesh spacing to improve accuracy in regions of high field curvature. The data can be processed by a graph plotting routine to produce mappings of magnetic flux contours (field lines) and |H| as used in this report.

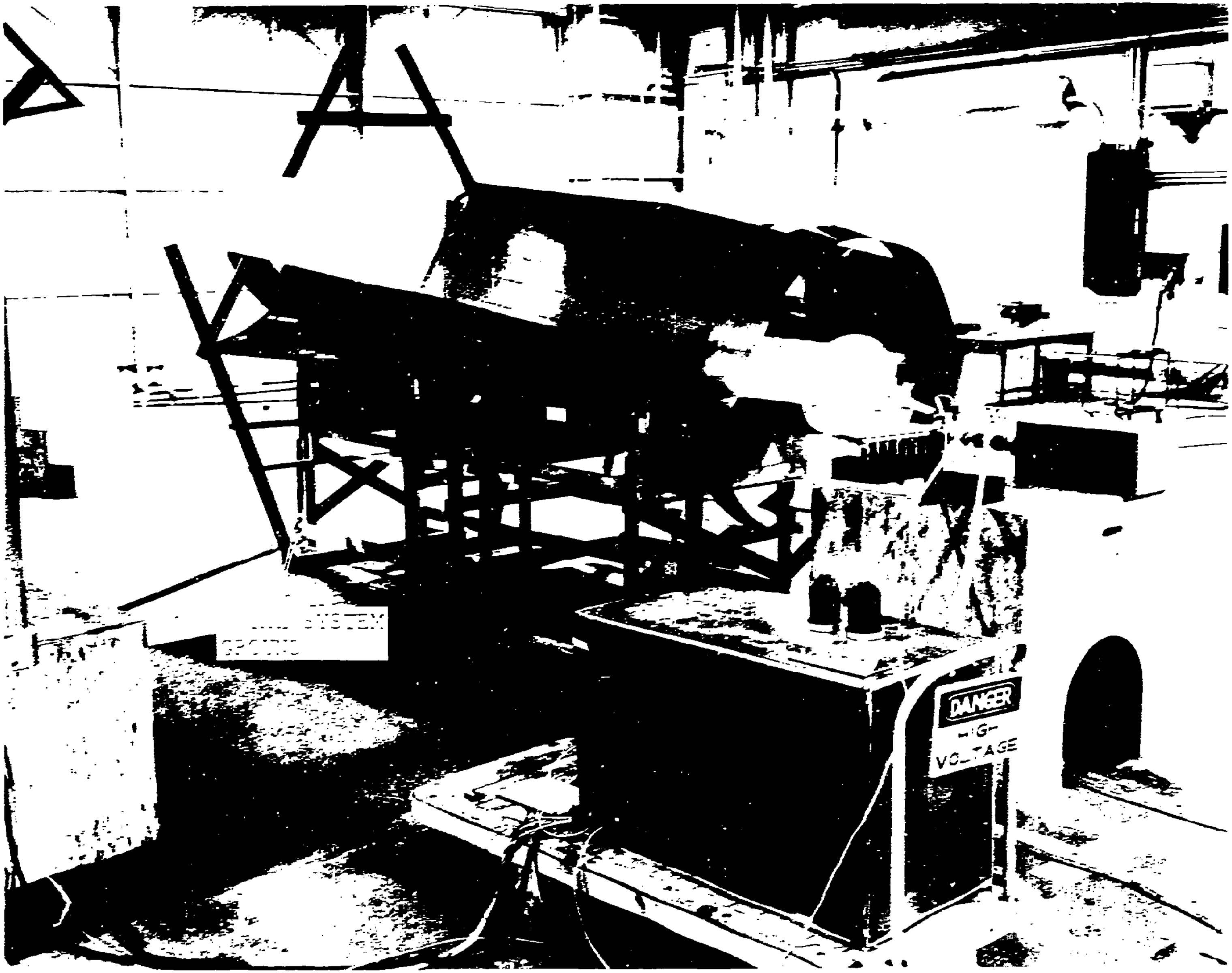

Figure 6 Overall Forward View of Test Setup for Simulated Lightning Strikes

the return conductors to fuselage was varied along the length of the fuselage in an attempt to keep r_2/r_1 approximately constant at two. The inductance at representative stations as calculated from the POTENT field maps were as follows:

CONDITION	STATION 75 (FORWARD BAY)	STATION 150 (COCKPIT)	STATION 273.5 (FUEL TANK)
Current on fuselage skin	.177 μH/m	.172 μH/m	.14 μH/m
Current in metal or high conductivity regions	.286 μH/m	.277 μH/m	.179 μH/m

As can be noted, the tabulated values show very close agreement to the .14 μH/m calculated from equation (1) above.

The first utility of the above values of inductance is to facilitate calculation of total inductance of the test configurations. The forward fuselage is approximately 4.9 meters long without its instrumentation breakout box (See Section 6) and 5.6 meters long with the box. Therefore, the inductance of the load assembly, L_L, is given by

$$L_L = 0.14 \times 5.6\ \mu H$$
$$= 0.78\ \mu H$$

Thus, an inductance of $\sim 1\mu H$ can be realized. This low value of inductance enables the overall system inductance, L_O, of the capacitor bank, switch, busbars and load assembly to be kept very low consequently easing the problem of generating large I and di/dt with the simple bank.

4.2 DESIGN OF CAPACITOR BANK FOR CURRENT PARAMETERS

The next consideration was the design and expected output of the capacitor bank to the load assembly. These considerations are as follows:

The low frequency equivalent circuit of a capacitor discharge pulse generator is shown in Figure 7.

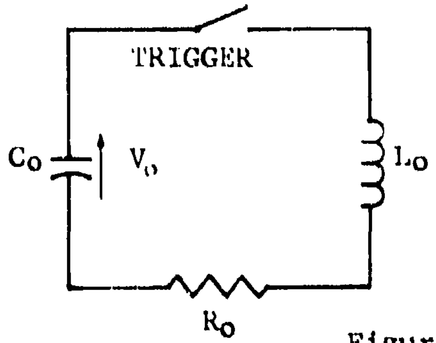

C_o = Bank capacitance
L_o = Total series inductance of bank, load assy, resistor, etc.
R_o = Total effective Series resistance

Figure 7
Lightning Generator Equivalent Circuit

When the capacitor bank is charged initially to V_o, the current pulse amplitude is given by

$$\hat{I} = V_o k_1 \sqrt{\frac{C_o}{L_o}} \quad \text{Amps} \qquad (2)$$

$k_1 < 1$ and is a function of $\dfrac{4L_o}{R_o^2 C_o}$

if $R_o = 0$, $k_1 = 1$

$$\hat{I} = V_o \sqrt{\frac{C_o}{L_o}} \quad \text{Amps} \qquad (3)$$

if $R_o = 2\sqrt{\dfrac{L_o}{C_o}} = R_c$ (the value for critical damping)

$$\hat{I} = \frac{V_o}{e} \sqrt{\frac{C_o}{L_o}} \quad \text{Amps} \qquad (4)$$

where $e = 2.718...$

if R_o is less than R_c the pulse is oscillatory. If $R_o = R_c$, a unipolar pulse with no overshoot is achieved.

Independently of R_o the maximum rate of change $d\hat{i}/dt$ is given by

$$\frac{d\hat{i}}{dt} = \frac{V_o}{L_o} \quad \text{Amps/s} \qquad (5)$$

4.2.1 Calculation of $\hat{I}$ and $d\hat{i}/dt$ Amplitudes

Information development to this point now allows some approximate calculations to be made of $\hat{I}$ and $d\hat{i}/dt$. These can then be compared to the magnitudes we sought for the reasons outlined in Section 3.2.

From Section 4.1, L_L is approximately 1 μH. As a first order approximation, we estimated another 1 to 1.5 μH in the capacitor, switch and resistor for a total circuit inductance, L_O, of 2-2.5 μH.

A capacitor of 4 μF, 45kV (working voltage) was available, thus

$$L_O = 2.25\,\mu H$$
$$C_O = 4.0\,\mu F$$
$$V_O = 45kV$$

Assuming $k_1 = 0.85$, from equation (2),

$$\hat{I} = 45 \times 10^3 \times .85 \times \sqrt{\frac{4 \times 10^{-6}}{2.25 \times 10^{-6}}} = \underline{51kA}$$

and equation (5) gives

$$\frac{d\hat{i}}{dt} = \frac{45 \times 10^3}{2.25 \times 10^{-6}} = \underline{20kA/us}$$

If $R_O = R_C = 1.5\Omega$ (unipolar pulse) equations (4) and (5) give

$$\hat{I} = \frac{45 \times 10^3}{2.7183} \sqrt{\frac{4 \times 10^{-6}}{2.25 \times 10^{-6}}} = \underline{22kA}$$

$$\frac{d\hat{i}}{dt} = \underline{20kA/us}$$

These are nominal values; actual test values are given in Section 5. However, the range of these values demonstrate that the configuration will provide the simulation we intended to achieve. (See 3.2 requirements)

4.3 DESIGN IMPLEMENTATION

Requirements and test configurations have been developed. However, the success of the test program was as dependent on the hardware and methods of implementing the design as on development of the requirements for the test configuration. The items of implementation such as grounding, impulse generator design, and instrumentation are discussed in this section.

4.3.1 System Grounding

Due to the simplicity and small size of the one stage bank, considerable flexibility is possible in the layout of the test configuration grounding. Conventionally, one side of the capacitor bank is grounded (as in Reference 3); other tests have grounding points at the fuselage midpoint (Reference 1) but choice of grounding should be determined from considerations (vi) and (vii) in Section 4.0 above. Various possible grounding configurations are shown in Figure 8. Choice of point (1) seemed to provide the simplest method for accomplishing all the constraints of articles (vi) and (vii). Additionally, point (1) also provided the most convenient place to provide a reference to the screen room which was used to house the measuring instruments. Further discussions on the screen room are contained in subsequent paragraphs.

With regard to spurious grounds, the small, compact bank allows large separation distances above the ground so as to minimize stray HF current through distributed capacitance.

Selection of point (1) does allow the capacitor bank to rise to several kV during the pulse but this effect is not detrimental. The charging and trigger leads also have high voltage impressed on them during the pulse. These leads are effectively isolated by a resistor string which prevents spurious currents from being injected back into the power supply units.

As noted in Figure 8, only one point was established as a ground for the total test configuration. Figure 9 shows the location of this ground with respect to the load assembly and the screen room (trailer in the background of Figure 9).

4.3.2 Impulse Generator

The high current impulse generator consisted of one 4μF, 50kV energy storage capacitor, an open gap switch, and a series damping resistor. These high current elements were arranged in a closely spaced circuit located at the nose of the fuselage about four feet above the floor as shown in Figure 10.

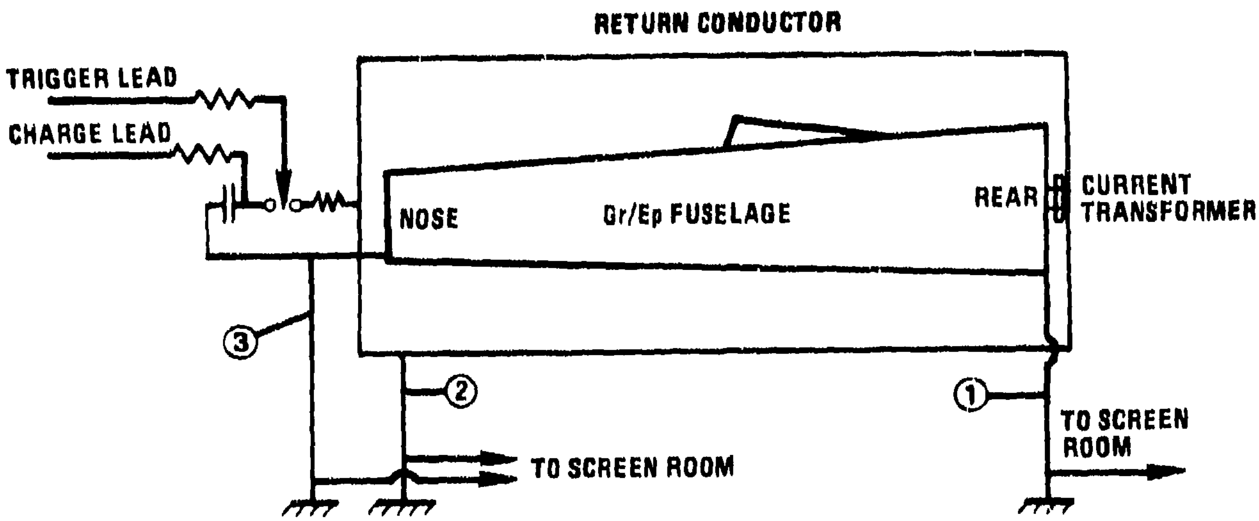

1, 2, and 3 are alternative grounding points of which only one may be used. 1 is the most convenient for instrumentation - see text.

Figure 8 Choice of Bank and Load Assembly Grounding Points

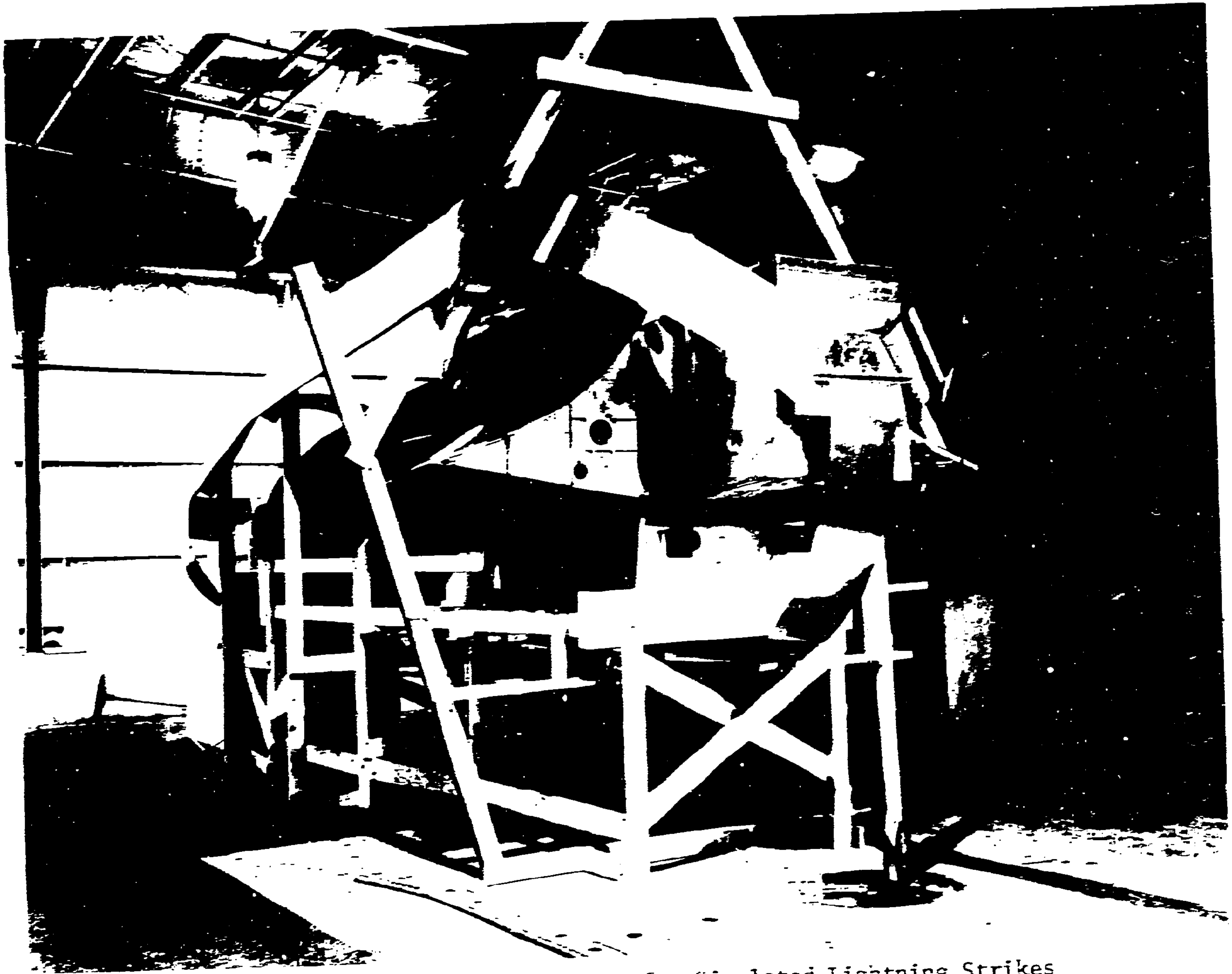

Figure 9 Aft View of Test Setup for Simulated Lightning Strikes

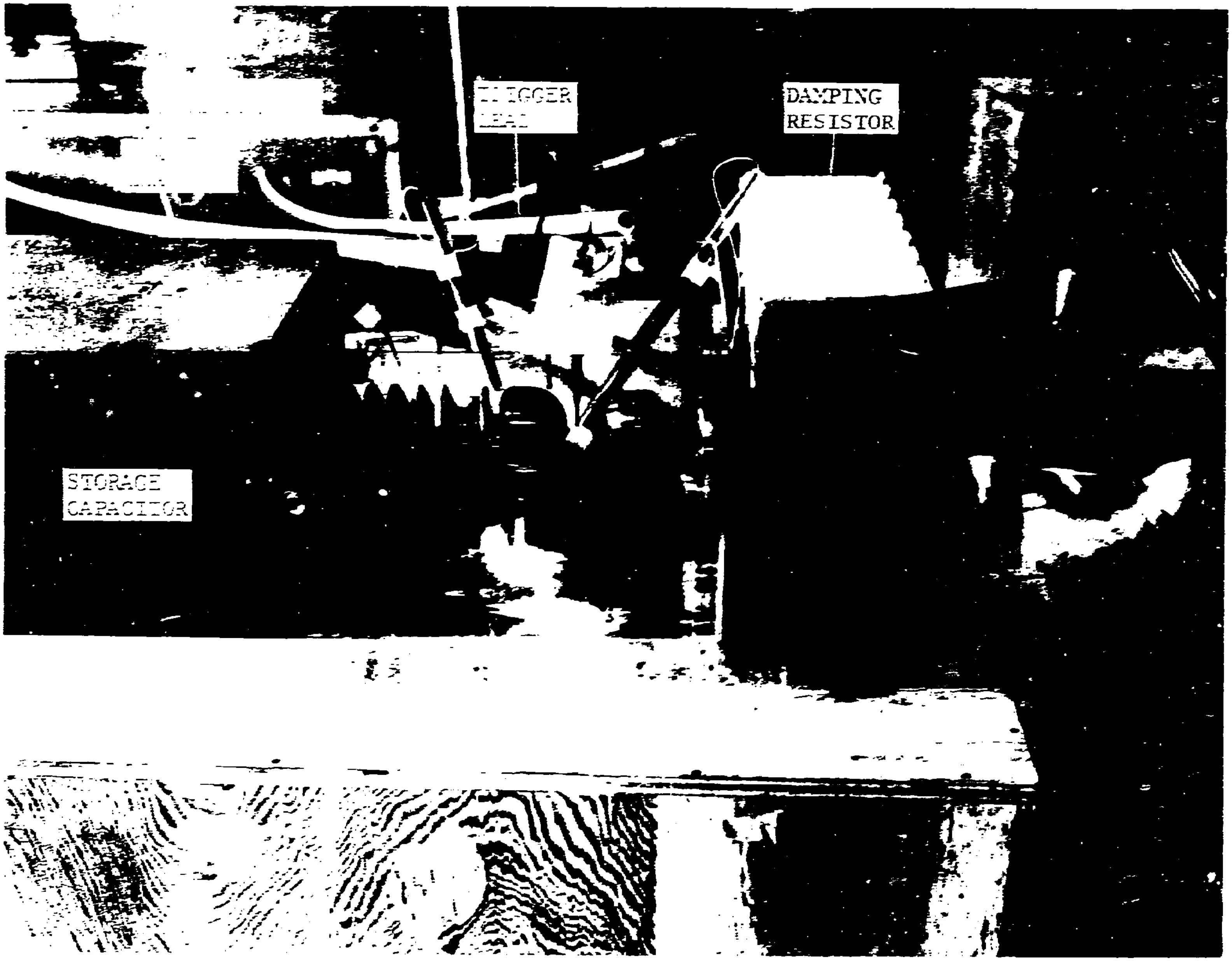

Figure 10 Close-up View of Impulse Generator at Front End of Test Setup

The gap switch was constructed with one electrode attached to the capacitor and it utilized a mid-plane trigger rod as shown in Figure 10. The series resistor was constructed with titanium strips to provide high resistivity and the strips were connected in alternate directions in a closely spaced stack for minimum inductance. The resistor parameters were 1.35 ohms resistance and 0.3 microhenries inductance.

Charging and triggering were provided from a power supply assembly located about six feet from the capacitor. Resistive isolation was provided in both the charging and trigger lines. The resistors were located inside plastic tubing that was extended between the units. Triggering was provided through a smaller trigger gap located inside the power supply assembly. (This trigger was also taken out to the screen room for oscilloscope trigger.)

The unique features of this part of the test configuration is the low inductance provided by the damping resistor, and the closed, broad connections between the capacitor/gap and the load assembly. A schematic of the test configuration is given in Figure 11.

4.3.3 Instrumentation

Instrumentation consisted of a mobile screen room, a Tektronix 7633 oscilloscope, a Pearson 1080 current transformer, a fiber optic transmitter/receiver, RG-58 and RG-22 coaxial cable, and various calibrated loops and divider networks. This section discusses the instrumentation arrangements.

4.3.3.1 Screen Room

For these tests, we obtained a trailer which had a 8X12 screen room with an ancillary unshielded operations room. This trailer was parked about 12-15 feet from the load assembly. All measurements were taken from inside the screen room. Figure 12 shows a portion of the internal arrangement.

The screen room received power from a self-contained transformer which was energized from facility power. The power entry points into the shielded enclosure were filtered and data indicated no spurious signals inside the enclosure. Hard-wire interface cables into the shielded enclosure were all shielded with shields grounded at the entry points. Reference was the single ground point established at the rear of the load assembly. Electrical connection from the trailer to the ground was effected by a section of aluminum pipe laid from the outside wall of the trailer to ground point. At the trailer side wall, a heavy braid was

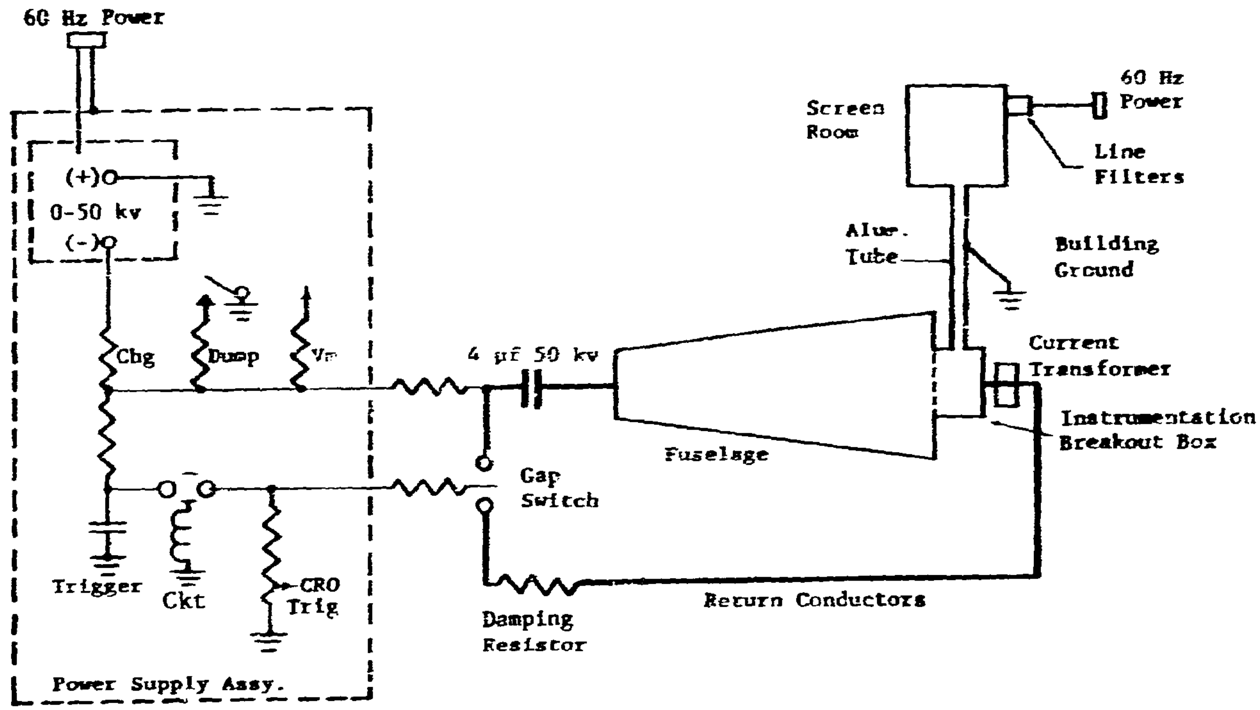

Figure 11 Test Configuration Schematic

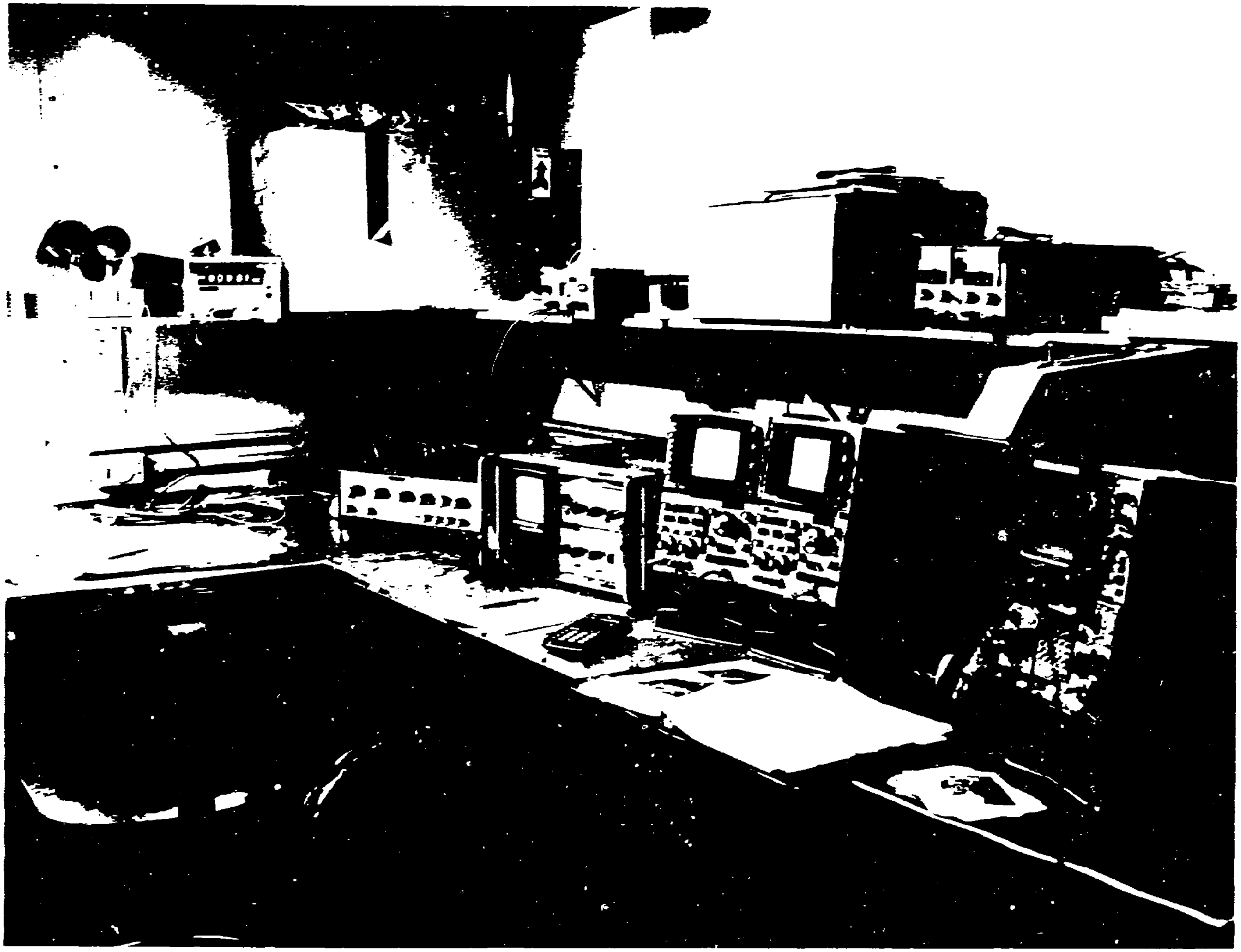

Figure 12 View of Shielded Screen Room and Diagnostic Equipment

fitted over and clamped to the aluminum pipe and routed through an air duct to the ancillary operations room, outside the shielded enclosure, where it was solidly fastened.

4.3.3.2 Measurement Instruments and Transducers

All measurements were made using an oscilloscope (CRO), Tektronix Model 7633 with a 7A13 differential preamplifier. This CRO has storage capability at sweep rates of 50 ns per division, a bandwidth of 105 MHz, and a common mode rejection ratio greater than 200 to 1 up to 20 MHz. It was calibrated to manufacturers specifications just prior to the tests and calibration checks were made periodically during the test period.

The CRO inputs were provided by a coaxial or fiber optic interface. The coaxial interface (RG-58 or RG-22) was used in measurement of IR voltages developed along the fuselage, and flux (both diffusion and external) voltages induced into "looped" circuits inside the fuselage. The coax was routed from the screen room to the fuselage inside the aluminum pipe used to establish ground between the screen room, local facility ground and the fuselage. As can be seen from Figure 9, a vertical aluminum pipe makes the ground connection between the fuselage and facility ground. The vertical pipe is attached to an aluminum fixture (instrumentation break-out box) which is in turn connected to the metal bulkhead which exists at station 253 of the fuselage. This instrumentation break-out box was used to facilitate instrumentation connections and to provide an extra length to promote a particular longitudinal HF resonance as discussed in Section 3.3.2.

From inside the break-out box, the instrumentation coax was routed inside the fuselage skin to the particular areas under test. The routing was made along metal substructure or graphite build-up areas where possible in order to minimize pick-up in the cable.

At the CRO, divider networks were provided to scale the measured voltages so that the common mode rejection voltage would not be exceeded at the CRO inputs. A typical divider is shown in Figure 13. Data was measured using the differential input feature of the scope.

During tests with coaxial cable diagnostics, spurious noise pick-up was periodically monitored by short and open circuit measurements in order to assure a high signal to noise ratio. Figure 14 illustrates a typical check where the short circuit signal was due to small loop coupling (i.e. simulated loop formed by the coax/test circuit interface). The largest detected values peaked in the tenths of volts range, Figure 14, which was negligible compared to tens or hundreds of volts measured by the test circuit.

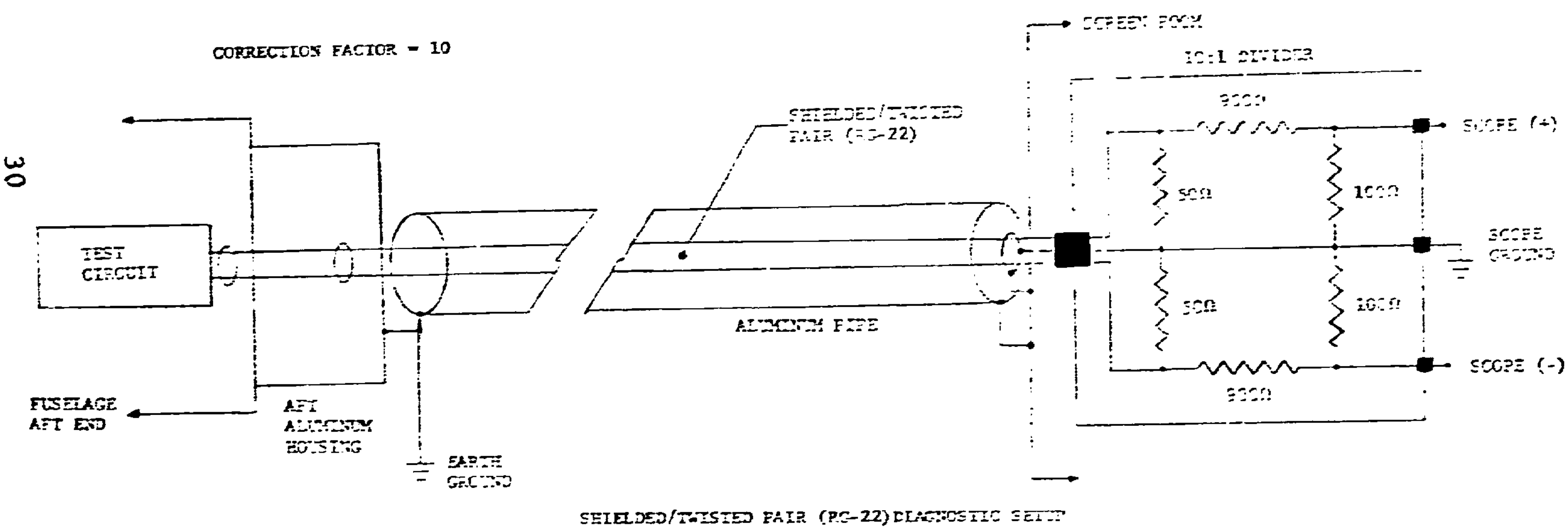

Figure 13 Coaxial Interface Configuration

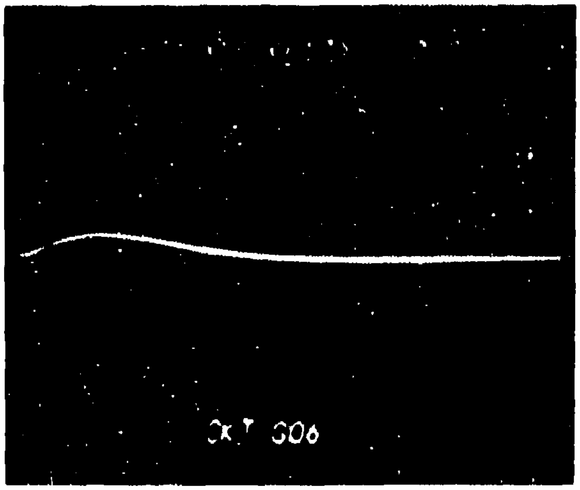

A. Short Circuit Test in Forward Bay.

Vertical: 1 V/Div.
Horizontal: 2usec/Div.

(Open Circuit Test showed negligible signal)

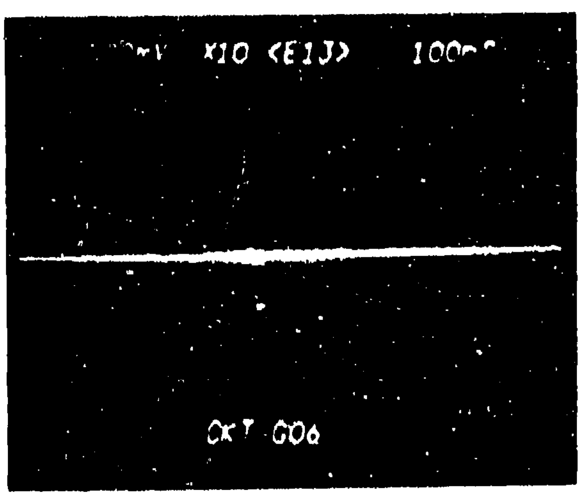

B. Expansion of Photo A above.

Vertical: 1 Volt/Div.
Horizontal: 100 nsec/Div.

Figure 14: Typical Noise Check Data with RG-22 Coaxial Cable

When a signal to noise ratio was small enough to become detrimental to data accuracy, a diagnostic setup was used which incorporated a low noise Fiber-optic link. This system eliminated high common mode voltages and spurious HF pick-up from shield leaks or interaction between the screen room and fuselage. A block diagram of the fiber optic link is shown in Figure 15. The transmitter and receiver units were obtained from Meret Inc., Part Number MDL238. Since these devices did not specifically meet our requirements, a few modifications were performed as indicated. The most important of these modifications involved designing a buffer and frequency compensation unit for the transmitter, and a frequency compensation and post amplifier unit for the receiver. The result of these modifications was to provide an analog system with a flat frequency response out to 30MHz and a 20dB/decade rolloff thereafter. This resulted in less than 12dB loss at our upper frequency limit of 50MHz.

The voltage divider located at the signal input was added because there was a 1 volt input limitation to the transmitter. The divider was made variable by resistor R for covering a wide range of induced voltage levels. The entire transmission system was placed in a metallic case (2 x 2 x 4 inches) and powered by NICAD batteries. A twisted pair was used for connections to test circuits in order to eliminate unwanted flux coupling. Open, loaded, and short circuit checks were continuously made during all test phases and on all diagnostic setups to define real zero and voltage levels not associated with the test circuit.

Figures 16 and 17 show examples of the loaded and open circuit noise levels, respectively. A few quick tests showed this noise was located essentially in the receiver unit. However, the noise level was sufficiently low and its frequency high enough as not to significantly interfere with accurate data acquisition.

For complete isolation from the high noise environment, the storage scope used for recording data was also triggered by a fiber optic link. This link was designed and built at G. D. and consists of simply a waveshaping circuit and transmitter receiver units. It can respond to a 20 nanosecond pulse up to 50 volts and has a delay time comparable to that of the data link.

The tranducers in general were circuits which were placed inside the fuselage in particular places to evaluate effects such as diffusion and apertures. The circuits consisted of loops, coax, open circuit wires, twisted pair and twisted-shielded pair. In addition, small, calibrated one and four-turn loops were used to measure flux (and indirectly current) distribution both inside and outside the fuselage shell.

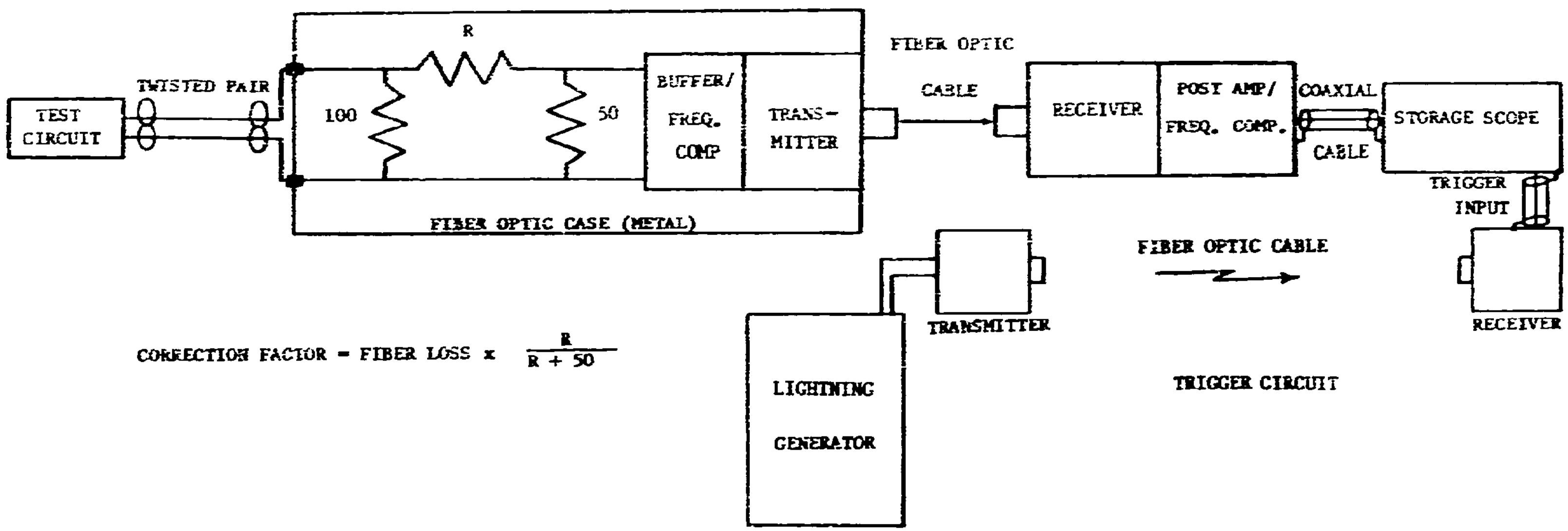

Figure 15 Fiber Optic Diagnostic Setup

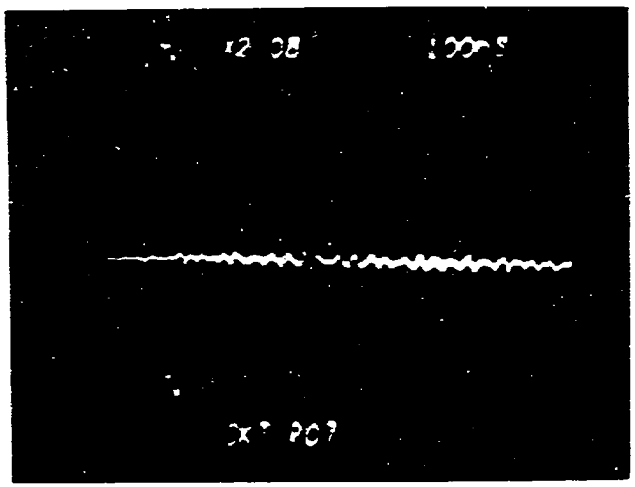

Vertical: 0.208 V/ Div.
Horizontal: 100 nsec/ Div.

Figure 16 Loaded Circuit Noise

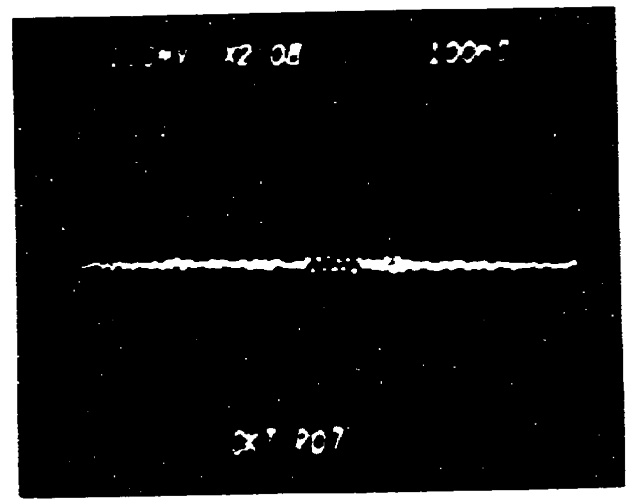

Vertical: 0.208 V/ Div.
Horizontal: 100 nsec/ Div.

Figure 17 Open Circuit Noise

The primary current pulse was measured using a Pearson Model 1080 transformer connected around the connection point between the fuselage shell and the return conductors. This instrumentation point is located at the aft end of the fuselage between the instrumentation break-out box and the returns.

SECTION V
DRIVING POINT WAVEFORM AND FLUX (CURRENT) DISTRIBUTION

The current waveform developed by the impulse generator was an over damped unipolar pulse with a peak value of 20,000 amperes rising to peak in 3.2 microseconds and falling exponentially to 50% at 8.5 microseconds from turn-on. The initial rate of current rise was 17 kA/μs. It was generated from a charge voltage of 45 kV on the 4μF capacitor.

The current was measured with a calibrated current transformer, Pearson Model 1080, located at the aft end of the fuselage. The transformer provided an accurate trace of the basic current waveform but it was found that it acted as a differentiator of high frequencies and exaggerated components that were faster than its rated rise time of .25 microseconds. The current wave contained faster components and they were measured separately as described below.

The output of the current transformer was recorded and a computer analysis was made by using a digitizer to collect input data points from the current trace. The waveform and its characteristics are shown in Figure 18. A Fourier transform of the low frequency components was made and is shown in Figure 19.

Parameters of the test circuit were determined from component measurements, from waveform analyses and from measurements of impulse voltages. The circuit inductance was determined from an underdamped waveform that was obtained by shorting the damping resistor and discharging the capacitor at 45 kV. The waveform and its analysis are shown in Figure 20. The division of the circuit inductance between the components was determined by measuring impulse voltages around the circuit. Voltage was measured with respect to the screen room through a voltage divider located at the screen room wall with the sensing lead connected to the circuit at right angles to the current path. The initial impulse voltage across each component was determined from the traces and the inductance of the underdamped circuit was divided among the components in proportion to the initial voltage drops. The measured and calculated values of R, L, and C are tabulated in Table 1.

In comparing the values obtained with the requirements we developed in Section 3, there is a very good agreement with what was expected.

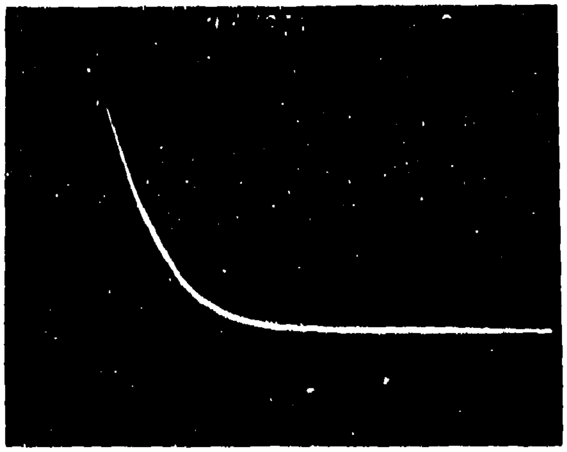

Vertical: 4 kAmps/ Div.

Horizontal: 5 usec/ Div.

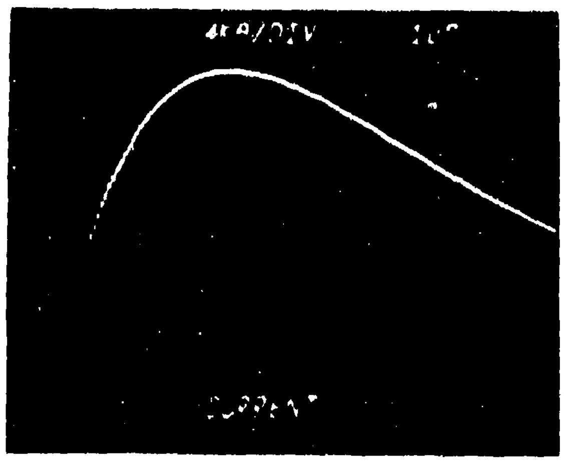

Vertical: 4 kAmps/ Div.

Horizontal: 1 usec/ Div.

Capacitance	=	4.0 uF
Voltage	=	45 kV
Current Maximum	=	20 kAmps
dI/dt Maximum	=	17.2 kAmps/usec
Peak Time	=	3.2 usec
Natural Frequency	=	49.2 kHz
Charge Transfer	=	0.18 Coulombs
Action Integral	=	2.4×10^3 A^2 sec
Total Resistance	=	1.67 Ohms

Figure 18 Driving Point Waveform-Overdamped

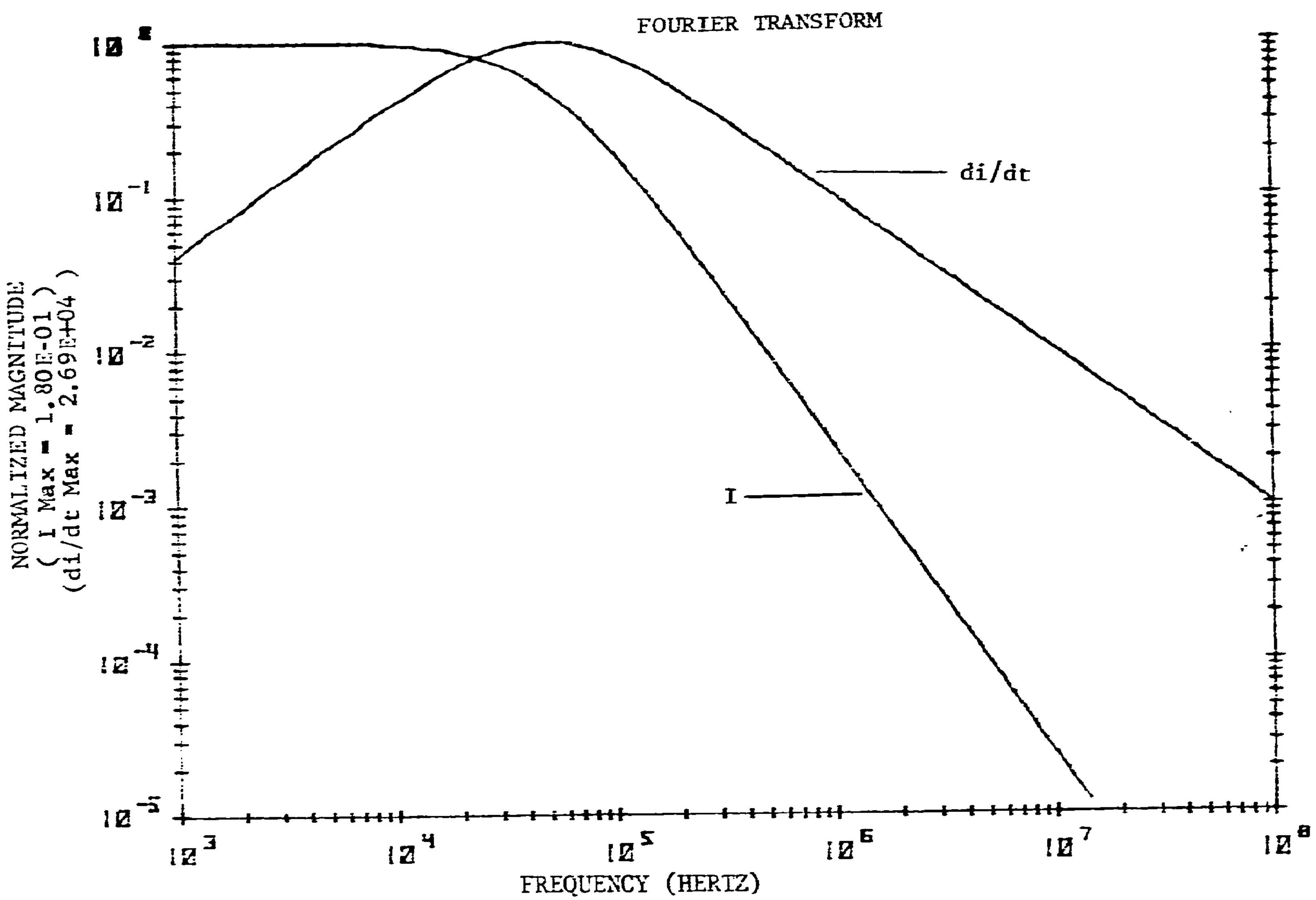

Figure 19 Fourier Transform of 20kA Current Waveform

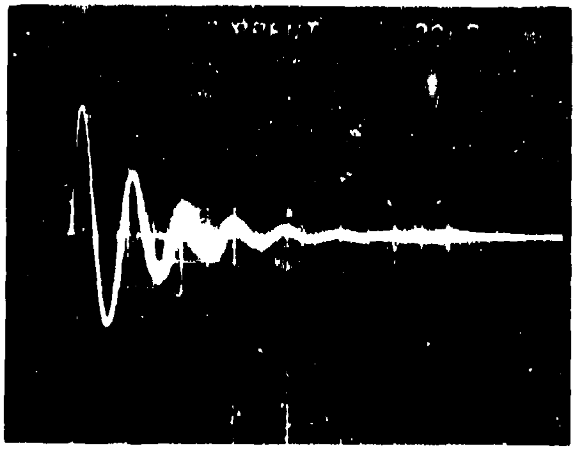

Vertical: 20 kAmps/ Div.

Horizontal: 20 usec/ Div.

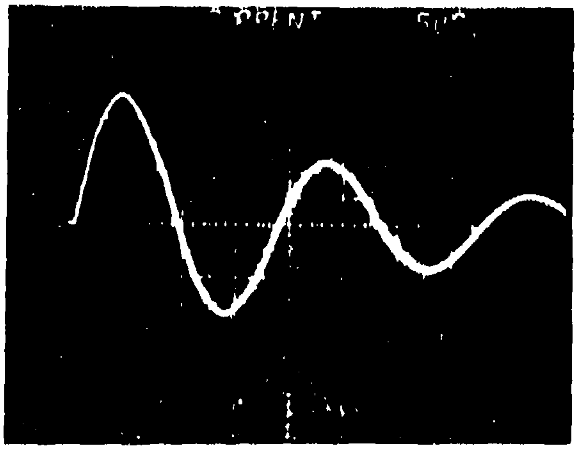

Vertical: 20 kAmps/ Div.

Horizontal: 5 usec/ Div.

Capacitance	=	4.0 uF
Voltage	=	45 kV
Current Max	=	48 kAmps
Natural Frequency	=	52.9 kHz
Inductance	=	2.26 uH
Stored Energy	=	4050 joules
Action Integral	=	22060 A^2 sec
Resistance	=	.165 ohms
di/dt Max	=	19.9 kAmps/usec

Figure 20 Driving Point Waveform-Underdamped

TABLE 1

TEST CIRCUIT PARAMETERS

A.	Capacitance:	
	Bridge, Brown Elec. Co. Model 312A	
	Capacitor, CSI Model 50W588NP	4.05 μf
B.	Resistance Calculated from Waveforms:	
	Underdamped circuit	.165 ohms
	Overdamped circuit	1.686 ohms
	DC Resistance of components: Bridge, Rubicon Co. Model 1622	
	Damping Resistor	1.350 ohms
	Fuselage and return conductors	.0228
	Fuselage forward compartment	.0105
C.	Inductance Calculated from Waveform:	
	Underdamped circuit	2.26 μH
	Inductance of components calculated from voltage division:	
	Capacitor and gap assy.	0.23
	Damping resistor	0.28
	Generator connections	0.79
	Generator total	1.30 μH
	Fuselage Sta. 60 to 253	0.56
	Return conductors Sta. 60 to 253	0.34
	End connections Sta. 253	0.34
	Load total	1.24 μH
	Total test circuit	2.54 μH

5.1 LOW FREQUENCY (LF) DISTRIBUTION

The field distribution around the forward compartment was measured in detail at fuselage station 85. The forward compartment was totally composite except for metal ring members at stations 60 and 98. All equipment, wiring and equipment mounts were removed from the compartment prior to the tests sothat the results would indicate characteristics of an all composite structure. The 20 kA test current was applied end to end for each measurement.

Loops were placed initially in six locations around the outside of the fuselage. Field traces (integrated voltages) are shown in Figure 21. The flux waveshape with time was found to be similar to that of the driving current as can be seen from a comparison with Figure 18.

The magnetic field pattern produced by the test current pulse was measured with small wire loops. Six identical loops were constructed by winding four turns of No. 24 wire on a 3/4 x 2 inch wooden form. The resultant coil looped an area of .00108 m with four turns and had an inductance of 1.8 μH. Each coil was connected to RG58 cable which was routed through the fuselage to the CRO and was terminated with 50 ohms. The signal was divided at the CRO for voltage measurements and was connected to a 100 μs integrator for flux measurements. The time constant of the loop-cable system was determined to be adequate for the LF traces but was too long to permit scaling of the high frequency components of voltage.

As can be seen from Figure 21, the distribution around the fuselage is very uniform (as would be the case in free space and as was an initial requirement in the design of the test configuration).

To provide a check on the data, the magnetizing force around station 85 was calculated from the measured field strength and was compared with the magnetizing force that was calculated from the driving current and the fuselage dimensions. For example, the peak field of circuit A03 in Figure 21 was .0089 webers/meter^2. The magnetizing force at that point was this field intensity divided by the permeability of free space, or $.0089/4\pi \times 10^{-7} = 7082$ Amp/meter. This value is in good agreement with the average magnetizing force of the driving current which was 20 kA and a fuselage circumference at station 85 of 2.74 meters, or 7290 Amp/meter. This value also compares favorable with values predicted by POTENT as shown in Section 6.

Next, the loops were placed inside the fuselage at the same six locations. The results are shown in Figure 22. The internal flux did not follow the driving current, but followed a diffusion/ redistribution pattern that was determined by characteristics of the fuselage. Note that the general shape of the flux (which is a measure of internal skin current) follows the shape suggested by the theory. (See Section 6.)

5.2 HIGH FREQUENCY (HF) DISTRIBUTION

As discussed in Section 3.3.2, a longitudinal distribution of HF current was expected in our test configuration. Measurements were made in a similar manner as in the LF tests. The expected predominant frequencies were 14MHz and 42MHz. These currents were expected to be maximum at the aft end and minimum at the forward end.

Figures 23(a) and (b) show the loop voltage and current (integral of loop voltage) at the aft end and Figures 23(c) and (d) show the comparable values at the generator. At 300 nanoseconds from turn-on, the current at the aft end measures 198 amperes peak-to-peak (0.6 x 330 amps) and at the forward end 92 amperes peak-to-peak (0.2 x 463 amps).

The predominant frequency shown in the integrated waveform is 14MHz. The integration time was too long to show any higher frequency component. However, the higher frequency (approximately 46MHz) is evident in the voltage shown in Figures 23(a) and (c).

To demonstrate that the effect (HF components) is due to transmission line mis-match, the characteristic impedance of the set-up was calculated (40Ω) and this value resistance was connected across the forward end of the fuselage between the return conductors and the fuselage. The measurement of current was repeated, with the results shown in Figure 24(a) and (b). Clearly, the HF components are a transmission line effect as the 14MHz component is almost completely damped out. During tests, the damping resistor was removed.

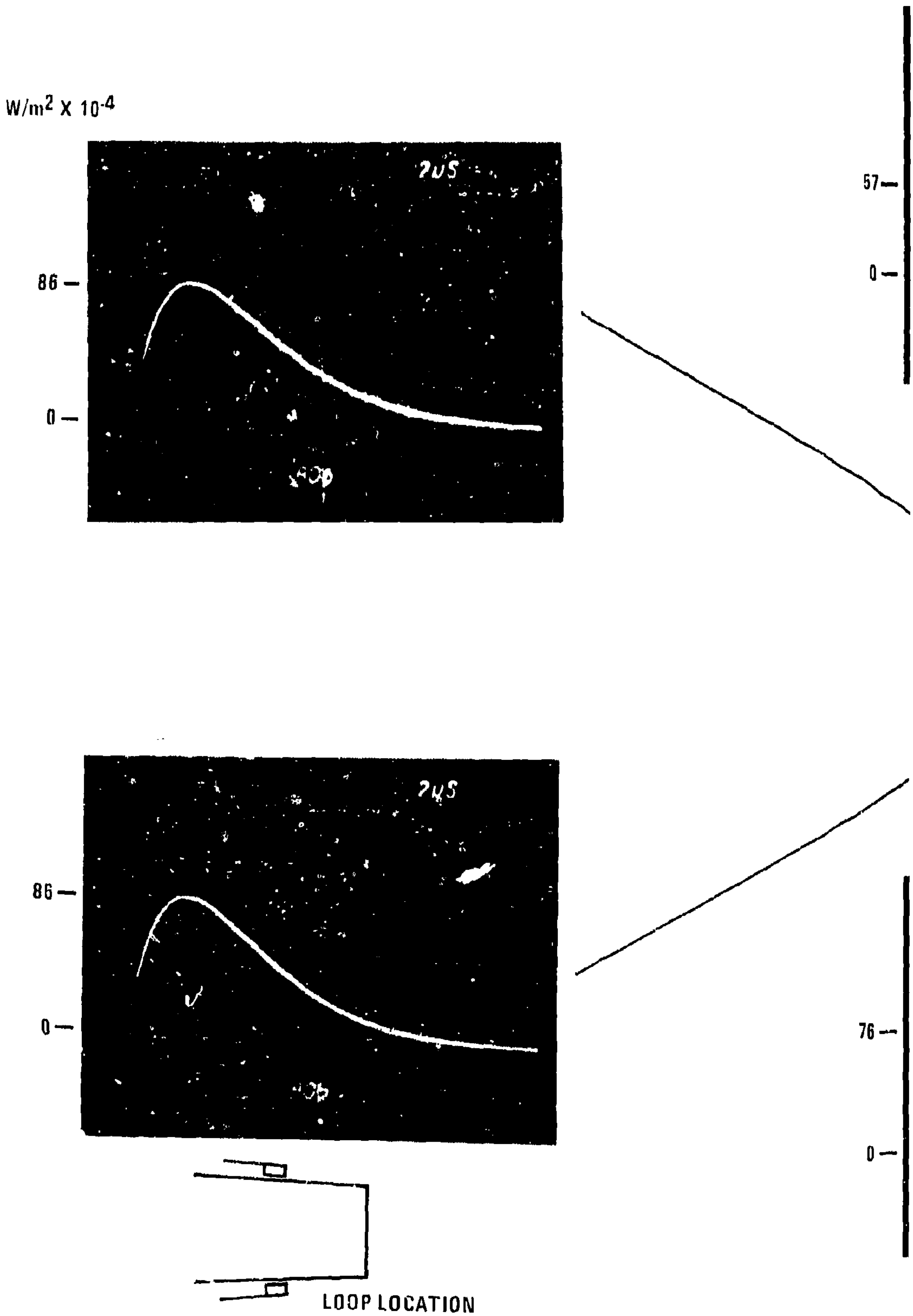

Figure 21 E

Oscillogram Scaling:
Vertical: 27×10^{-4} Webers/Meter^2/Div.
Horizontal: 2 usec/Div.

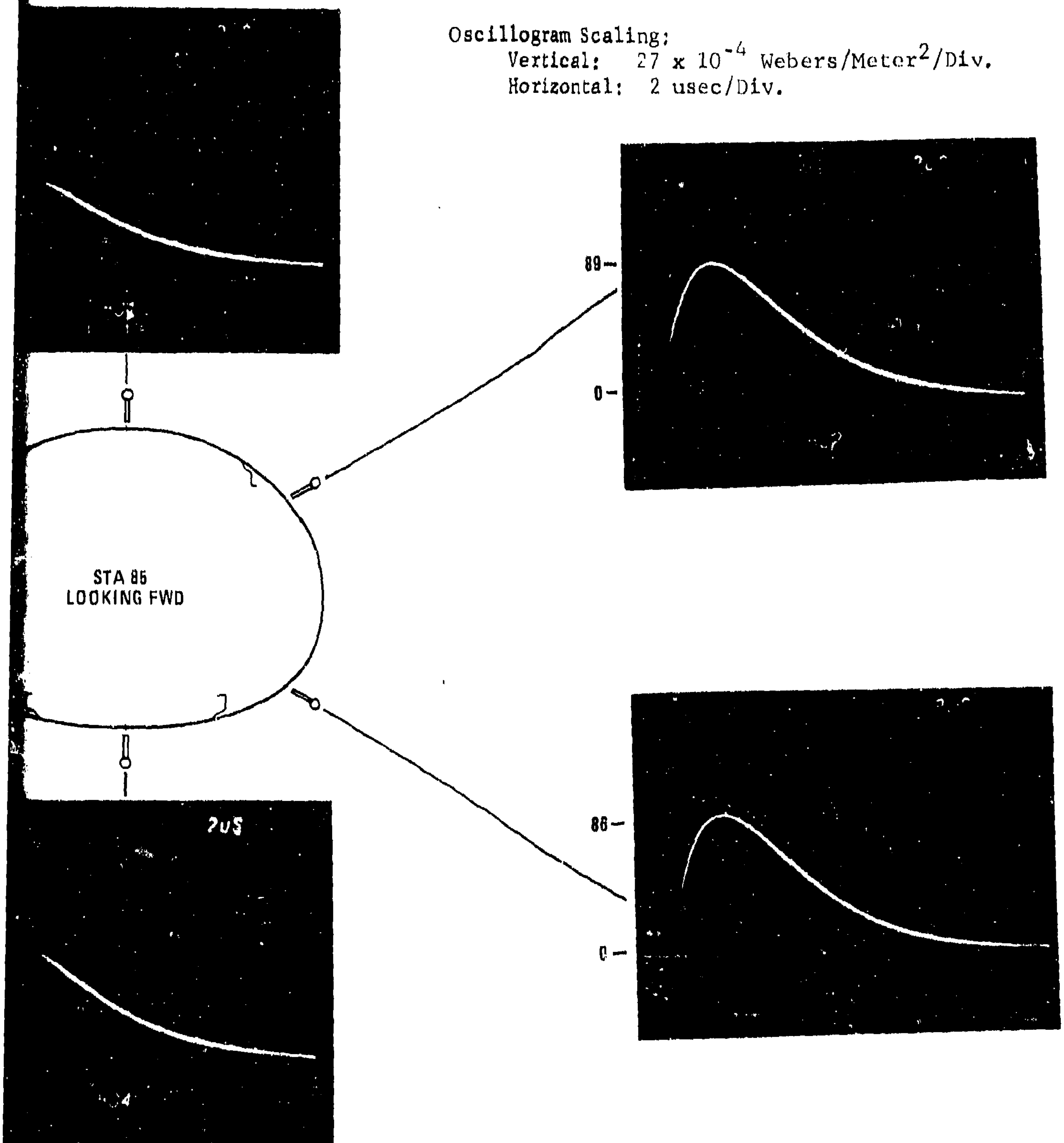

Field Distribution (STA 85) - Low Frequency

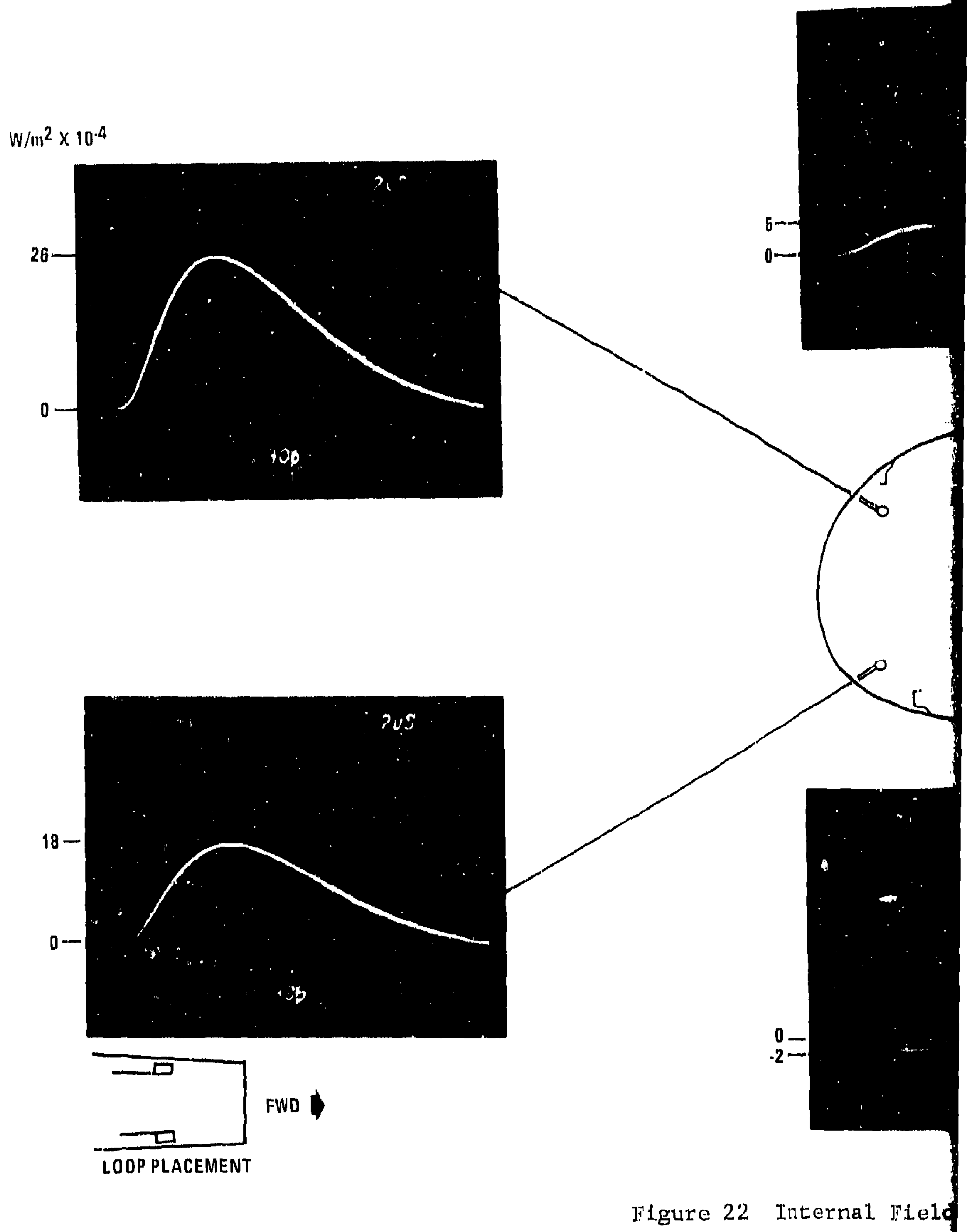

Figure 22 Internal Fiel

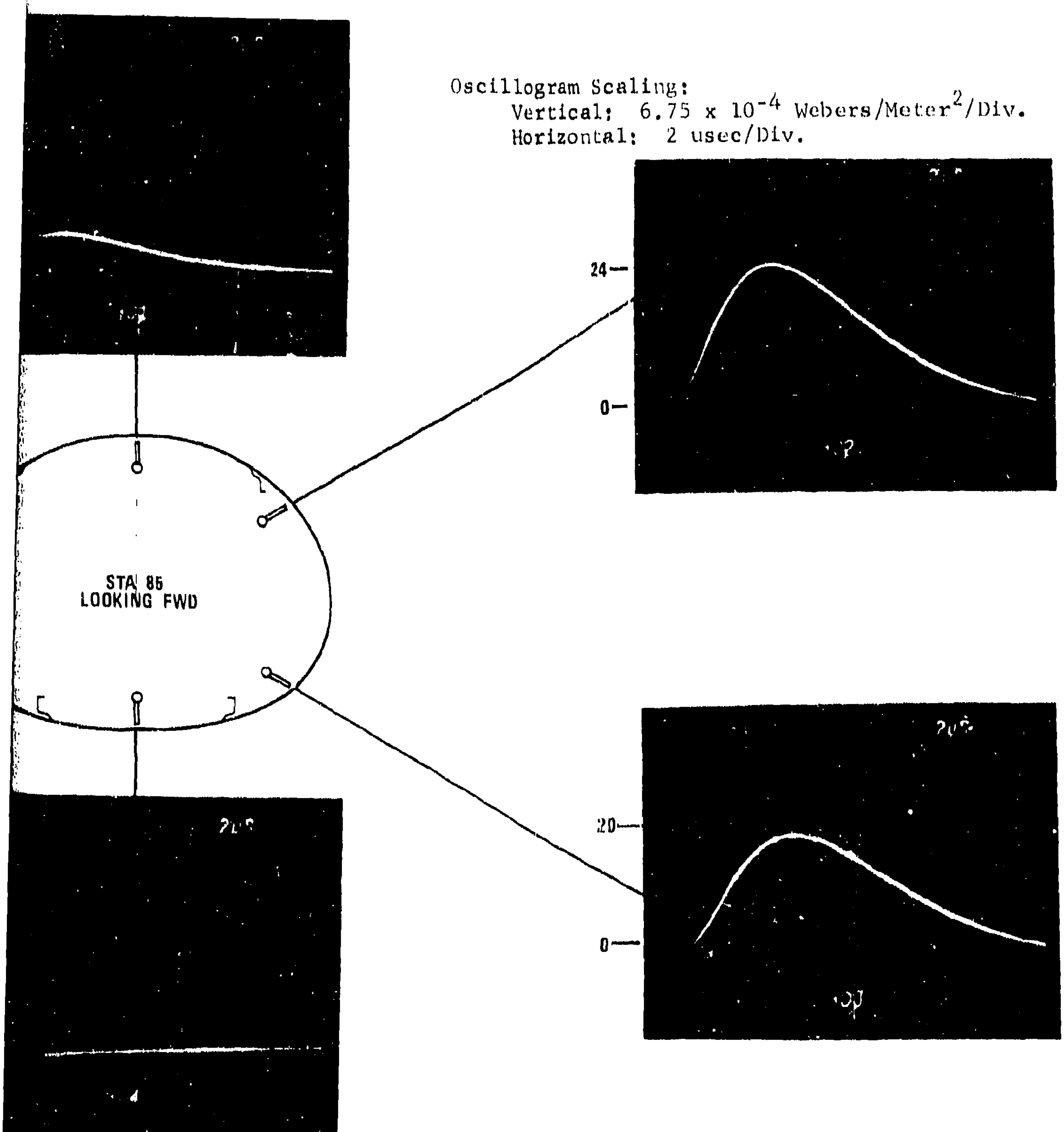

Field Distribution (STA 85) - Low Frequency

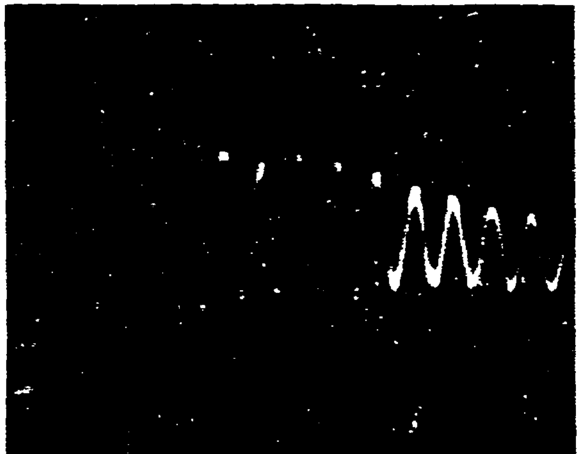

(A) Vertical: 10 Volts/Div.
Horizontal: 100 nsec/Div.

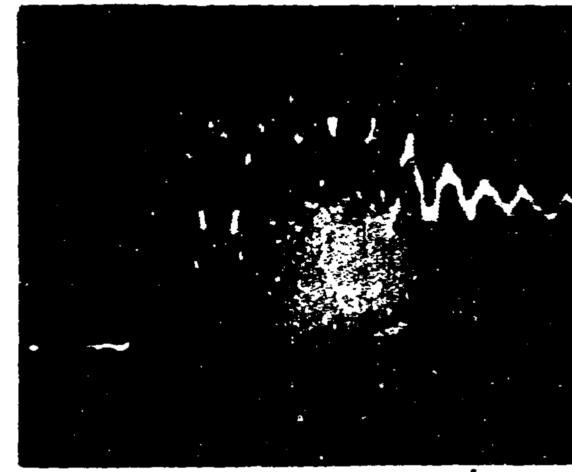

(C) Vertical: 5 Volts/Div.
Horizontal: 100 nsec/Div.

Loop Voltages

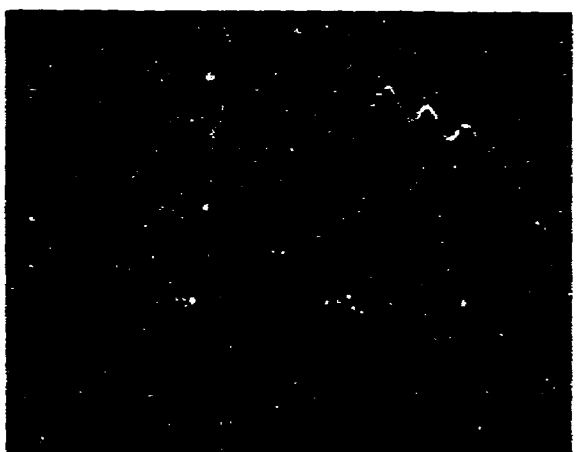

(B) Vertical: 330 Amps/Div.
Horizontal: 100 nsec/Div.

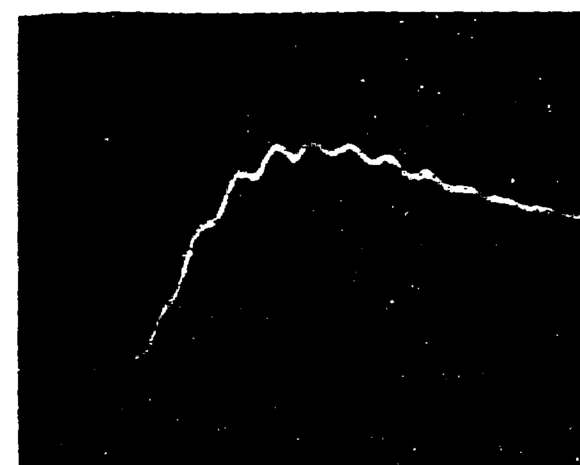

(D) Vertical: 463 Amps/Div.
Horizontal: 100 nsec/Div.

Current waveform indicated by 100 nsec integrator

Figure 23 HF Current Distribution--(A) & (B) Aft End; (C) & (D) Forward End

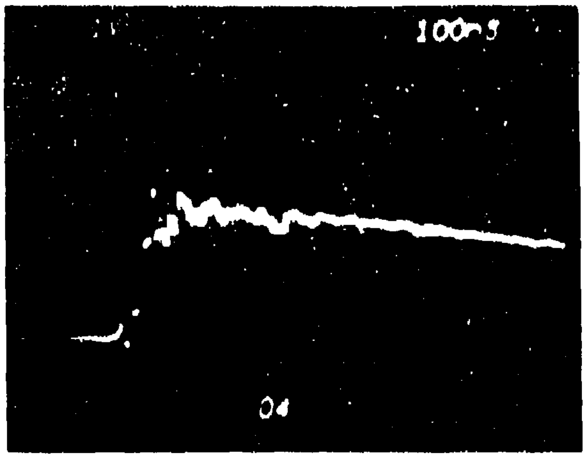

(A)

Loop Voltage

Vertical: 10 Volts/Div.
Horizontal: 100 nsec/Div.

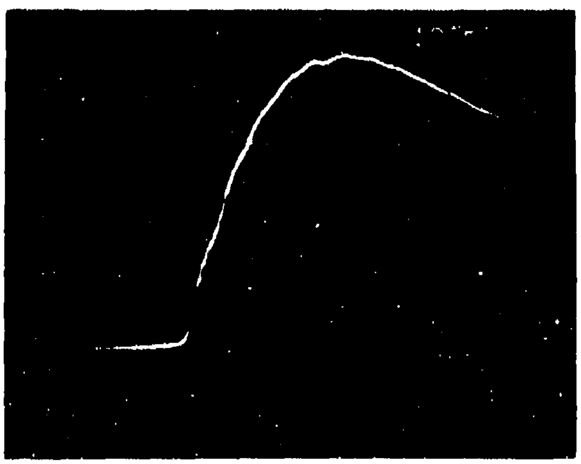

(B)

Current waveform indicated by 100 nsec integrator.

Vertical: 330 Amps/Div.
Horizontal: 100 nsec/Div.

Figure 24 Effects of Matching the Impedance of the Test Configuration

SECTION VI

TEST APPROACH AND COMPARISON OF PREDICTED AND MEASURED RESULTS

In Section 3.4, we stated the primary mechanisms for induced effects. Induced voltages are either due to an aperture, or resistively generated voltages resulting from diffusion of the flux through the fuselage skin, or a combination effect.

For aperture effects there is no fundamental difference between a metal or a Gr/Ep fuselage. Hence, calculations of, and measurements on apertures in a composite fuselage, e.g., the cockpit, will in principle be unaffected by the graphite. However, due to the comparatively large IR drops to be expected in graphite (perhaps hundred or thousands of volts since ρ is ~ 1000 times larger than for aluminum), IR and aperture voltages will be comparable in magnitude, and may add or subtract to give complex waveforms. Examples will be shown.

Graphite is a conductor, although a poor one. Therefore, it is essentially different from Kevlar and glass fiber which are insulators and give aperture type voltages behind them. Since graphite is a conductor both resistive and diffusion flux induced voltages measured internally will therefore be proportional to the waveform of the current and not di/dt.

To make the output of these tests as general as possible, we needed to determine the principal characteristics of a complex structure comprising graphite, metal and non-conductors from the viewpoint of lightning and the electrical system. Due to the mechanical and electrical complexity of the fuselage, three typical sections were tested:

1) Forward Equipment Bay (FEB), Stations 60-98. Fully enclosed, mainly graphite with four thickened up longerons, but little metal, with two removable graphite doors, one with a small Kevlar access panel in it.

2) Cockpit. Stations 98-168. Large aperture dominated section, mainly graphite wall and floor (including graphite front strake section) but with a metal sill (the canopy seal) and the metal right-hand equipment console.

3) Central and R.H. Aft Bays. Stations 227-253. This section has a lot of metal in the strakes, the rear transverse bulkhead, and fore and aft panels. The

graphite bay doors are secured to all metal substructure. The right hand side panel has metal inserts for the screw heads.

In all sections the predominant modes of induced voltage were determined. Surface IR* and loop voltages were predicted and measured, including the dependence on circumferential position, and depth within the bay (i.e., distance in from skin). Also the effect of metal fasteners and of screening of the wires to induced voltages is shown.

Additional measurements included:

(a) Small aperture effects

(b) Attenuation of H.F. fields through graphite panels

(c) Performance of twisted pairs, coaxial cables and shielded twisted pairs in presence of aperture and diffusion fields.

(d) Effect of additional metal conductors and their impact on the circumferential variation of voltages

(e) H. F. effects inside enclosed areas (fwd bay) due to capacitive coupling

(f) Flux distribution inside the fuselage.

The test series also included an "electronics powered up" test on the aircraft to check for interference or damage.

6.1 PREDICTED RESULTS: FORWARD EQUIPMENT BAY (F.E.B.)

6.1.1 Surface IR Voltages

A POTENT (Reference 6) field mapping of the front fuselage at station 75, with the specified load assembly return conductor positions, yielded the surface magnetizing force H shown in Figure 25(a). These values are identical to the surface current density (i.e., current per unit width for longitudinal current),

*The term surface IR voltage means that the resistively produced voltage is measured by sensing connections along the inner face of the panel whose outer surface is the outer surface of the aircraft skin.

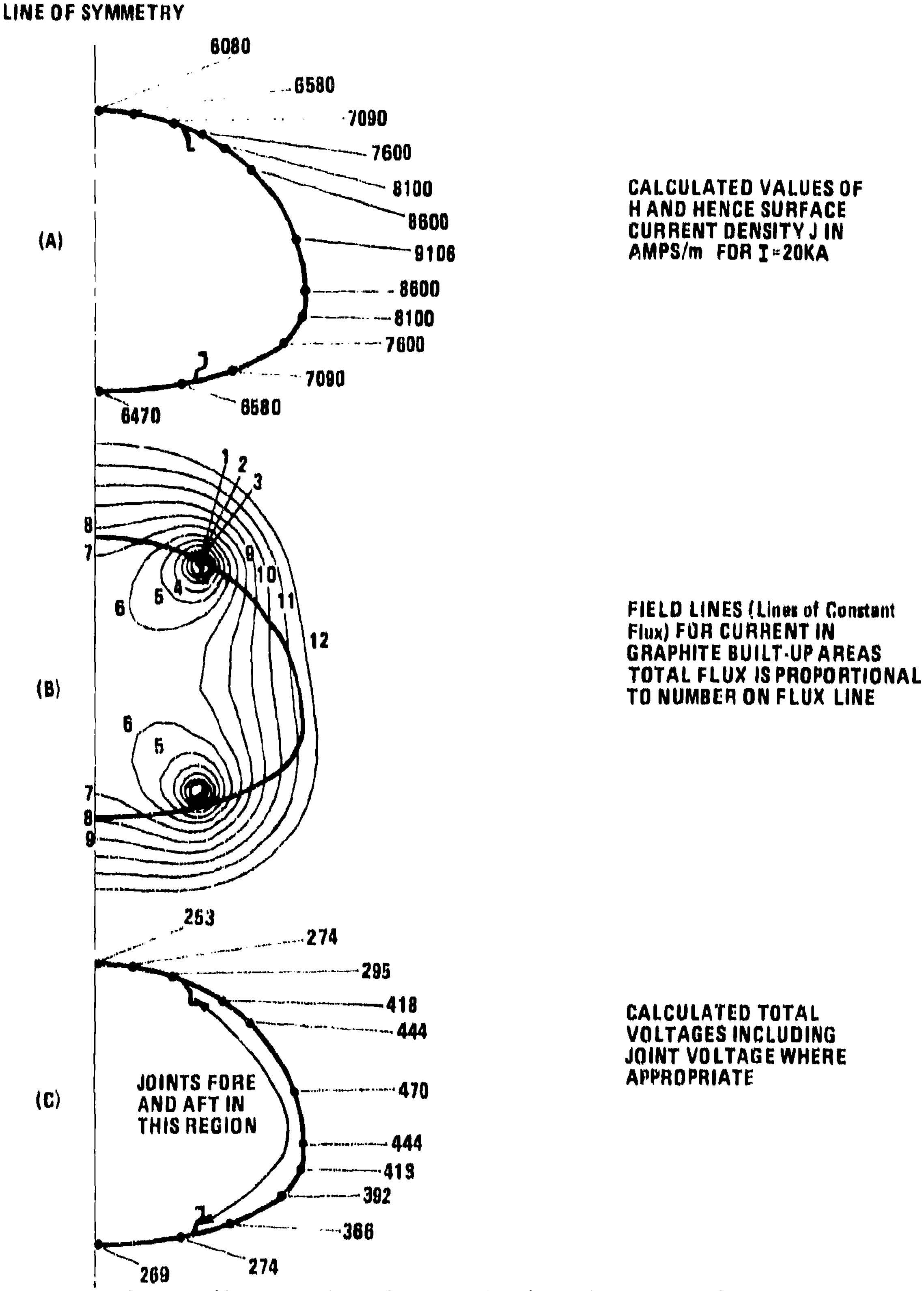

Figure 25 Station 75 - Calculated Flux and H Values

also in Amps/meter, in the condition where the current distribution is essentially inductively shared around the entire fuselage periphery. It can be shown that current redistribution is small up to peak current. Since current penetration through the graphite is so fast, the inside surface voltage follows the current pulse. Therefore the external current produces a voltage on the inside surface of the graphite panel given by an Ohm's Law calculation:

$$V_R = \frac{J \cdot \rho_{eff} \cdot \ell}{h} \text{ Volts} \tag{6}$$

where J = local surface current density
ρ_{eff} = effective resistivity of graphite panel
ℓ = panel length
h = panel thickness

J is obtained from Figure 25(a) and in the F.E.B; ℓ = 38" (.965m); h for 6-ply is 0.84×10^{-3}m; and ρ_{eff} is taken from measured data. For calculations in this report, the value of ρ_{eff} is taken to be the resistivity of the surface ply, ρ_0 . This value is $3750 \times 10^{-8}\Omega$m and was measured as described in Volume 1 of this report. This value of resistivity is lower than most published values and is lower than would be predicted for a $(0, +45)_s$ panel using ρ_{45} and ρ_0 as measured in Volume 1. The fact is, an effective bulk resistivity for the fuselage will vary considerably around and along the fuselage periphery due to metal substructure, ply build-up such as around access doors and other ply and construction anomalies as discussed in this report. Such anomalies would always tend to make the effective resistivity lower than would be predicted for uniform structure containing only graphite and epoxy.

Using above values for ℓ , h, ρ_{eff}, and J (from Figure 25 a) the calculated voltages are shown in Figure 25(b). To allow for the screw joints in the access panels, a resistance of 5mΩ-m will be used based on measurements on Environmental Conditioning Tests made at General Dynamics. For 2 joints per panel (fore and aft), the total joint voltage V_J to be added to the Figure 25(b) values are:

$$V_J = J \times 10 \times 10^{-3} \text{ volts.}$$

Thus the total metal ring-to-metal ring (station 60 to 98) voltage at any IR wire (see Figure 38) will be $V_R + V_J$.

Total voltages, including joint voltages as appropriate, are given in Figure 25(c).

6.1.2 Internal Loop Voltages Generated by Diffusion Flux

Internal voltages in loops are induced by the diffusion flux, that is, flux which passes through, as distinct from around, a conductor. To estimate internal loop voltages the field pattern of the diffusing flux is required - this is shown in Figure 25(b). (also obtained by POTENT). For this calculation, current flow is in four conducting paths only - the regions of graphite build-up.

The flux adopts the same pattern throughout the entire diffusion process. Flux which has passed through a conductor has a rate of change depending on that conductor material, (thickness resistivity, etc.) and cannot change as fast as the external flux. Voltages of a generally similar waveform and amplitude as the skin $J\rho$ voltages will be generated on loops (cf Theorem 1 in Appendix).

Using equation (A13) in the appendix, the voltages on separate small loops can be calculated by a difference technique. That is, the loop voltage can be considered to be the difference between two loops, each comprising one longitudinal arm of the test circuit, and a common return close to the graphite build-up.

Thus, voltages on the 8" x 2" loops #1, #2 and #3 (see Figure 38) are calculated by the difference in the flux ϕ at the position of longitudinal wires as follows:

$$\frac{V_{loop\ \#1}}{V_R} = \frac{\phi_1 - \phi_2}{\phi_s}$$

where ϕ_s is the flux at the graphite surface where V_R is measured, and ϕ_1 and ϕ_2 are the fluxes linking the two longitudinal sides of the 8" long loop; ϕ_1 being the closest to the graphite panel. Likewise for loop #2, the voltage is calculated from $\phi_2 - \phi_3$ and so on. The flux values from the POTENT tabulation are:

ϕ_1	ϕ_2	ϕ_3	ϕ_4	ϕ_s
.5217	.4677	.4167	.3733	.5558

Example Calculation Loop #1 - Using the predicted panel $J\rho$ voltage for V_R which was given as 379V, and allowing for the reduced length of the loop (8" instead of 38" used for calculating V_R), the predicted voltage is

$$V_{\#1} = \frac{(\phi_1 - \phi_2)}{\phi_s} \times V_R \times \frac{8}{38} = \frac{.054}{.5558} \times 379 \times \frac{8}{38} = 7.75\text{V}$$

Similarly for loops #2 and #3:

$V_{\#2} = 7.3V$

$V_{\#3} = 6.2V$

A comparison with measured data follows the sections on predictions for the cockpit and the aft bay.

6.2 PREDICTED RESULTS: COCKPIT AREA-STATION 126-168

Voltages in the cockpit area will be induced by both resistive/diffusion coupling and aperture coupling. The two mechanisms are treated separately, but in any general case instantaneous voltages produced by the two mechanisms can be added algebraically for total voltage.

6.2.1 Cockpit IR Voltages

The calculation method used is the same as used above for the F.E.B.; and is simplified by the absence of removable access panels (Station 126 is behind the lower equipment bay). However, the many changes of skin thickness both along and around the cockpit make calculations difficult. The strakes further complicate the problem since they are different material and different thickness (thermoplastic resin 8-ply, right; regular resin 16-ply, left). On the cockpit floor, between the longeron, 10-ply increasing to 14-ply toward the back is used. The longerons are concentrations of 0° fiber. Above the longerons up to the waist joint is 10-ply, changing to 6-ply up to the canopy sill except at the left side at the rear (adjacent to the gun muzzle) where it is 10-ply. Figure 26(a) shows the external surface field (calculated by POTENT) thus giving the surface current density from which the voltage drops were calculated. Calculated and measured values are shown in Figure 28.

6.2.2 Cockpit Aperture Flux Induced Voltages

This calculation will use the same assumptions for a graphite fuselage as for metal; that is, the initial aperture field is unaffected by current re-distribution. This has been demonstrated to be true for metal. The POTENT calculation, referred to in the above paragraph, also produced the flux contours ('field lines') shown in Figure 26 (b). From the POTENT tabulation which produced Figure 26 (b), calculation of voltages can be made by calculating M_{TF}, which is defined in the Appendix, equation A2 in terms of L' and M. M_{TF} in effect is the fraction of the total flux which couples the circuit or loop; multiplied by L':

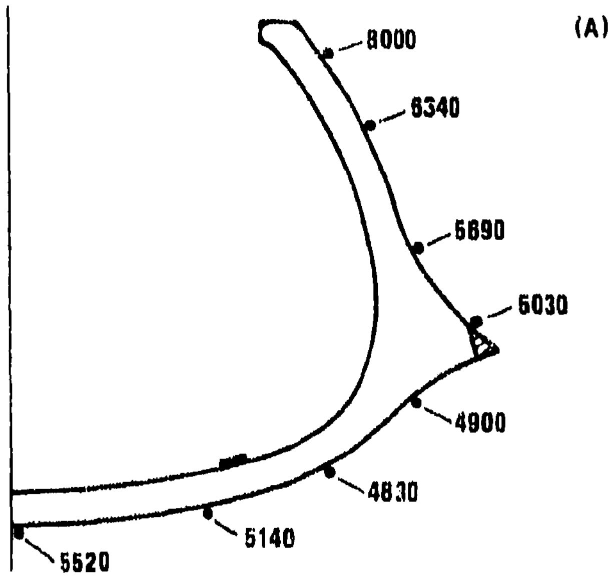

CALCULATED VALUES OF H (and hence J) IN AMPS/m FOR $I = 20$ kAmp

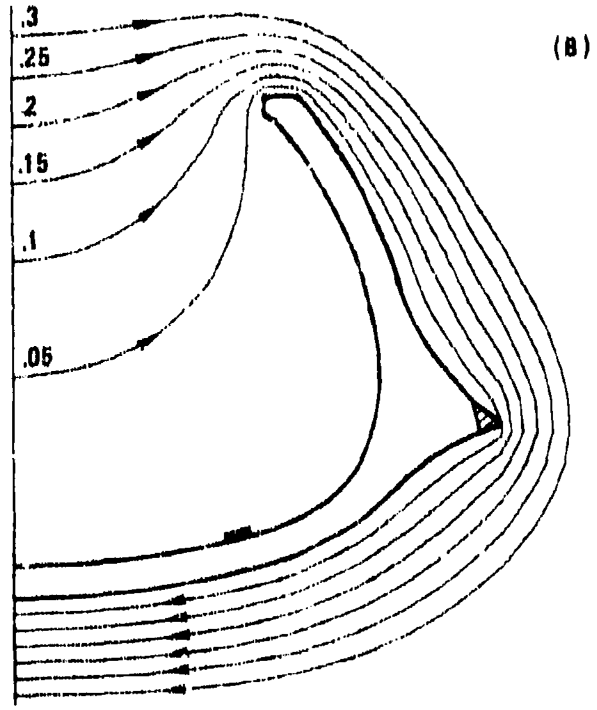

FIELD LINES (Flux Contours) AROUND COCKPIT AT STATION 150

THIS DEMONSTRATES THE INTRUSION OF APERTURE FLUX INTO THE COCKPIT (Geometry is Simplified)

Figure 26 Station 150 - Calculated Flux and H Values

$$M_{TF} = L' \times \frac{\phi_1}{\phi_T} \text{ H/m} \qquad \phi_1 = \text{flux linking loop or circuit}$$

$$= L' \times \frac{\phi_1}{1} \text{ H/m} \qquad \phi_T = \text{total flux between fuselage and return conductors } (\equiv 1 \text{ weber in POTENT technique})$$

in any circuit of arbitrary length, ℓ,

$$V_M = \ell \times \frac{di}{dt} \times L' \times \frac{\phi_1}{1} \quad \text{volts.}$$

Using this method, the calculated voltage for a longitudinal loop, 'Loop 1' in the floor of the cockpit is as follows:

ℓ = 36" = .91m, vertical wire spacing = 1.5" (=3.81cm), height from floor = 2" (=5.08cm). From tabulation ϕ_1= .0124 - .00654 (that is, difference of flux at + 3.5" level and +2" level).

ϕ_T = 1, L' = 0.172 uH/m (see para. 4.2.4), and $\frac{di}{dt}$ = 17.2 kA/us.

$$V_M = 17.2 \times 10^9 \times 0.172 \times 10^{-6} \times .91 \times .00586$$
$$= 15.8\text{V}$$

Loop 2 has the same orientation and dimensions as Loop 1 but is raised to 14.5" from the cockpit floor. By a similar calculation, using the appropriate value of ϕ_1

$$V_M = 27\text{V}$$

Three loops #1, #2, and #3 (shown in Figure 52) were situated along the cockpit side wall. Voltages were also calculated by a similar technique giving 2.7V, 3.0V and 2.9V respectively. All aperture flux within the cockpit is transverse, in simple theory, and hence the predicted voltage in loops which have no loop area orthogonal to the flux direction will be zero. Figure 26(b) shows the direction of the field lines across the cockpit.

6.3 PREDICTED RESULTS AFT BAYS-STATION 227-253

Voltages in both the upper (ammo handling bay) and aft right-hand strake bays are resistive/diffusion voltages only. Therefore, the prediction technique follows that used in the F.E.B.

As in the forward bay an extra potential drop caused by the joint resistances are included since both panels are removable.

6.3.1 IR Voltages in Upper Bay

(See Figure 27(a) for surface field) Calculations were made for the following wire numbers (see Figure 56).

#1	central
#2	7" off center toward right
#3	17" off center toward right

The bay cover panel is 10-ply, and the calculations are made on a 27" length to compare with measurements. J obtained from POTENT was as follows:

	#1	#2	#3	
J	3575	3520	3492	Amps/m
V_R (graphite only)	65	64	62	V
V_J (10 mΩ total joint resistance)	36	35	35	V
V_{TOTAL}	101	99	97	V

6.3.2 Loop Voltages in Upper Bay

Two loops are calculated, corresponding to the measured loops, #1 and #2 of Figure 58. These are 26" long centrally placed, 8" down and 15.5" down respectively from the top graphite panel. The loop calculation assumes that the loop is completed by running wires across to the metal bulkheads and back along the side metal panel as shown in Figure 58. As before, for loop calculations in the F.E.B.,

$$V_R\ (\text{loop}) = V_T \times \frac{\phi_1}{\phi_{\text{Surface}}}$$

ϕ_1 and ϕ_s are obtained from the tabulation from which Figure 27(b) is derived. Figure 27(b) shows the pattern of the diffusing flux.

For loop #1

$$V_R \text{ (loop)} = 120 \times \frac{0.357}{0.474} = 90V$$

For loop #2

$$V_R \text{ (loop)} = 120 \times \frac{0.272}{0.474} = 69V$$

The total measured voltage, metal ring-to-metal ring was used for V_T.

6.3.3 IR Voltages in Aft RH Strake Bay

These IR voltages were calculated as in paragraph 6.1.1 above. The graphite is 6-ply, a 22" (.56m) measuring length is used and the other data is as below:

Circuit	#4	#5	#6 (See Figure 56)	
Distance from Strake Edge	22" (.56m)	15"(.38m)	5½" (0.14m) (and 1½" from strake metal)	
J	2860	2780	3450	Amps/m
V_R	69	67	83	Volts
V_J (10 mΩ total joint resistance)	29	29	35	Volts
V_T	98	96	118	Volts

6.4 COMPARISON OF CALCULATED AND MEASURED DATA

6.4.1 IR Comparisons

Figure 28 shows a comparison between predicted IR voltages in the three areas tested. Agreement is generally very good with some exceptions as discussed below.

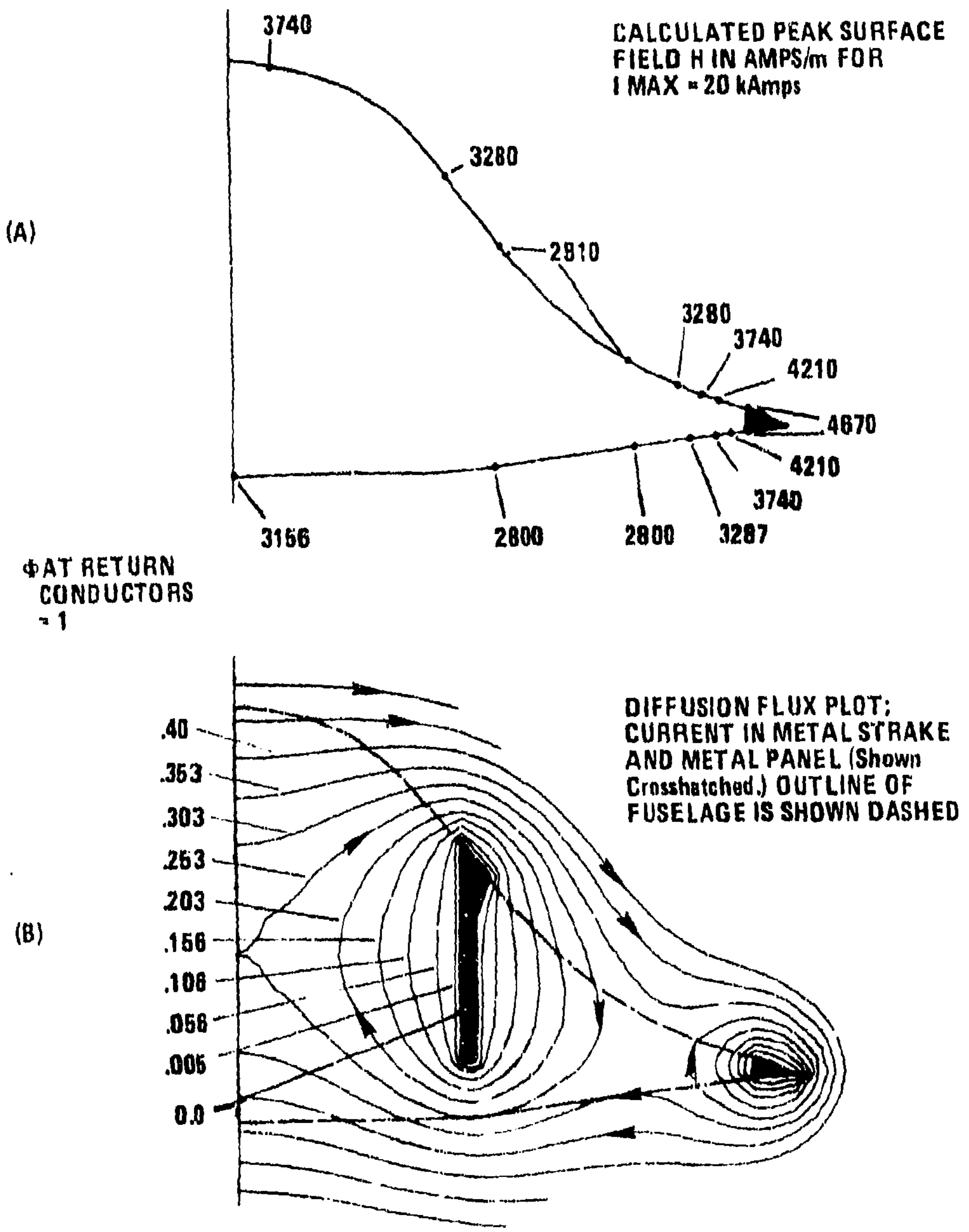

Figure 27 Station 237.5 - Surface H Field and Diffusion Flux Plots Calculated Using Field Mapping Program

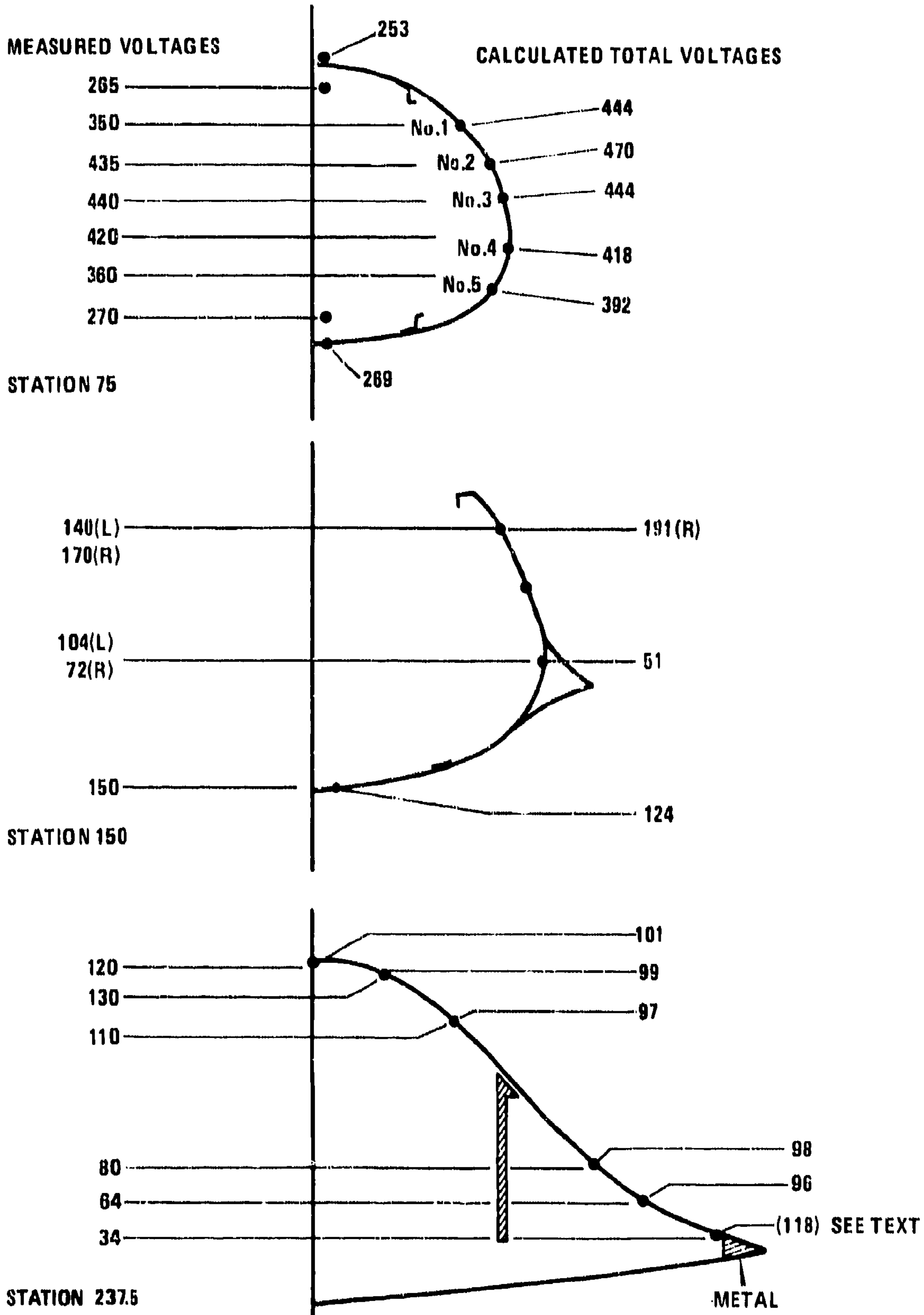

Figure 28 Comparison of Measured and Calculated IR Voltages on Graphite

A. F.E.B.

Consistent agreement was obtained in all values; the predictions are within 10% of measured values. This agreement confirms the choice of low value for ρ_{0° and ρ_{45° for the graphite panels.

B. COCKPIT

Because of the complexity of the cockpit area in terms of ply thickness, strake geometry, etc., the predictions were not expected to be as reliable as in the F.E.B.. The simplest geometry was the cockpit floor where agreement was adequate. At 'waist' level inside, 51V was calculated compared to 104V (L) and 72V (R) measured. This indicates that the strakes do not contribute much to the fuselage conductivity, perhaps because of inadequate electrical bonding (Mechanical bonding strength is not being questioned.) The results are all the more surprising because the thicker strake is on the right side which may have contributed to the lower value there than on the left. The voltages higher up the side, toward the sill, are in somewhat better agreement.

C. AFT EQUIPMENT BAYS

The geometry is simpler here, except for possible influence of the metal boundary on the panel around its entire periphery. On comparison of the voltages shown in Figure 28, the upper bay measured voltages are all higher, and the RH bay voltages lower, than the calculated values. Examination of data and the test system has ruled out many possible sources of error, leaving only variations of J and ρ as likely causes. The most likely cause is the 'end effect' of the test rig, created by the shape of return conductors, the aluminum extension box and the fuselage, which may have tended to increase current centrally at the expense of current in the strakes. Also, the shape of the rear cockpit fairing just in front of the panel may have increased J too. While these arguments are speculative, the data is in qualitative support of such an explanation.

The prediction of 118V at 1½" from the metal strake is in any case not a reasonable prediction since current flow in the metal alongside influences and reduces the graphite current.

A significant effect can be seen in the joint voltages, see Table 8. The sum of the two joint voltages is .3 of the graphite panel voltage for the RH bay, but .62 for the upper bay. These figures give joint resistances of 3.5mΩ and 6mΩ for the side and upper panel joints respectively. This may be accounted for by the presence of metal inserts in the graphite for the screw heads on the side panel.

6.4.2 Diffusion Flux Loop Voltage Comparison

		Loops		Calculated V	Measured V (Figure 28)
A.	F.E.B.	#1	Figure 38	7.75	7
		#2		7.3	6.5
		#3		6.2	5
B.	Aft Bay	#1	Figure 56	90	85
		#2		69	51

These show excellent agreement with predictions.

6.4.3 Aperture Flux Comparison in Cockpit

Loops		Calculated Voltage	Measured Voltage
36" on floor	See Para. 6.2.2	15.8	12
36" raised 14.5"		27	24
#1	Figure 52	2.7	2.4
#2		3.0	2.2
#3		2.9	2.5

These results also show good agreement and indicate that the assumption used in the calculations is justified, that is, the aperture flux in a graphite fuselage cockpit can be predicted as if the fuselage were metal.

6.4.4 General Conclusions

All voltages which were predicted to be generated by resistive/diffusion coupling, includes the measurements in the F.E.B., IR voltages in the cockpit and all the Aft bay circuits did in fact produce voltages generally similar to the current pulse. Diffusion flux generated loop voltages in general lack the extreme L.F. components since they must show a zero crossing and polarity reversal to conserve the total quantity of flux which enters and leaves the loop. However, they show the essential features of the current pulse shape and have an initial rate of rise similar to the current pulse and therefore a similar HF spectrum. This can be seen by comparing the spectrum of a diffusion flux generated voltage on a loop shown in Figure 44 with the current pulse spectrum shown in Figure 5.

Conversely, all the measured aperture flux voltages in the cockpit have the characteristic di/dt wave shape which implies a fast rise to peak voltage at $t = 0+$ and a zero crossing at approximately 3us. Due to the effect of diffusion flux, the zero crossing in Loop 1 test in the cockpit floor occurred early because a diffusion flux induced voltage subtracted from the aperture flux voltage.

SECTION VII

TEST DATA COMPILATION

The composite forward fuselage, Figure 29, was basically divided into three different test areas: forward bay area (stations 60 to 98), cockpit area (stations 98 to 168), and the aft section (stations 168 to 253). The following presentation of data will be sectioned relative to these areas for ease of categorization. Data tables, charts, and typical oscillograms will be given throughout this write-up to describe fuselage response to the lightning current pulse and to illustrate representative waveforms measured during the various test phases. Data will also be correlated between a severe 200kA lightning strike and the 20kA test current pulse.

7.1 DATA EXTRAPOLATION TO 200kAMPS

Reference 1 defines a severe lightning strike as having a 200kA peak amplitude and 100kA/us rate of rise with these values being exceeded only about 0.5 percent of the time. Since aircraft are now being designed to withstand this level of current, test data reported herein will be extrapolated up to that amplitude for comparison. Two basic extrapolations were required for data measurements because of different coupling mechanisms. These extrapolations correspond either to current amplitude, or to current rate of rise, di/dt. Initially, each scaling factor was assumed to be a linear extrapolation from the 20kA-17kA/usec current waveform to a 200kA-100kA/us severe lightning strike and was defined as follows:

$$\text{Current (I) Scaling Factor} = \frac{200\text{kA}}{20\text{kA}} = 10:1$$

$$\text{Current Rate of Rise (di/dt) Scaling Factor} = \frac{100\text{kA/usec}}{17.1\text{kA/usec}} = 5.85:1$$

The scaling factor applicable to particular data was determined by an analysis of the test circuit, expected response, and shape of voltage waveforms measured on the test circuit.

In order to verify applicability of linear extrapolation between different current and di/dt amplitudes, a series of tests was performed at varying generator outputs. The first test of the scaling verification series was relative to a voltage drop

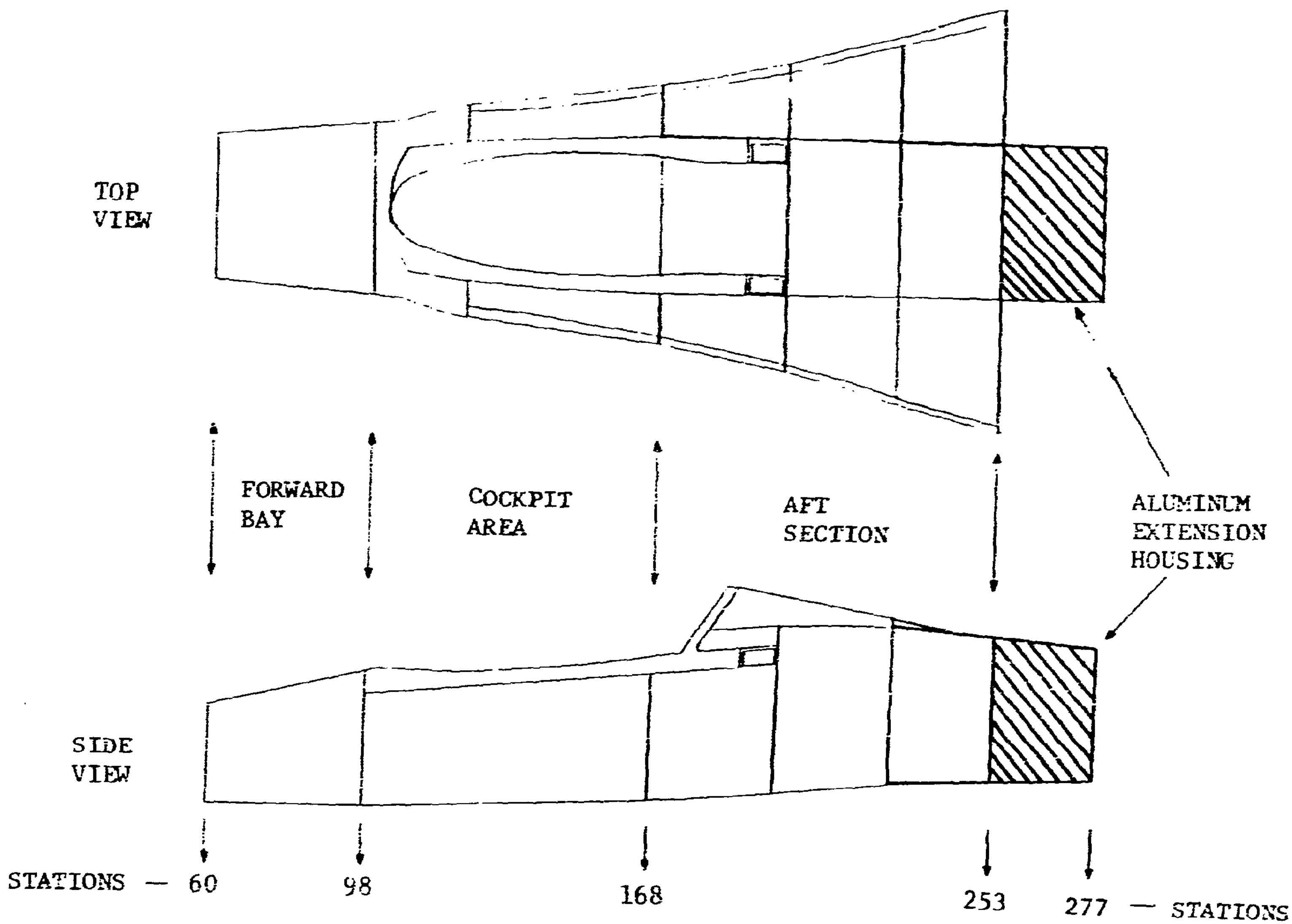

Figure 29 Composite Forward Fuselage and Basic Test Areas

between two points in the fuselage. In the forward bay, measurements were taken between the aft/forward bulkheads at stations 98 and 60. Oscillograms taken during these tests are shown in Figure 30 for input current amplitudes of 20kA and 10kA. The peak voltages show a 2:1 ratio for the corresponding 2:1 peak current change.

Another similar test was performed on the cockpit floor (center line) between stations 130 and 168. This test compared the 20kA unipolar pulse to a damped oscillatory current at 48.7kA peak amplitude or a 2.43:1 current increase. The resultant voltage drop between the two stations at peak values showed a 2.33:1 increase in voltage amplitudes which is in close agreement to the current increase. That the scaling is indeed current scaling is demonstrated by the fact that the measured voltage waveforms correspond in time to the current waveforms. More significantly, the di/dt for the 20kA unipolar and 48.7kA oscillatory was the same. Had the induced voltage been proportional to di/dt, then there would not have been a change in induced levels.

The second of the verification series dealt with di/dt scaling. Due to the physics of coupling, these tests must be performed in an area where the primary coupling mechanism is external flux. The area chosen was in the center of the cockpit. A loop was placed 8 inches above the cockpit floor and the generator was modified to produce high current damped oscillatory waveforms. Figure 31 shows the induced voltages in the loop at three different current levels and three different di/dt's. The peak currents were 31.2kA, 48.6kA, and 72.9kA. The corresponding di/dt's were 8.9kA/us, 13.1kA/us, and 19.4kA/us, respectively.

Since the di/dt changes from pulse-to-pulse at the same rate as I (i.e. amplitude change at a constant frequency), the key to determining whether the induced voltage is proportional to I or di/dt is the initial waveshape. A review of the oscillograms in Figure 31 shows an initial value at t=0+ which follows a di/dt coupled waveform rather than an IR induced voltage where V(0+)=0.

Some anomolies do exist in this data, Figure 31, which must be accounted for in order to validly extrapolate by di/dt ratios. The time from initial turn-on to first zero-crossing should ideally be one-quarter cycle rather than the much shorter time durations observed in the three oscillograms. The apparent shift from a cosine wave to spike at t=0+ is due to an additional diffusion flux component. However, an extrapolation value is based on the ratio of di/dt components at different generator outputs (e.g. ratio of peak values of Figures 31a to time corresponding values of Figure 31b). Since the separate ratios of external or diffusion flux components equal a constant (ratio of current amplitudes),

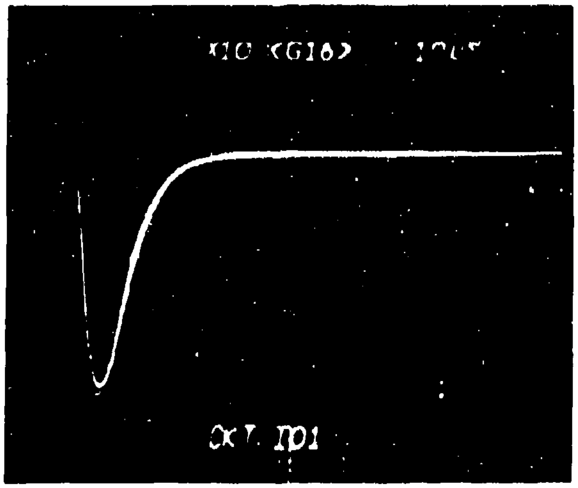

A. IR drop (Sta 98 to 60) measured at a 20kAmp level.

Vertical: 50 Volts/Div.
Horizontal: 10 usec/Div.
(220 volt peak amplitude)

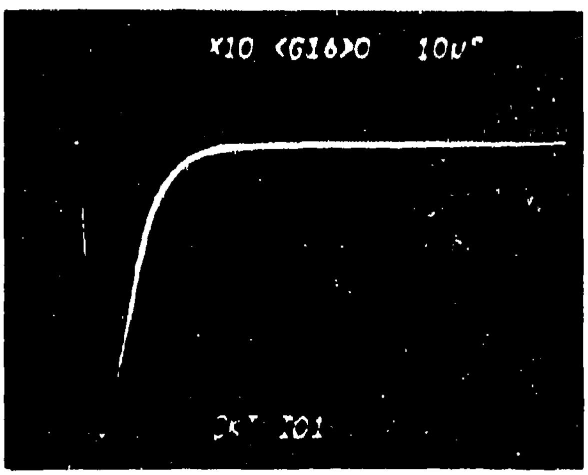

B. IR drop (Sta 98 to 60) measured at a 10 kAmp level.

Vertical: 20 Volts/Div.
Horizontal: 10 usec/Div.
(110 volt peak amplitude)

Figure 30 Linear IR Voltage Waveforms Taken in the Forward Bay at 20 kAmp and 10 kAmp

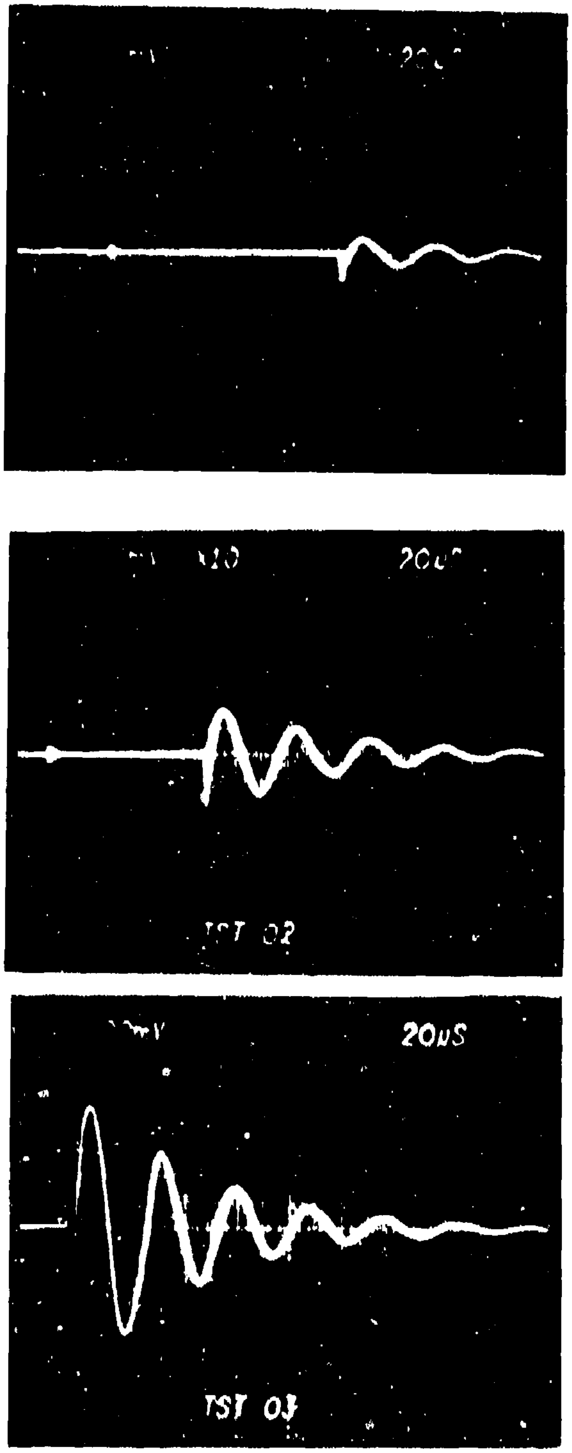

A. Loop voltage measured at a 31.2 kAmp level.

Vertical: 2 Volts/Div.
Horizontal: 20 usec/Div.

B. Loop voltage measured at a 48.6 kAmp level.

Vertical: 1 Volt/Div.
Horizontal: 20 usec/Div.

C. Loop voltage measured at a 72.9 kAmp level.

Vertical: 1 Volt/Div.
Horizontal: 20 usec/Div.

Figure 31 Loop Voltage Variation Measured in the Cockpit at Three Damped Oscillatory Levels.

the ratio of the sum of external plus diffusion flux components yields a simple algebraic relationship equal to the same constant current ratio.

The ratio of peak values between the di/dt waveforms of Figure 31 should thus equal the change in generator output. When comparing 31(a) to 31(b), the voltage ratios from the first six peak amplitudes yield an average value of 1.58:1 which corresponds to the source di/dt ratio of 1.56:1 (also equal to the ratio of current amplitudes for constant frequency or 48.6kA/31.2kA=1.56). The next comparison, six peak values from 31(b) and 31(c), gives a ratio of approximately 2.7:1 while the source di/dt ratio comes to 1.5 (72.9kA/48.6kA).

As can be seen, the linearity of scaling did not hold through the 72.9kA/19.4kA per usec pulse. The induced level is 1.8 times higher (2.7/1.5) than would be predicted from either I or di/dt scaling, thereby indicating some parameter change. It was during this higher current (i.e., 72.9kA) level that arcing was first observed along the joints of the metal canopy interface (the interface is not a continuous piece of metal structure). It is suggested that the non-linear scaling condition is due to the arcing. The arcing in effect creates a lower impedance path in the area around the top of the canopy, and this in turn allows greater current densities to exist near the top of the cockpit area. Additionally, the arcing mechanism may tend to alter local di/dt conditions at the canopy interface.

This test points out an important aspect of scaling, particularly in graphite/metal fuselages. Assumption of linear scaling in areas where arcing can occur may result in errors when extrapolated to high levels.

From the above test data, we feel the cockpit di/dt scaling factor should be 10.5 (5.85 x 1.8) rather than the 5.85 which will be used in fuselage areas other than the cockpit. The effect of this arcing on current amplitude related measurements is not known and we estimate voltage drops between points on the cockpit wall can be either lower or higher than actual data taken at 20kA. However, we will assume the 10:1 extrapolation because of lack of data.

7.2 FORWARD BAY

The forward bay area afforded the best closed area in the fuselage as there exists a minimum number of apertures and no metallic ribs except for the ring members at the front and aft bulkheads (stations 60 and 98). This configuration represented an ideally controllable test area which was approximately cylindrical in shape, closed in all planes or open via small apertures, and comprised of all composite side walls. The aft bulkheads (station 98) was also composite with small apertures located in various positions (cable feed-thru points) while the forward bulkhead (radome interface) was sealed off with aluminum foil in order to provide a completely closed area. By adding or subtracting apertures, open or closed sections, internal racks/equipment, etc., we were able to obtain specific changes in current and flux patterns in the bay. In this manner, we have been able to study the characteristics and responses of a closed composite fuselage section to lightning currents.

7.2.1 Basic Test Data

Two basic test circuits have been used to define primary electromagnetic rules associated with composites. The first of these circuits was a wire loop for measuring magnetic flux penetration into the bay. By varying loop cross-sectional area and orientation relative to the fuselage axes, we obtained field patterns and field strengths that will be applicable to defining exposure levels to internal aircraft equipment and cables. A typical example of this type of experiment can be described in the following test. Magnetic flux coupling by a small aperture situated in the fuselage surface can be illustrated from the experiment performed in Figure 32. An access port (4.5 X 3.25 inches) was located on the left hand side of the forward bay starting at station 92.75. Measurement of the magnetic flux density was made with a single wire loop (3 X 7/8 inches) which was positioned at various depths into the bay. A 50 ohm coaxial cable was used as the instrumentation lead to the oscilloscope where scope polarity is indicated by the (+) and (-) markings on the loop. A typical oscillogram which was taken during these tests is shown in Figure 33 when the loop was at position #3. The voltage waveform is described by Amperes' flux coupling law and is directly portional to the rate-of-change of magnetic flux density normal to the plane the loop bounds. A time integration of the loop voltage, Figure 34, could then be scaled to Webers/square meter by a (1/loop area) factor (see equation 7). Table 2 is a list of peak loop voltages and peak flux densities obtained from the eight loops with the voltage zero-crossover time equal to the time-to-peak of the flux density.

Results show that the external field penetration into the aperture is only predominant at a distance of two inches into the bay or less than one maximum aperture dimension. As we increase distance into the bay, the diffusion flux becomes the greater coupling vector which resulted in the increase in the zero-crossover times shown. From loop #2 to #5, this time varies

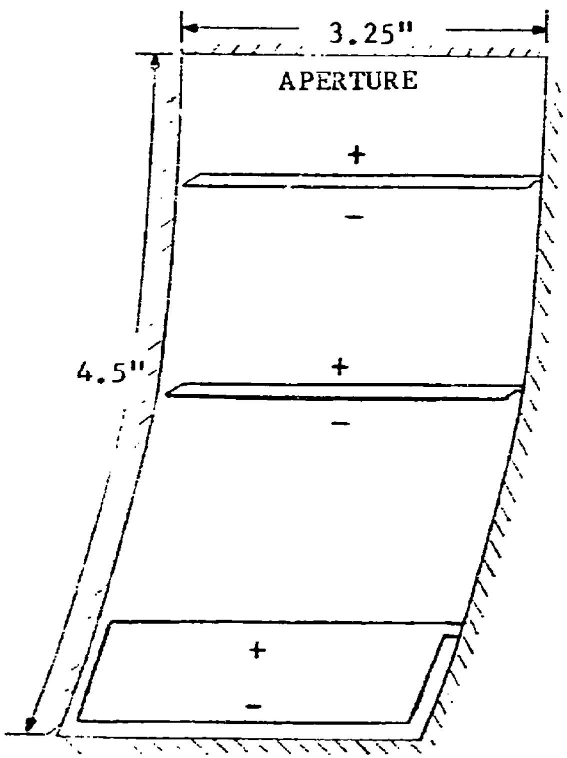

APERTURE - FRONT VIEW

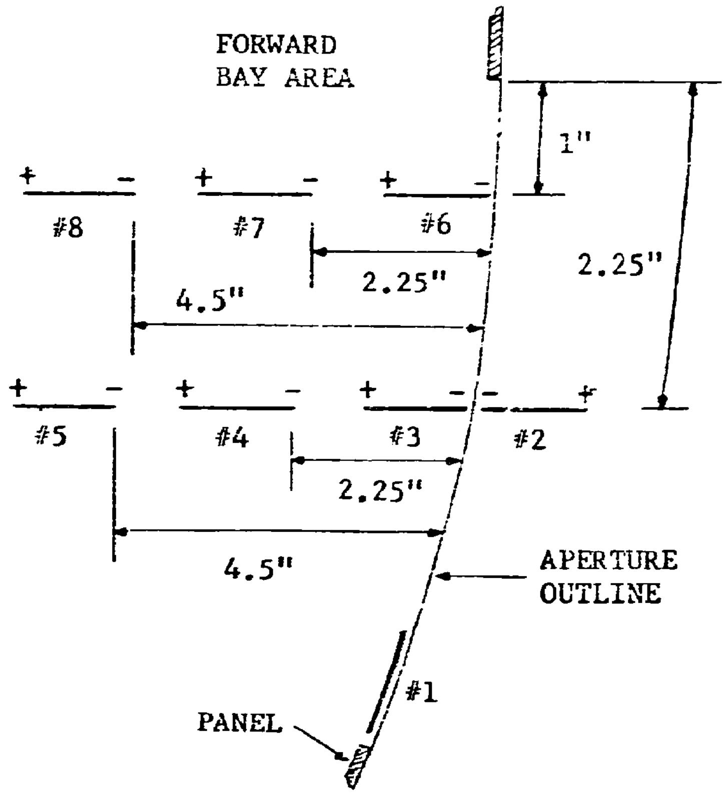

APERTURE - SIDE VIEW

Note: The loop used for this test was 3x7/8 inches. Voltages were measured by the coaxial cable with (+) and (-) marks indicating connection to center conductor and shield, respectively. The cable was terminatd in 50 ohms.

Figure 32 Loop Orientation Relative to Aperture (Forward Bay)

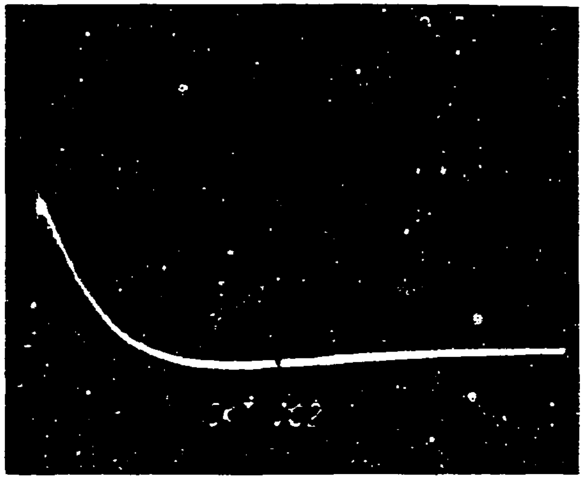

A. Voltage measured across 50Ω at loop position 3.
Vertical: 2 Volts/Div.
Horizontal: 2 usec/Div.

B. Expansion photo of the same waveform in part A.
Vertical: 2 Volts/Div.
Horizontal: 200 nsec/Div.

Figure 33 Typical Oscillogram From Loop Tests in the Forward Bay

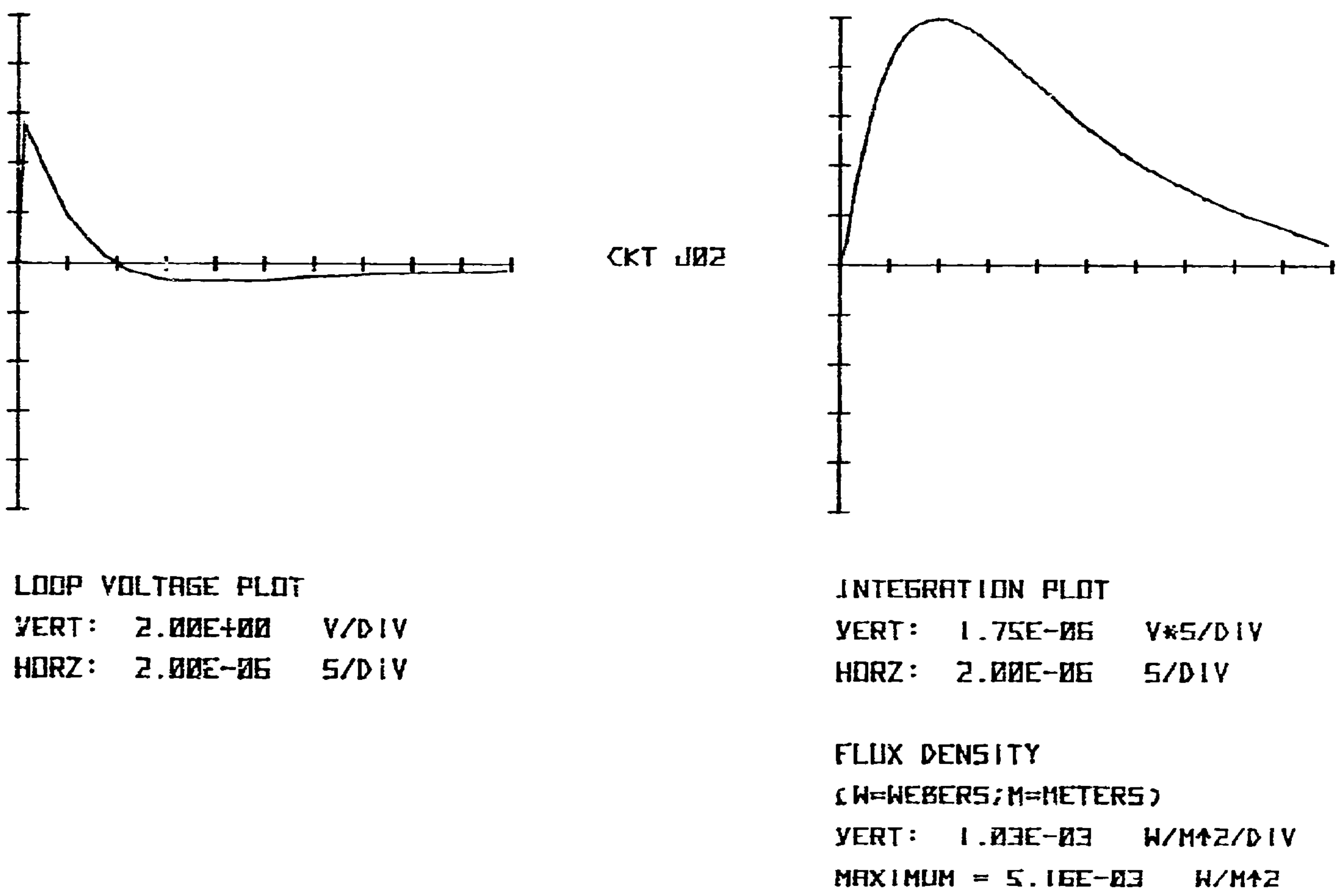

Figure 34 Time Integration of the Loop Voltage Measured in Loop 3

Table 2 DATA FROM LOOP TESTS AROUND THE ACCESS PORT IN THE FORWARD BAY

LOOP NO.	PEAK VOLTAGE (VOLTS)	ZERO CROSSOVER (uSeconds)	PEAK FLUX DENSITY (10^{-3} Webers/m^2)
1	7	-	-
2	8	3.4	5.9
3	6	3.9	5.2
4	1.5	5.8	2.9
5	1.2	6.3	2.6
6	4	4.3	4.1
7	1.2	6.1	2.5
8	1	6.2	2.3

from values close to the current source peak time, 3.2 usec., to diffusion flux peaks at approximately 6 usec. Alternately, when the loop is one maximum aperture dimension inside the structure, there is no external flux coupling to the loop.

A calculation of external flux density at station 94, had the aperture not been there, also yielded a peak flux density of 10.5×10^{-3} W/m and is about twice the density measured on loop #2. This phenomenon is a basic property of small apertures in metal structures where the flux density in the opening can be approximated by one-half the density without the aperture. This rule of thumb can also be applied to composites with values only being slightly smaller because diffusion flux addition is not accounted for. However, this error will be small as shown by the previous data.

The second basic test circuit measured IR drops across different sections of the forward bay. The test technique was to connect the RG-22 instrumentation to different points along the fuselage and measure the differential voltage developed across two 50 ohm resistors in a 10:1 divider. Because these tests were constructed for measurements of IR drops, care was taken to assure that wire routing would not produce loops which could couple spurious flux.

One area of major emphasis in taking IR data was determination of the effects of metal straps in reducing voltage potentials between two points. An example of this type of test is illustrated in Figure 35. The IR drop was measured between stations 60 and 98 with the potential sense wire to station 60 routed on the lower left flange (longeron) which is constructed of twenty-two ply composite and interfaces with the side access doors. The wire was routed on the flange in order to eliminate flux coupling and was returned to the scope along with the potential sense wire at station 98 on the RG-22 setup (with 10:1 divider). Four different tests, A, B, C and D, were conducted with a varying number of aluminum straps (flashings) which were run between stations 60 and 98. Table 3 lists peak voltages and typical voltage waveforms are shown in Figures 36 and 37.

Results show that a potential of 220 volts peak, Test D, was developed with no flashings but a 45% drop to 120 volts, Test C, was achieved by having one flashing routed between the two tie-down points. Tests A and B show that the major percentage drop achieved in Test C was not improved upon significantly (approximately 9% more drop) by having the flashings installed in

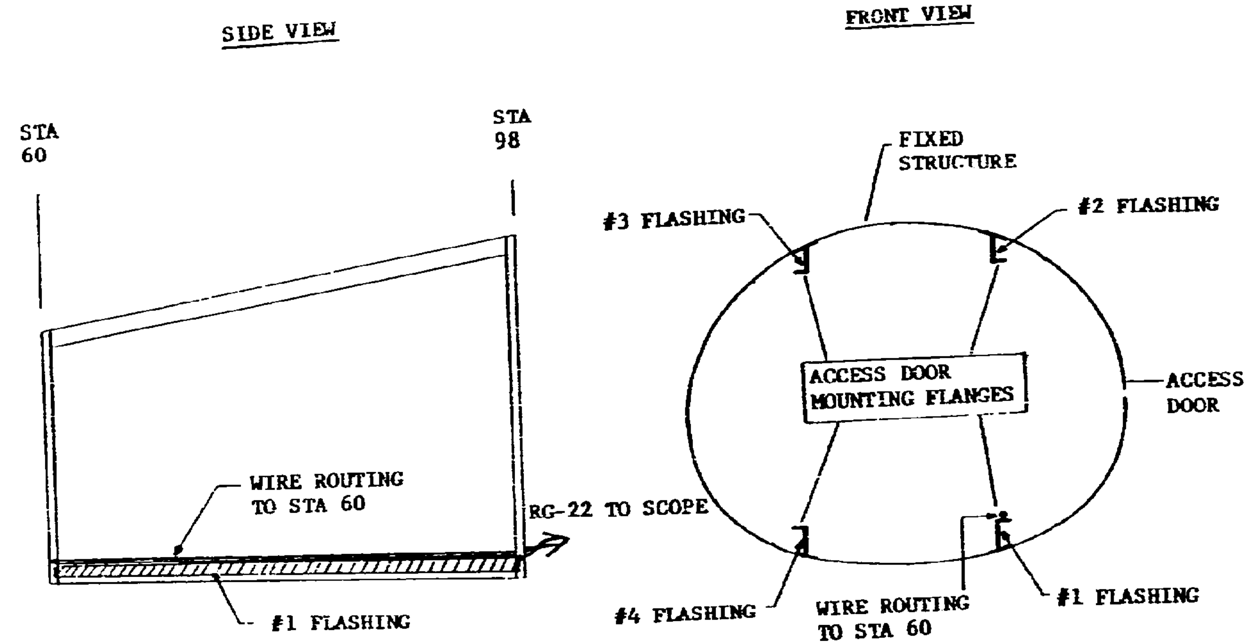

TEST A: All flashings installed.
TEST B: #1 flashing removed.
TEST C: #2,3,4 flashings removed.
TEST D: All flashings removed.

Note: Flashings are 25 mil thick/1 inch wide/38 inch long aluminum strips

Figure 35 Test Setup in The Forward Bay for Taking Voltage Drops With/Without Metal Flashings

Table 3 VOLTAGE MEASUREMENTS IN THE FORWARD BAY WITH/WITHOUT METAL FLASHINGS

TEST	INSTALLED FLASHINGS #1	#2	#3	#4	MEASURED POINTS STA to STA	PEAK VOLTAGE (Volts)	EXTRAPOLATION @ 200 kAmps (Volts)	COMMENTS
A	Al	Al	Al	Al	60-98	112	1120	Al Flashing installed with plain screws.
A	Al	Al	Al	Al	60-253	308	3080	Al Flashing installed with plain screws.
A	Al	Al	Al	Al	60-98	98	980	Al Flashing #1 installed with taper pins.
A	½Al	Al	Al	Al	60-98	162	1620	Al Flashing #1 only a half strip (sta 77-98).
B	-	Al	Al	Al	60-98	211	2110	
C	Al	-	-	-	60-98	120	1200	
C	Al	-	-	-	98-253	250	2500	
D	-	-	-	-	60-98	220	2200	
D	-	-	-	-	98-253	242	2420	
D	-	-	-	-	60-98	110	1100	10 kAmp current source.
D	-	-	-	-	98-253	123	1230	10 kAmp current source.
E	Ti	-	-	-	60-98	188	1880	Titanium Flashing.
E	Ti	-	-	-	98-253	282	2820	Titanium Flashing.

1. Measurements taken at 20 kAmp unless specified.
2. Flashings are 25 mil thick/1 inch wide/38 inch long strips.
   Equivalent Resistance: Aluminum (Al) = 1.6 milli-ohms.
   Titanium (Ti) = 30 milli-ohms.

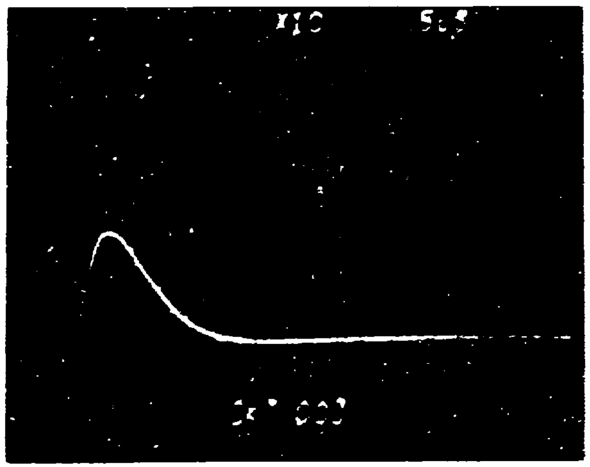

A. Differential voltage between station 60 (+) to 98 (-).
   a. 4 Al Flashings installed.
   Vertical: 50 Volts/Div.
   Horizontal: 5 usec/Div.

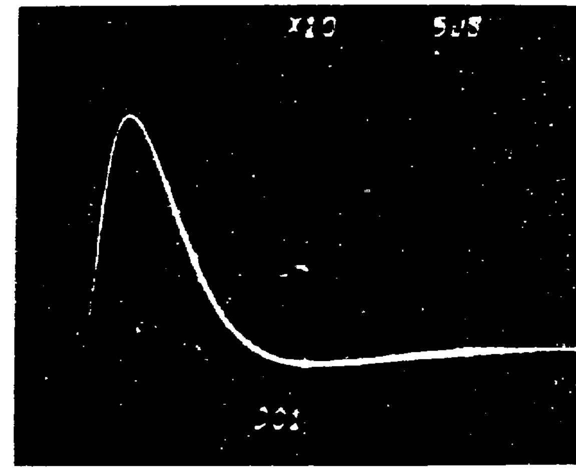

B. Differential voltage between station 60 (+) to 98 (-).
   a. 3 Al Flashings installed.
   b. #1 Al Flashing removed.
   Vertical: 50 Volts/Div.
   Horizontal: 5 usec/Div.

Figure 36 Oscillograms From IR Tests (A,B) in the Forward Bay

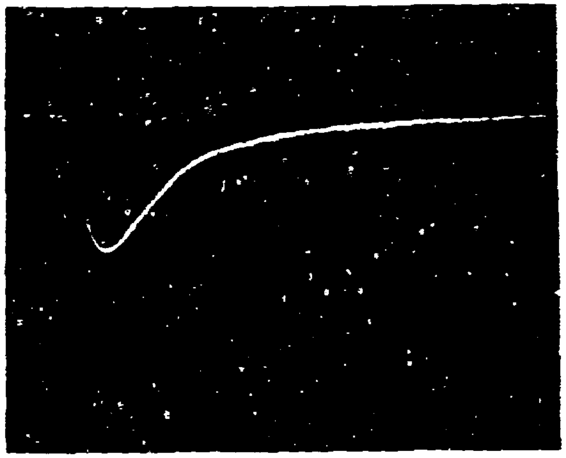

C. Differential voltage between station 98 (+) to 60 (-).
   a. 3 Al Flashings removed.
   b. #1 Al Flashing installed.
   Vertical: 50 Volts/Div.
   Horizontal: 5 usec/Div.

D. Differential voltage between station 98 (+) to 60 (-).
   a. All Al Flashings removed.
   Vertical: 50 Volts/Div.
   Horizontal: 10 usec/Div.

Figure 37 Oscillograms From IR Tests (C,D) in the Forward Bay positions 2, 3 and 4. Tests of this nature were conducted to determine IR reductions from metallic straps in different positions along the fuselage or wire routes between equipment in order to obtain overall guidelines for protection against IR drops that would affect aircraft avionic performance.

Another similar test involved the effects of metal straps on both IR drops and flux density along the right access panel, as illustrated in Figure 38. The entire forward bay was cleared of unwanted wires and equipment racks to eliminate current paths other than the composite structure. Voltage drop measurements were made between stations 60 and 98 at five different points (wire numbers 1-5). In the test setup, holes were drilled through the fiberglass ribs along the panel such that wires could be routed to station 60 with no unwanted loops which would have otherwise coupled spurious flux. Reference points for the IR measurement were the two metal ring members at stations 60 and 98 with the station 98 reference being a single point at the wire #3 position. Three 2 X 4 inch loops (one after the other) were also installed perpendicular to the panel with the first loop being 1.25 inches from the wall and center opposite to IR wire #3. When metal straps were installed between stations 60 and 98, they were tied to the metal ring members, routed along IR wire #3 and placed through drilled slots in the fiberglass ribs similar to the IR wire routing. All flux and IR measurements were made with the RG-22 cable instrumentation setup.

A typical oscillogram from the IR measurements is shown in Figure 39. This voltage was measured along wire position #3 and was taken when no straps were installed along the panel.

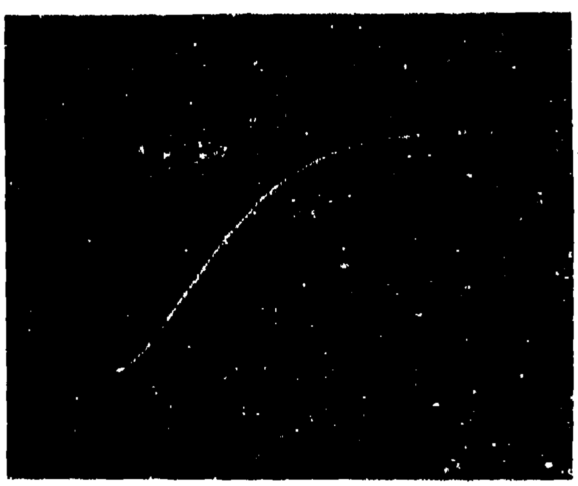

Voltage Drop Between Sta 98 to Sta 60.
Vertical: 100V/Div.
Horizontal: 2 usec/Div.
(Peak Amplitude = 438 Volts)

Figure 39 Voltage Drop Along Wire Position #3

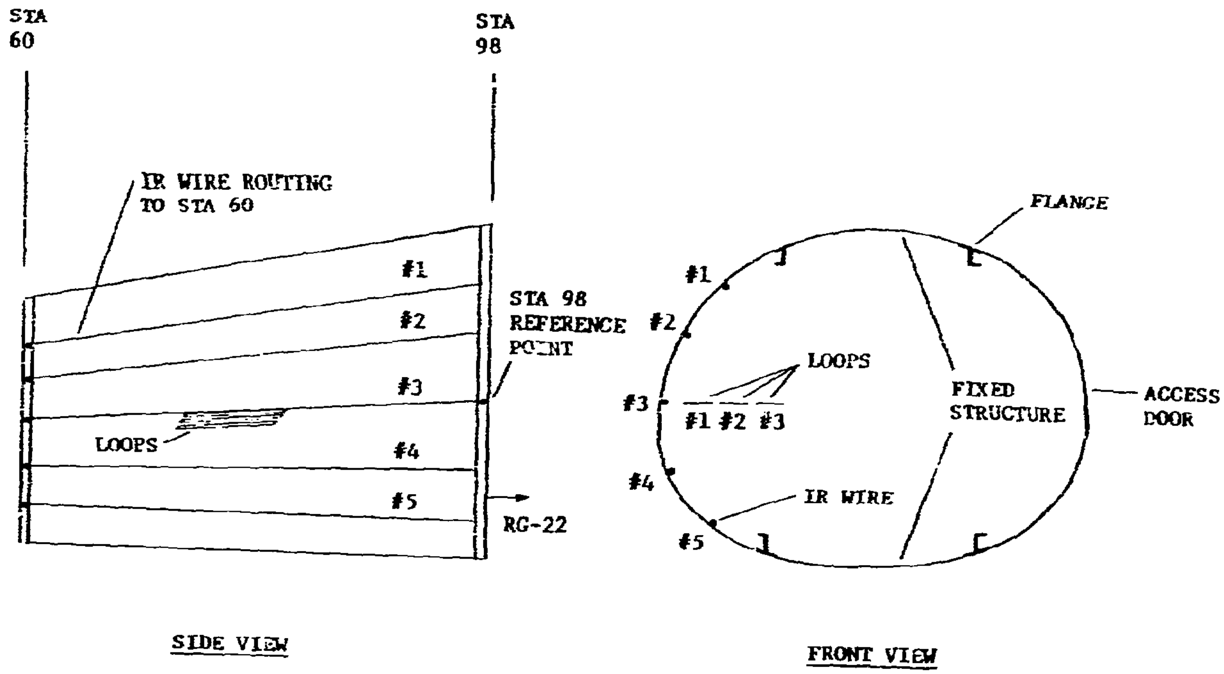

The grounding straps were routed along IR wire #3 between STA 60 and 98.

Figure 38 Test Setup on the Forward Bay Right Access Panel

Figure 40 is a compilation of the peak voltage drops along all wire positions with and without grounding straps. Table 4 is a list of the types of metal straps used during these measurements and defines the appropriate point markers used in Figure 40. (Note that the dashed lines in the figure are an approximation of what we felt the voltage drops would look like

TABLE 4: METAL STRAPS/RESISTANCE AND SYMBOLS FOR GRAPHS

SYMBOL	METAL STRAP SIZE	RESISTANCE (Milli-Ohms)
○	No Strap	N/A
△	38" x 24 AWG Wire	85
×	38" x 1" x .6 MIL Strip	65
⬡	38" x 1" x 25 MIL Strip	1.6
◇	38" x 2" x 25 MIL Strip	0.8

as one approached position 3 from wire routes 2 and 4, respectively.)

Results show that the voltage drop along wire position #3 dropped from the 400 volt level to the 50 volt range (an 88% drop) with aluminum straps installed in that position. However, the voltages measured at the other positions (1, 2, 4, 5) were only slightly affected by the straps. The average circumferential distance between reference points at station 60 was approximately 3 inches which illustrates the fact that substantial drops in peak voltages between two points is obtained only with a strap tied between those two points. This fact is also in coincidence with the previously described experiment where the IR drop across flange #1 was only affected by a metal flashing at that position.

The effect of the straps on magnetic flux density was determined from voltages measured across the three loops in Figure 38. Peak magnetic flux densities were obtained by time integrations of the loop voltages in accordance with Amperes' Law. The basic conversion equation was

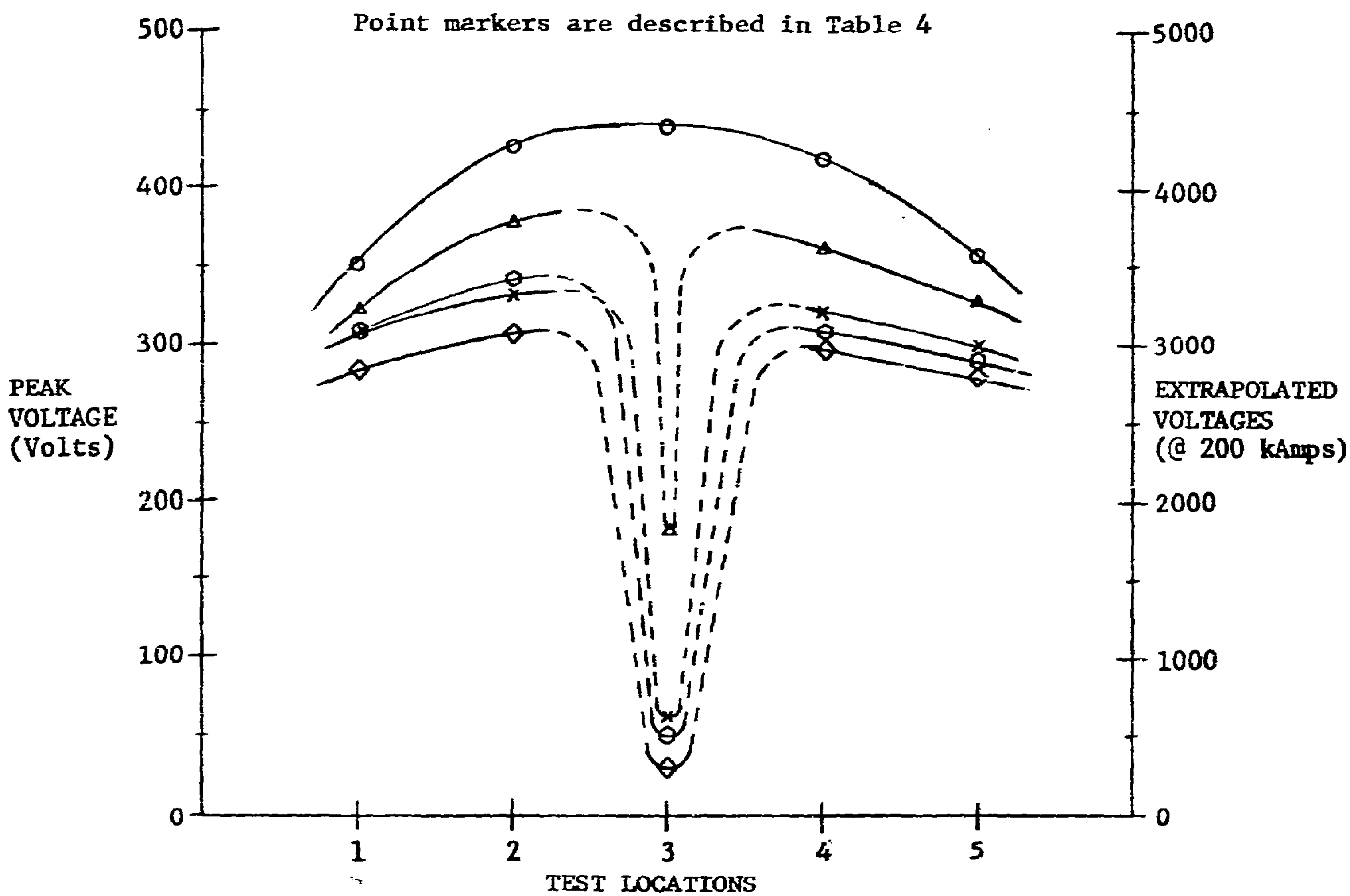

Figure 40 Plot of Voltage Drops Across the Right Access Panel in the Forward Bay

$$|B| = \frac{1}{A}\int_0^T V dt$$

where, $|B|$ = Magnetic flux density (W/m^2) (7)

A = Loop area

Figure 41 is a plot of peak flux densities from all three loops and Figures 42 and 43 are oscillograms of loop #1 voltages which shows waveshape variation for all test setups. Figure 42A is the diffusion flux into the forward bay and is the same waveshape measured from loops #2 and #3 except for decreasing amplitudes (i.e., loop #3 has a peak value of 5 volts). The result of adding metal straps along the wire #3 position was to introduce a lower resistance path in the right access door. This alters current distribution in that area and consequently changes the diffusion flux pattern as detected by the loops. By injecting a higher current down a strap, the resultant flux vector and thus loop voltage reverses direction from voltage A (Figure 42A) to that of voltages C, D and E. By adding a 24 AWG wire which has a higher resistance than the metal straps, the current down the wire is smaller such that we observe an intermediate offset (Figure 42B). The voltages are due to usual diffusion flux and an oppositely directed flux vector from the wire which subtracts from each other to yield a voltage B waveform. This can be seen by a voltage C type wave plus a voltage A wave. As we moved away from the straps to loops #2 and #3, the magnitude of the flux from current in the straps decreases by an inverse distance factor. This effect resulted in waveforms between voltage B and C with loop #2 following voltage B to a greater extent than loop #3.

A Fourier transform plot was made of the loop #1 voltage (Figure 42A) and is shown in Figure 44. This plot was obtained by a computer digitization of the waveshape and performing a Fourier integration from these points. It should be noted that variations in the high frequency region of the plot were a result of the digitizer limitations. The straight line drawn through that region is an approximation of what the plot should look like had the digitizer been more accurate (i.e., point readout was limited to $\pm$.01 inches on the oscillogram). The important fact of this plot is that it essentially follows the frequency spectrum of the current waveform, Figure 5, except for a deficiency of low frequency components. This data was treated in more detail in Section 6.

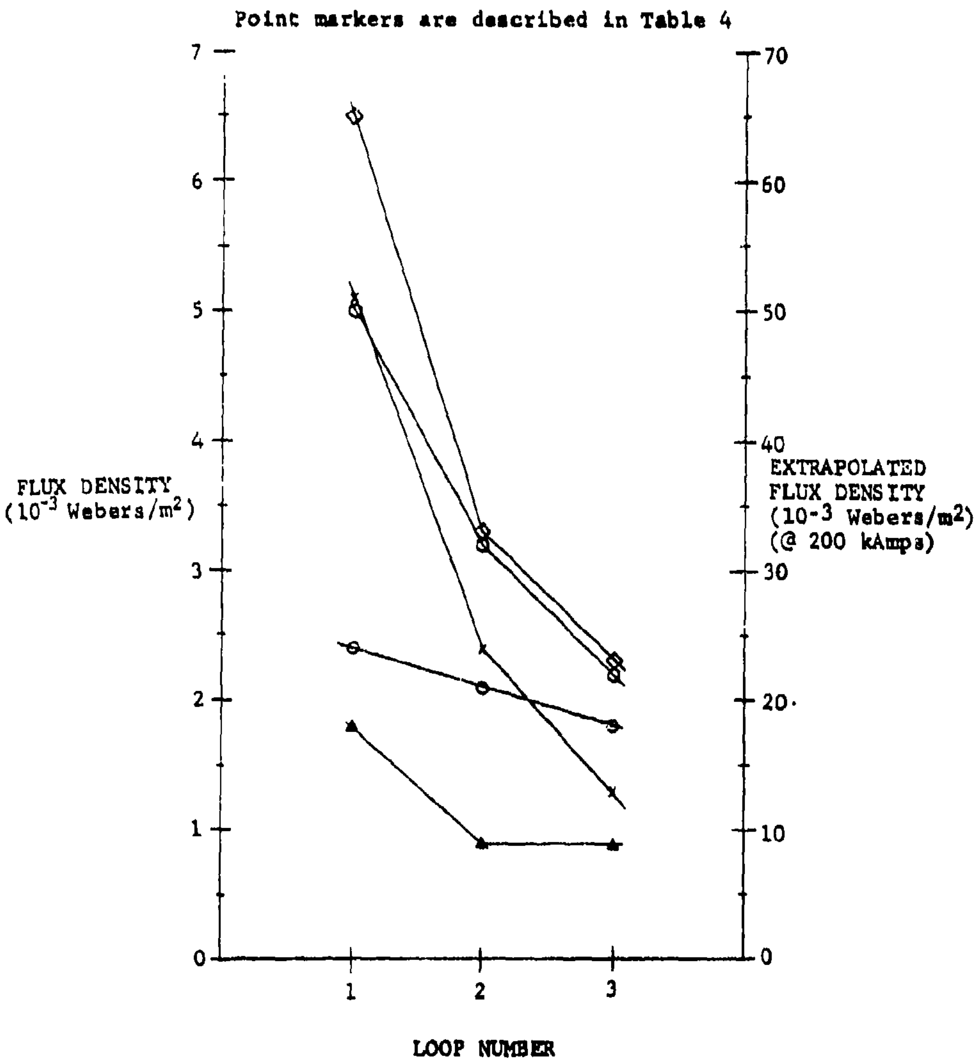

Figure 41 Flux Density Calculations From Three (2 x 4 inch) Loops in the Forward Bay

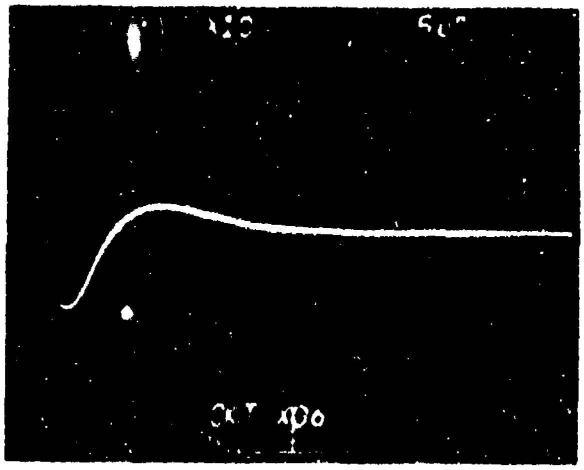

A. Loop voltage with no metal straps.
Vertical: 5 Volts/Div.
Horizontal: 5 usec/Div.

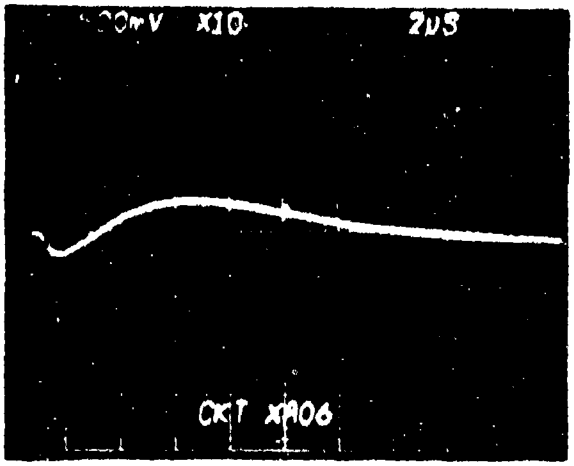

B. Loop voltage with 24 AWG wire.
Vertical: 5 Volts/Div.
Horizontal: 2 usec/Div.

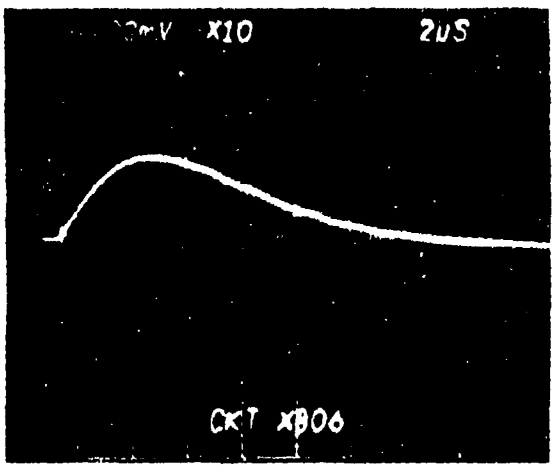

C. Loop voltage with 25 mil/1" wide Al strap.
Vertical: 5 Volts/Div.
Horizontal: 2 usec/Div.

Figure 42 Loop #1 Voltage Measurements Taken Along the Forward Bay Right Panel

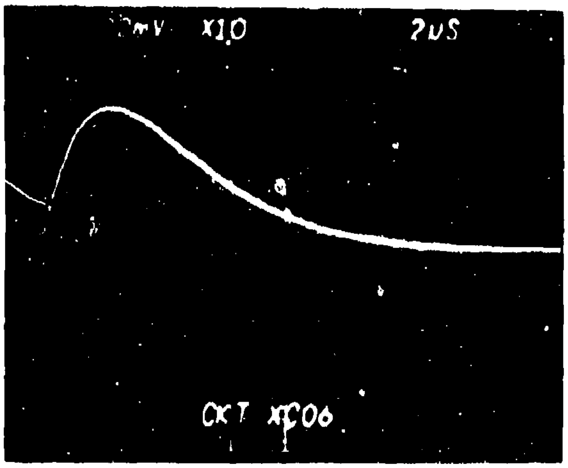

D. Loop voltage with
25 mil/2" wide Al strip.
Vertical: 5 Volts/Div.
Horizontal: 2 usec/Div.

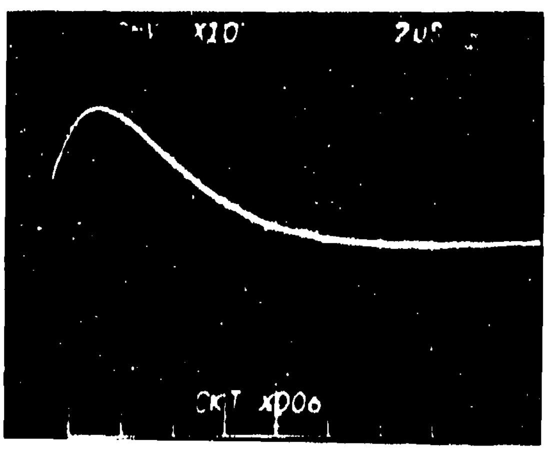

E. Loop voltage with
0.6 mil/1" wide Al strip.
Vertical: 5 Volts/Div.
Horizontal: 2 usec/Div.

Figure 43 Loop #1 Voltage Measurements Taken Along the Forward Bay Right Panel

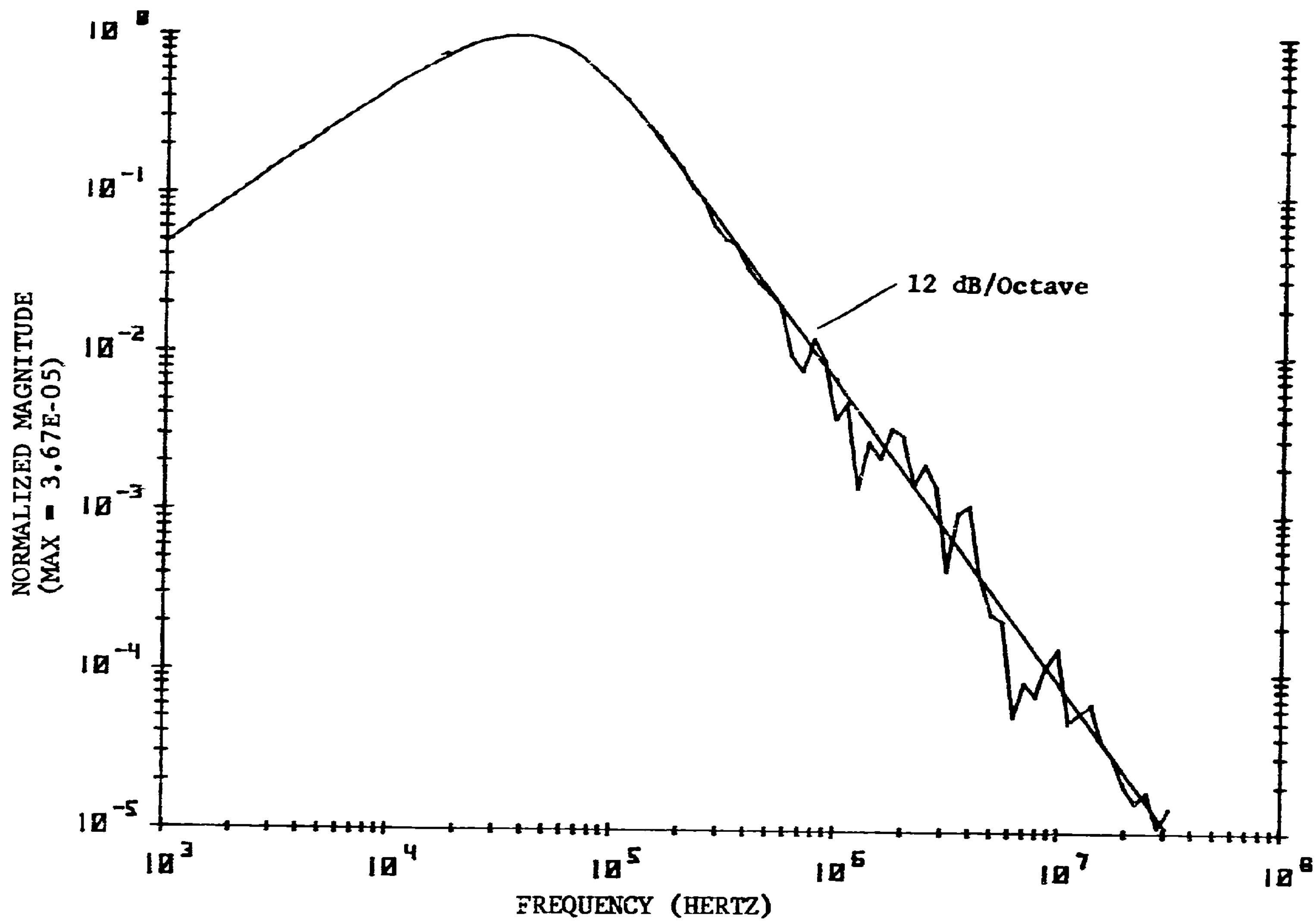

Figure 44 Fourier Transform Plot of Loop #1 Voltage Waveform

7.2.2 Special Tests

Final testing in the forward bay centered around the induced effects on coaxial cables and twisted pair transmission lines. Tests were designed to study coupling mechanisms and relative amplitudes in the low and high frequency ranges. When high frequency components were detected, a fiber optic instrumentation link was used in order to read low signal levels in the presence of high common-mode signals. It should be noted that extensive testing was not accomplished in all areas because of test time limitations. However, those tests which were performed in the forward bay were specially selected to provide general information concerning equipment interfaces. Coaxial cable data will be presented first with twisted pair testing immediately following.

7.2.2.1 Coaxial Cable Test Data

A comparative study was performed between an unshielded single wire and a coaxial cable (type RG-58) as shown in Figure 45. Table 5 is a list of data obtained from those tests and is subdivided between shielded/unshielded circuits and different load terminations, R_L. Peak voltages which were measured across the instrumentation load, R_D, are provided in terms of equivalent current at the instrumentation input (i.e., V_O/R_D). Cable/wire routing was directly atop the bottom left flange (composite) except for Tests 11 through 13. Ground points for shield and load terminations were the metal ring members at stations 60 and 98. Shields were grounded at both ends unless specified.

Tests 1 through 6 provided a basic insight into the different coupling mechanisms which result from the flux and current patterns in the forward bay. When we were dealing with an unshielded wire having forward and aft loading, there existed three forms of coupling in the line. The first of these was an injected diffusion current, IR, at station 60 which resulted from the simple parallel combination of resistance; i.e., the line load ($R_L + R_D$) in parallel with the composite flange resistance (R_C). By varying the line load, we changed the amount of line current by an $R_C/(R_C + R_L + R_D)$ factor or $\simeq R_C/(R_L + R_D)$ knowing that $R_C << (R_L + R_D)$. (It should be noted that this resistance ratio is on the order of 10^{-4} such that any current drawn into the line would have a negligible effect on current in the flange.)

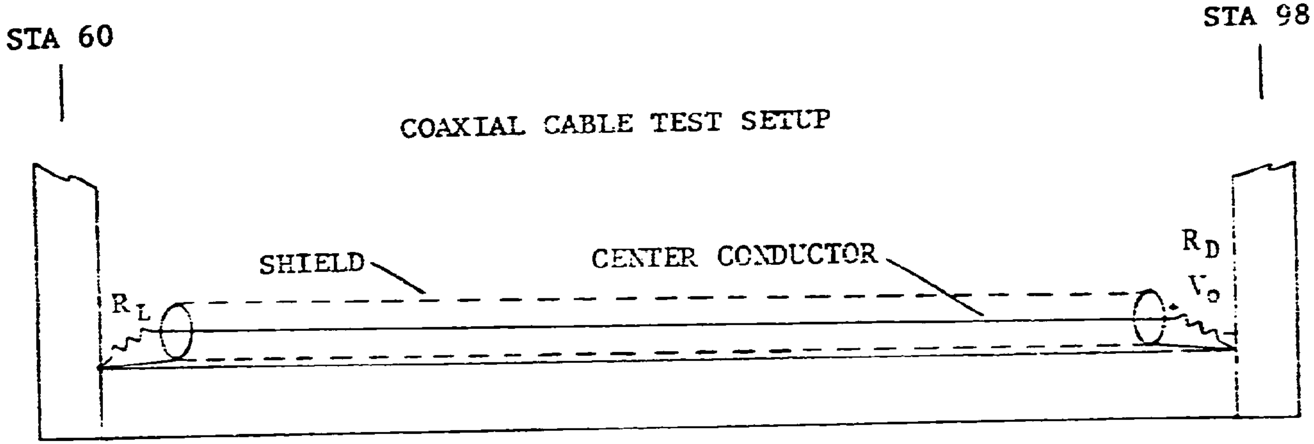

R_L = 0,100,10K,OPEN (OHMS)
R_D = EQUIVALENT DIAGNOSTIC LOAD
V_o = MEASURED VOLTAGE DROP ACROSS R_D

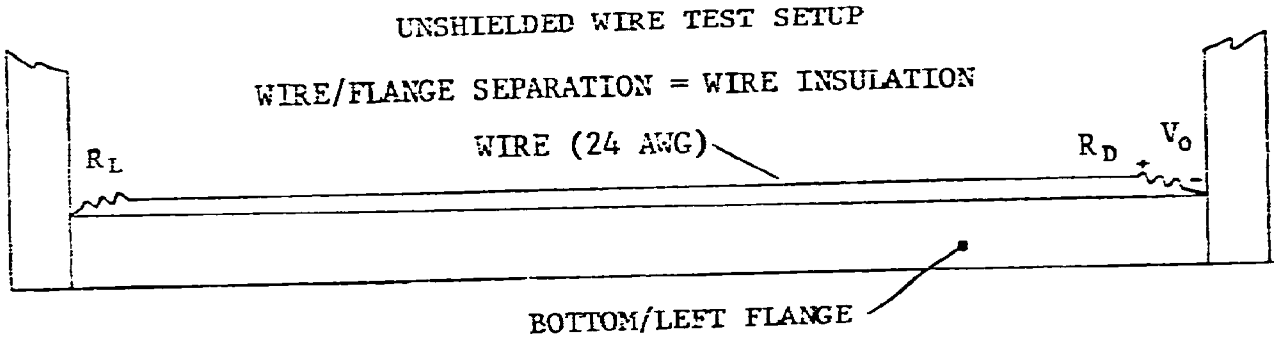

Figure 45 Coaxial Cable Test Setup in the Forward Bay

Table 5: Data From Coaxial Cable Tests In The Forward Bay

TEST NO.	LOAD RESISTOR (Ω)		COAX SHIELD		PEAK LINE CURRENT *				MISCELLANEOUS
					CURRENT (mA)		TIME (us)		
	R_L	R_D	YES	NO	20kA	200kA	PEAK	50%	
1	0	50		X	4.1K	41K	4.0	9	
2	100	97		X	649	6490	4.5	10	
3	10K	84.6		X	9.9	99	5.0	12	
4	0	50	X		300	3000	~6	--	
5	100	97	X		88	880	5.5	13.0	
6	10K	33.3	X		5.5	55	4.5	10.5	
7	OPEN	1100		X	1.7	17	0.8	--	dV/dt waveform
8	OPEN	100		X	1.7	17	0.8	--	dV/dt waveform
9	OPEN	100	X		NEGL	NEGL	--	--	
10	OPEN	100	X		0.3	3	0.8	--	Shield open at forward end.
11	0	95		X	2.9K	29K	3.2	10	Cable rerouted to center.
12	0	95	X		242	2.4K	5.3	28	
13	0	95	X		2.9K	29K	3.2	9.7	Shield open at aft end.

* Equivalent current thru the diagnostic load, R_D.

1. Groundpoints for shield and load termination were the metal ring members at stations 60 and 98.
2. Shields were grounded at both ends unless specified.
3. Measured peak currents given for a 20kA and 200kA source current (i.e. 10:1 scaling factor.)

The second item was diffusion flux coupling through the loop formed between the line and flange surface. The flux coupled current in the line should be constant assuming constant loop area; however, the emf measured across R_D will be a fraction of the total loop emf by $R_D/(R_D + R_L)$. The final coupling mechanism is with respect to the distributed capacitance between the line and flange. The load resistor, R_L, plays an important role in this effect such that the degree of capacitive coupling will depend on its value. The resistance can shunt out the capacitance ($R_L = 0$) or increase upward until an open circuit is approached, yielding a maximum capacitive admittance. The voltage source as seen by this distributed capacitance will be the IR voltage down the flange. The following test results will illustrate these overall effects.

Coaxial cable results of Tests 4, 5 and 6 will be presented first since diffusion flux coupling to the center line is shielded out by the cable shield. In Test 4, the shorted load, $R_L = 0$, in essence, shunted out the capacitive effect on the line. The measured voltage across the instrumentation load, 15 volts peak, is thus an accurate measure of the voltage drop between stations 60 and 98 at the flange. When the flange is paralleled with the coax shield, the addition of the low resistance cable shield shows a similar effect, as seen in previous tests, when metal strips were installed between two points.

When resistance, R_L, was added to the line, Tests 5 and 6, we start introducing line capacitance. Because the resistive voltage drop between stations 60 and 98 was only 15 volts, the difference in capacitance effects with the 100 ohm and 10 k-ohm loading should be small. We can thus assume that any current component through R_D as a result of distributed capacitance is a constant. Equations describing the voltage drop, V_0, across R_D at 6 useconds are as follows:

$$97\,(I_{R1} + I_C) = 8.15 \text{ volts} \tag{8}$$

$$33.3\,(I_{R2} + I_C) = 0.175 \text{ volts} \tag{9}$$

$$I_{R1}/I_{R2} = 10033.3/197 \text{ volts} \tag{10}$$

where, I_C = Capacitive Component in R_D

I_R = Line Resistance Component

$(R_L + R_D) >>$ Shield Resistance

Solving these equations for I_C yields:

$$I_C = 3.7 \quad mA$$

$$I_{R1} = 80.3 \quad mA$$

$$I_{R2} = 1.56 \quad mA$$

or

$$V_R = I_R(R_L + R_D)$$

$$= 15.8 \text{ volts} \quad (197\Omega)$$

$$= 15.6 \text{ volts} \quad (10033.3\Omega)$$

These values, V_R, are the equivalent drops across the line minus the capacitive voltage across R_D. We thus see that these values are in close agreement with the 15 volts in Test 4 at 6 us and, assuming a constant I_C in R_D is a good approximation. Figure 46 shows a typical voltage waveform which was measured during Test 5. Note that the scale for 46 MHz was at 86.6 V/Div. or x4 which is due to the fiber optic loss in that frequency range (50 MHz). The expanded photo shows little or no 46 MHz component except for the fiber optic receiver noise which is barely detectable. At the low frequency voltage levels that were measured, HF levels were so much lower we cannot accurately make any statement from this data.

When a single wire (unshielded) was tested, tests 1, 2 and 3, all three coupling mechanisms come into play with diffusion flux being the extra component from the shielded case. However, we are now dealing with IR voltages down the flange which are in the 100 to 200 volt range. These amplitudes mean that we can no longer assume a constant capacitive effect on R_D and, therefore, end up with more variables than equations. At any single time in a voltage plot, our basic equation for V_0 becomes:

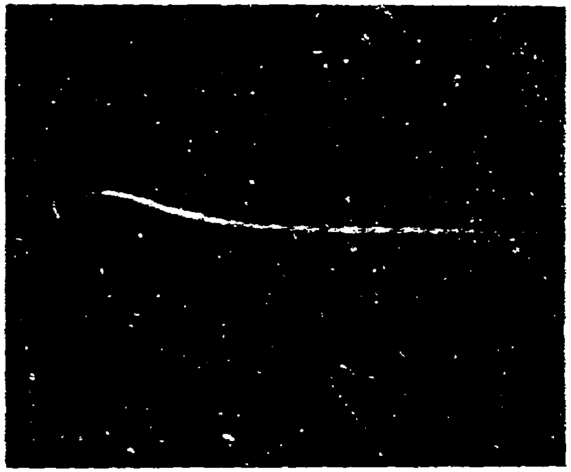

A. Voltage across R_D (97 Ω).
Vertical: 10.86 Volts/Div.
Horizontal: 5 usec/Div.

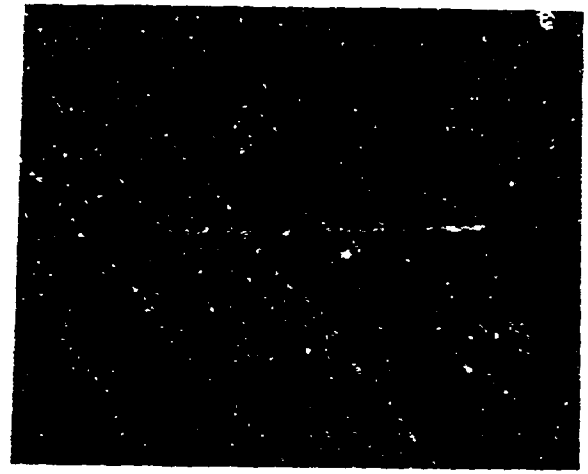

B. Expanded picture of left photograph (A).
Vertical: 21.72 Volts/Div.
Horizontal: 200 nsec/Div.
(46 MHz component scaled at 86.9 Volts/Div.)

Figure 46 Test 5 Coaxial Cable (Shielded) Voltage in the Forward Bay (Fiber Optic Instrumentation)

$$V_o = R_D I_R + \frac{R_D}{(R_D + R_L)} V_{emf} + R_D I_C$$

The only variable which we can assume constant is the total loop voltage, V_{emf}, for constant loop areas. Figure 47 is the voltage measured across R_D during test 2. We again see in this photo that HF components are much lower than LF components.

In order to observe capacitive and HF effects more clearly, we performed tests 7 thru 10 with an open circuit at station 60. As expected, the distributed capacitance results in a dV/dt waveshape due to the IR drop down the flange. Figure 48 is the voltage measured across a 50Ω resistor in the fiber optic transmitter line (another 50Ω resistor in series with this resistor yielded $R_D = 100\Omega$). Since we are dealing with capacitive coupling, the dV/dt coupling (constant current) should remain the same regardless of the R_D value. This fact was shown in test 7 with R_D raised to 1.1k ohms. The voltage measured across the same 50 ohm resistor as in test 8 yielded an identical voltage as in Figure 48A or constant current. The HF voltages shown in Figure 48B have the 46 MHz component superimposed on a much smaller 14 MHz component. The equivalent test circuit is a parallel RC combination which would behave as a high pass filter. We calculated the total capacitance between the line and the flange to be about 41 pico-farads. Therefore, the high pass frequency transfer function of a 41 pico-farad capacitor has a 3 dB point with 100 ohms at 40 MHz and 33 MHz with 1100 ohms. We see the 14 MHz and 46 MHz components with this type spectral response, but the transfer loss, as measured across the 50 ohms scope input, is much less with 100 ohms than with 1100 ohms. The expanded photo from test 7 (1100 ohms) did indeed show the 46 MHz component to be smaller by about 1:5 from Figure 48B. The 14 MHz component in both cases were practically the same as would be expected. As an alternate check, the magnitude of the displacement current (capacitance) can be roughly calculated by multiplying the initial rate-of-change of the voltage measured along the flange by the distributed capacitance (41 uuf). This gives a current of approximately 1.5 mA as compared to the 1.7 calculated from the voltage measured at the scope.

The final testing in this area was performed with a coaxial cable that was open circuit at station 60. Test 9 resulted in capacitive effects being eliminated and subsequently no LF or HF components through R_D. By ungrounding the shield at

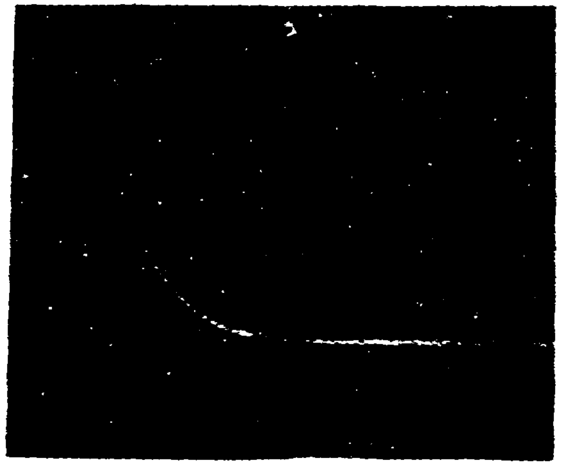

A. Voltage across R_D (97 Ω).
Vertical: 21.72 Volts/Div.
Horizontal: 5 usec/Div.

B. Expanded picture of left photograph (A).
Vertical: 21.72 Volts/Div.
Horizontal: 200 nsec/Div.
(46 MHz component scaled to 86.9 Volts/Div.)

Figure 47 Test 2 Unshielded Line Voltage in the Forward Bay (Fiber Optic Instrumentation)

A. Single wire/open circuit voltage across 50 Ω.
Vertical: 0.208 Volts/Div.
Horizontal: 1 usec/Div.

B. Expanded picture of left photograph (A).
Vertical: 0.208 Volts/Div.
Horizontal: 100 nsec/Div.
(46 MHz component scaled to 0.832 Volts/Div.)

Figure 48 Voltage Measured From Test 9 (Open Circuit) Across 50 Ω (Fiber Optic Instrumentation) the forward end, we did see a very small signal injection but felt this was a result of fringing effects at the open end of the cable which was exposed (i.e., the cable was simply cut at that end and not covered over). The important result of the open circuit testing was a demonstration of capacitive coupling to a line internal to the fuselage and how this effect can couple HF components.

In summary, the HF effects seen can be qualitatively evaluated but the data we obtained is only cursory. However, in observing the overall effects, the magnitude of the HF levels is so low compared to other (LF) levels as to indicate a minimal HF problem.

7.2.2.2 Twisted Pair Data

Tests on shielded/unshielded twisted pairs were primarily conducted in the forward bay. Lines were run between stations 60 and 98 with instrumentation connected at the back end (station 98). Loading was normally 100 ohms across both ends of the line. Original testing was performed with the RG-22 cable but initial results indicated the measured signals were mostly due to spurious noise and loop pickup at the twisted pair/instrumentation interface. We then switched over to the fiber optic system which greatly improved this condition and found our induced signals to be less than 1 volt peak. However, a simulation of the small loops formed by interfacing the twisted pair to the fiber optic transmitter showed diffusion flux coupling that was similar to a majority of our data. In order to eliminate even these lower levels of spurious pickups, it would have required a detailed analysis of the entire instrumentation system and a complete redesign of the fiber optic transmitter. Time did not permit this form of improvement. Therefore, data which we did obtain can only be applied in a general sense.

Testing in the forward bay on unshielded twisted pairs positioned over the bottom left flange or 2 inches above the center of the floor produced diffusion flux pickup through the loops formed between twisted lines. A typical oscillogram is shown in Figure 49A and shows an expanded view of the HF/46MHz component. The scale, 5.68V/Div., takes into account the 12dB fiber optic loss at that frequency. The low frequency waveform, which is not shown here, was a typical $d\phi_D/dt$ loop voltage with a peak at 0.15 volts. However, the spurious loop pickup at the twisted pair instrumentation interface was

A. HF pickup on unshielded twisted pair in forward bay.
Vertical: 5.68 Volts/Div.
Horizontal: 100 nsec/Div.
(Scale is set for 46 MHz component of x4 fiber optic loss)

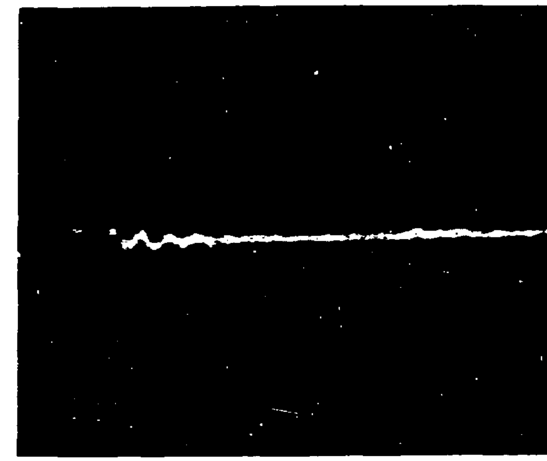

B. Voltage on shielded/twisted pair (transverse mode) Mux Bus line.
Vertical: 0.672 Volts/Div.
Horizontal: 500 nsec/Div.
(46 MHz component scaled to 2.67 Volts/Div.)

Figure 49 HF Induced Voltages - Unshielded and Shielded Pairs identical which indicated little or no LF pickup on the line. The HF noise was similar to Figure 49A but at half the amplitude. We thus felt that any HF voltages were from capacitive coupling.

For a shielded/twisted pair, we felt that our most representative data was obtained during aircraft system testing. During this phase, actual avionic equipment was installed and operated aboard the composite fuselage to observe system reaction while the generator current was incrementally increased to 125kA. Included in the setup was a multiplex (MUX) digital data system with transmitter/receiver boxes placed in the forward bay and the aft section (STA 253). The interconnecting MUX bus line was a shielded/twisted pair as used on F-16 aircraft which afforded us the opportunity to observe induced voltages on a closed loop system.

The fiber optic diagnostics, Figure 15, was com[illegible]ed across the twisted pair in the forward bay MUX box with measurements taken on both sides of a line isolation transformer. Figure 49B (at 20kA) is a photo of the voltage measured across an equivalent 36Ω series isolation resistance on the primary side of the transformer. In this situation, we see a predominant 4 MHz component and $d\phi_B/dt$ type waveform with a zero-crossover of approximately 6 useconds. It was felt that this voltage was more a result of flux coupling in the MUX box than through the MUX interface line. Each MUX receiver/transmitter was encased in a large rectangular box (metallic) with one side being entirely perforated with 1/4 inch diameter holes for ventilation. A fair amount of diffusion flux could then couple through these holes into circuit components/internal wiring. We feel that the 4 MHz component is a system reaction to this flux. Assuming that a voltage similar to Figure 49B is coupled into the MUX bus, an extrapolation to a 200kA level would mean that the peak voltage would reach a peak value of approximately 2 volts. The important fact here is that data systems operate at higher levels (normally +12 volts maximum) such that an induced voltage at 2 volts would not produce circuit damage. Worst case effects would be the possible injection of an error bit. However, since the systems are continuously recycling there would be no hazard to aircraft safety. It should be noted that an external bit comparator was tied to each MUX receiver/transmitter to detect error bit injection into the MUX line. The comparator was linked to the boxes through fiber optic lines. At the 20kA level, only 5 intermittent errors were observed out of 33 shots to the fuselage. As the current level increased, external field interaction with the comparator negated accurate error monitoring. At this point, we could only show that current levels up to 125kA did not damage the MUX system. This fact was shown by a post-test functional check.

7.3 COCKPIT AREA

The cockpit area represented on an opposite extreme to the forward bay in that approximately one-third of its surface area is an open aperture formed by the canopy interface. The impact of the opening is that the entire cockpit fuselage section in the electrical sense, is topologically external as compared to the forward bay which is a closed area. Metallic structures of importance in the cockpit were the canopy interface, a ring member at station 168, edge strakes, and a right-hand side console mock-up. Test results are described first for IR ($J\rho$) measurements and secondly for aperture and diffusion flux results on loops.

7.3.1 IR Voltage Test Results

Voltage measurements were taken between various points along the cockpit left wall as illustrated in Figure 50. This askew view was drawn to show all tie-down references in one picture and facilitate visualization of overall potential drops as listed in Table 6. A typical oscillogram is shown in Figure 51 from test 4.

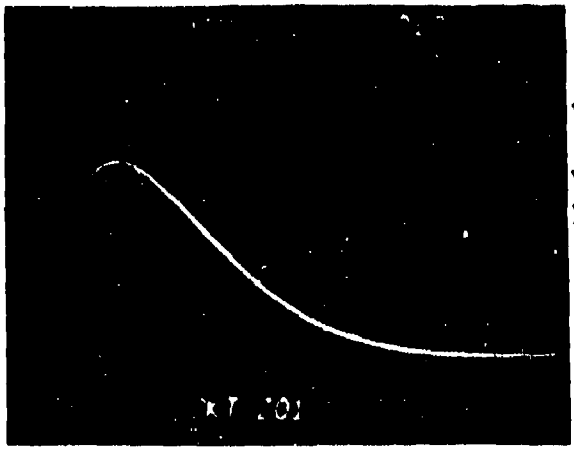

Voltage Drop With Wire Routing
1-1'-3'
Vertical: 50V/Div.
Horizontal: 2us/Div.

Figure 51: Voltage Measurement in the Cockpit Taken During Test 4

Primary importance with respect to voltage levels centered around wire routing from the forward potential sense (positive) point to the RG-22 instrumentation cable. For example, the voltage measured between points 1 and 3' with routing by 1-1'-3' showed a peak value of 160 volts. This voltage can then be broken down into its components as measured: points 1-1'

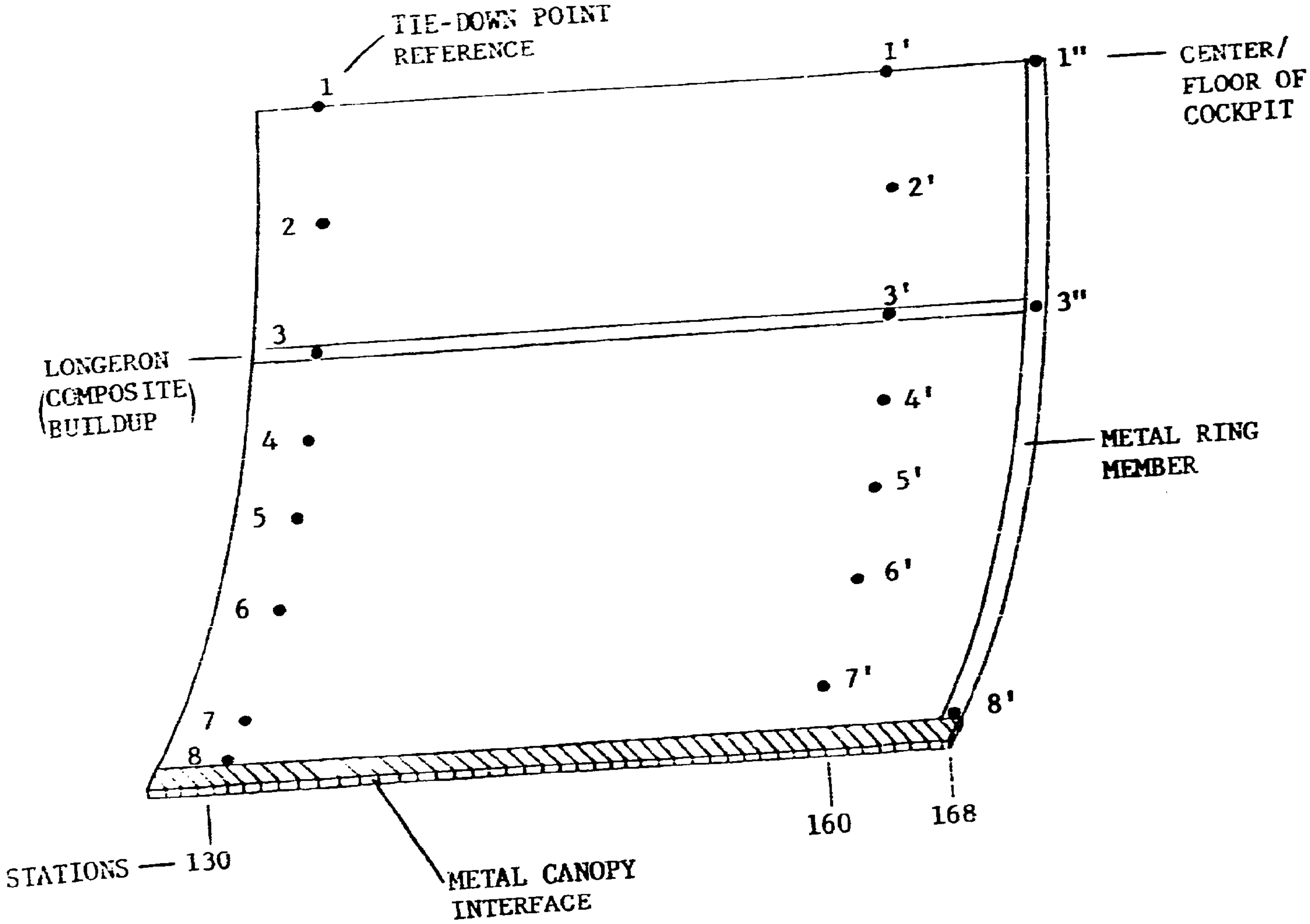

Figure 50: Askew View of Cockpit Left Side and Voltage Reference Points

Table 6 VOLTAGE MEASUREMENTS ON THE COCKPIT LEFT SIDE

Test	Wire Routing	Point Polarity		Peak Voltage		Peak Voltage With Metal Strap (3 to 3') (Volts)
		POS.	NEG.	(Volts)	@200KA	
1	1 - 1"	1	1"	150	1500	-
2	1 - 1'	1	1'	125	1250	125
3	1-3-3'-1'	1	1'	90	900	-
4	1-1'-3'	1	3'	160	1600	-
5	1'-3'	1'	3'	35	350	-
6	2-2'	2	2'	118	1180	118
7	2-2'-3'	2	3'	150	1500	-
8	2'-3'	2'	3'	30	300	-
9	3-3'	3	3'	70	700	Negl.
10	3-3"	3	3"	84	840	-
11	4-4'-3'	4	3'	130	1300	-
12	5-5'-3'	5	3'	115	1150	-
13	6-6'-3'	6	3'	140	1400	-
14	7-7'-3'	7	3'	167	1670	-
15	8-8'	8	8'	140	1400	-
16	8 - 1	8	1	9	90	-

1. Wire routing represents the path the positive wire lead was routed to the RG-22 diagnostic cable (e.g. Test 3 - the positive wire tie-down point was at point 1 with the wire routed to point 3, then point 3' and finally to point 1' where it was connected to the positive lead of the RG-22. The negative lead (RG-22) was tied to point 1').

yielded 125 volts and points 1'-3' yielded 35 volts. All voltage drop measurements are a function of wire routing with current injected into the wire being a property of $J\rho$ diffusion flux coupling between any two points along the wire. This phenomenon thus produces a voltage component addition from different wire directions. It should be noted that wire routing during these tests was directly atop the composite floor.

One last test series was made with a thick metal bonding strap tied between points 3 and 3' on the longeron. Results again showed a substantial voltage reduction between the two tie-down points (3 to 3') but negligible effects on surrounding areas. This data shows no new effects but demonstrates the magnitude of levels to be expected in the cockpit.

7.3.2 Loop Voltage Test Results

Magnetic flux measurements were made with the six loops positioned as shown in Figure 52. Loop voltages taken from loops 1, 2 and 3 are shown in Figure 53 with an expansion of loop #1 given in Figure 54 to illustrate initial rise and high

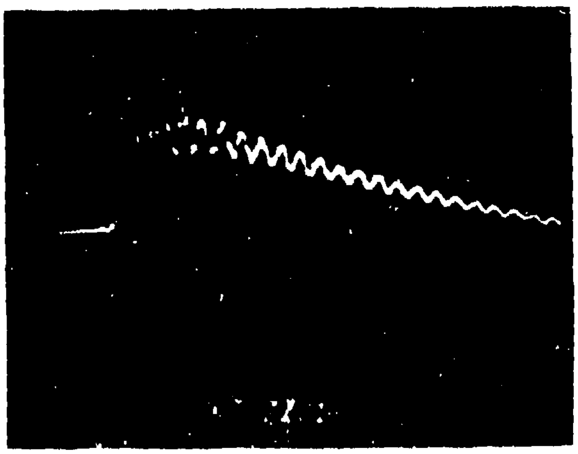

Initial Rise From Loop #1.
Vertical: 1 Volt/Div.
Horizontal: 200 nsec/Div.

Figure 54 Loop #1 Voltage Measured in The Cockpit

frequency components. Table 7 lists equivalent magnetic flux density peaks from all loops with these values obtained by computer time integration plots, see Figure 55.

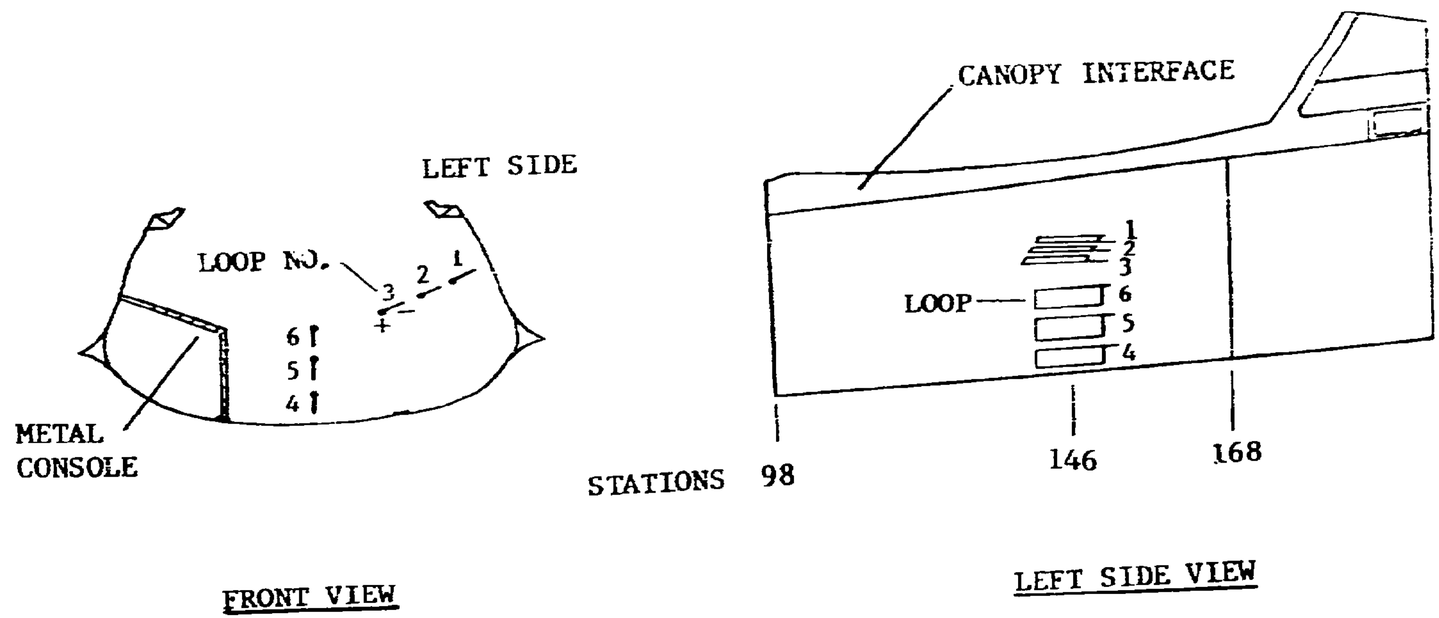

(LOOPS WERE 2 x 4 INCHES)

Figure 52: Loop Positions in the Cockpit

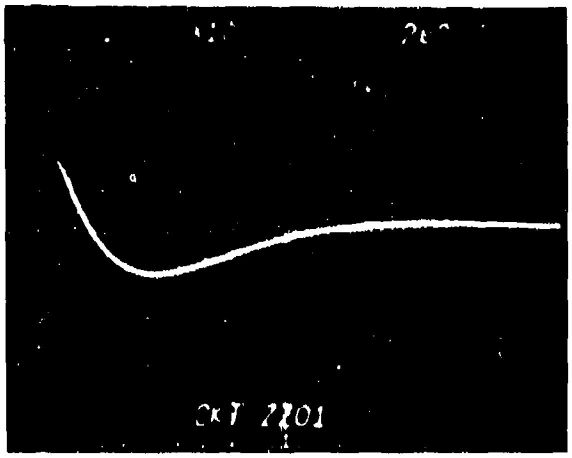

A. Loop #1 voltage.
Vertical: 1 Volt/Div.
Horizontal: 2 usec/Div.

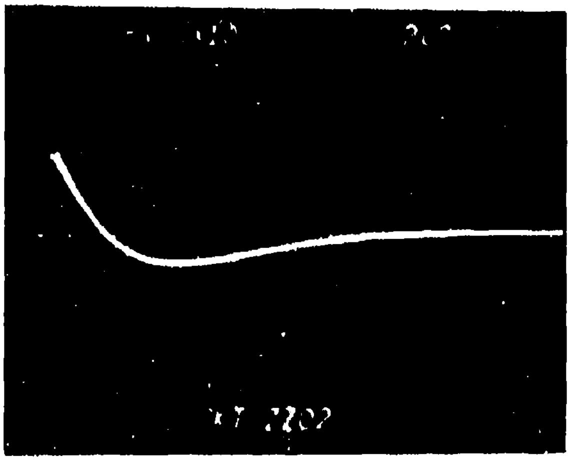

B. Loop #2 voltage.
Vertical: 1 Volt/Div.
Horizontal: 2 usec/Div.

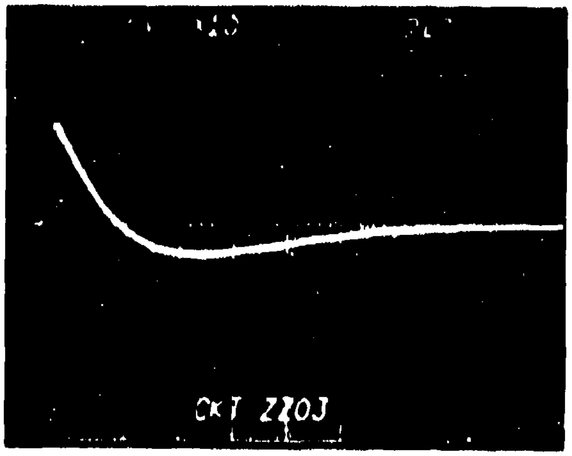

C. Loop #3 voltage.
Vertical: 1 Volt/Div.
Horizontal: 2 usec/Div.

Figure 53 Loop (#1, #2, #3) Voltage Measurements in the Cockpit

Table 7: Loop Measurements in the Cockpit

LOOP COUPLING IN TERMS OF MAGNETIC FLUX DENSITY

Loop No.	First Peak (10^{-4} Webers/m^2) @20kA	First Peak (10^{-4} Webers/m^2) @200 kA	Zerocrossing (μseconds)	Second Peak (10^{-4} Webers/m^2)	Second Peak (μseconds)
1	3.2	33.6	1.7	4.3	10.3
2	4.0	42.0	2.4	1.9	13.0
3	6.0	63.0	3.0	1.2	16.0
4	2.4	25.2	1.5	6.1	10.2
5	3.8	39.9	2.0	4.2	12.0
6	4.8	50.4	2.3	4.2	14.0

NOTE: First Peak scaling factor is x10.5. Second peak scaling factor is also x10.5 but values are not listed.

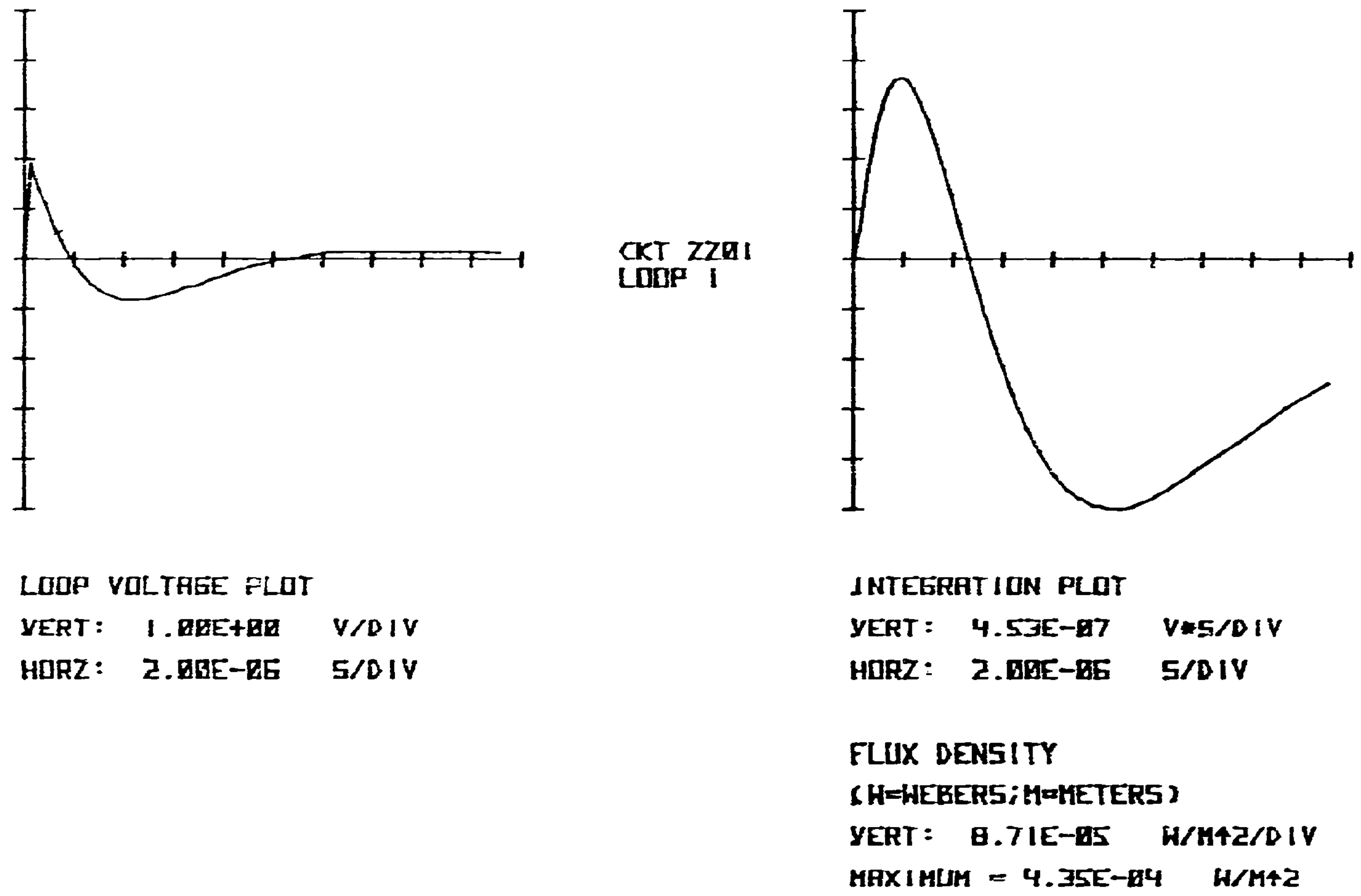

Figure 55 Typical Flux Density Plot From Loop 1 in the Cockpit

Results of this test show the vector combination (equivalent subtraction) of external flux and diffusion flux and their respective intensity variation for different loop positions. The loops closest to the cockpit sidewall and floor (#1 and #4) had the largest diffusion flux components and thus a greater subtraction from external flux as shown by first peak flux/time relative to the second peak. As the loop moved out to position #3 and #6, the diffusion flux decreased in magnitude such that we approached a predominant external flux component which can be seen by the approach toward a 3.2 usecond peak time (corresponding to a zero cross in the differentiation process). Loop #6 did not obtain as great a change as loop #3 and it was deduced that this was a result of the metal console being in close proximity and adding an extra component.

7.4 AFT SECTION

The aft section represents a combination of the forward bay and cockpit geometric and material conditions. The aft section is composed of composite panels/bulkheads, metallic ribs/bulkheads, and some small arbitrarily located apertures. Our major test area was located in the upper bay between stations 226 and 253 (ammo handling bay). It should be noted that the composite access panels in this bay are interfaced with the fuselage with metallic members on all sides. Additionally, some tests were performed in the right hand strake area which has metal substructure around the panel periphery. The panels in the right hand strake area also have metal inserts in the counter sunk fastener holes while other composite panels in other areas did not.

The organization of the data is by IR and loop measurements as in prior sections. The data illustrates the effect of joints and metal substructure on induced voltages and these effects have been treated in both Section 6 and in the theory of Appendix I.

7.4.1 IR Voltage Test Results

Voltage measurements along the length of the aft section (stations 226 to 253) are illustrated in the test setup of Figure 56. In each case, the forward tie-down point is the positive reference point, with the reference wire routed aft to the RG-22 diagnostic cable. A typical oscillogram taken during this test is shown in Figure 57 and has the external

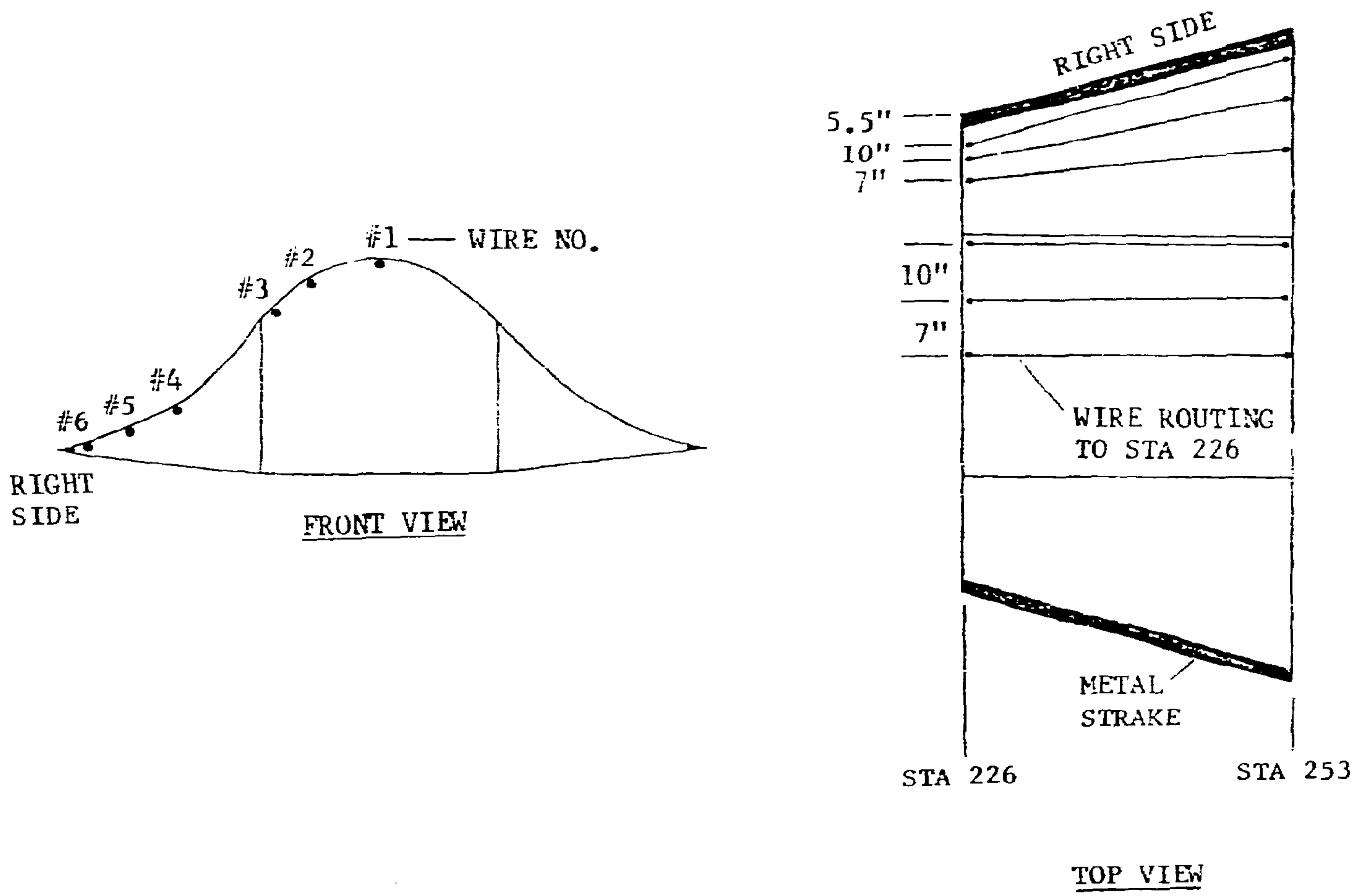

Figure 56 Voltage Drop Reference Points in the AFT Section

lightning current waveform (outer waveform on photo with arrow) superimposed on it for comparison of waveshapes. This photo illustrates the proportionality of the voltages which appear along the fuselage interior shell to the external current.

1. Current Pulse (arrow)
   Vertical: 4 kAmp/Div.
   Horizontal: 5usec/Div.

2. Voltage Drop (inner photo)
   Vertical: 20 Volts/Div.
   Horizontal: 4usec/Div.

Figure 57 Typical Voltage Waveform From the Aft Section With a Superimposed Current Waveform

Peak voltages measured during all tests are summarized in Table 8. At the bottom of Table 8, a description of three test modes is also listed. Basically, the tests were divided into three categories. Test 1 was with the reference points connected to composite only in the upper bay and with every other fastener in place along the joint which is perpendicular to direction of current flow. Test 2 was with reference still connected to the composite panel but with every screw in place, and Test 3 was with the reference connected to the metal substructure at the fore and aft ends of the panel and every screw in place. As can be seen from Table 8, Test 3 voltages are higher than Test 1 and 2 voltages. The increased voltage measured is due to the added joint resistance with the current distribution staying about the same in the respective areas. In comparing test results from Test 1 and 2 for wire positions 1 through 3, we see that a slightly higher voltage is measured in the Test 2 condition. This might seem counter to expected results because in Test 2, there were more fasteners installed and, therefore, lower resistance at the joint. However, the lower joint resistance also attracts slightly more current into the panel, and the predominant resistance is still the panel resistance. Therefore, a slightly higher voltage reading in Test 2 would be a normal result.

Table 8: Voltage (IR) Measurements in the Aft Section

Wire No.	Test 1 Peak Voltage (Volts) V_1	Test 2 Peak Voltage (Volts) V_2	Test 3 Peak Voltage (Volts) V_3	Test 3 Peak Voltage (x10) (@200kA)	$(V_3 - V_2)/V_2$ Ratio
1	70	74	120	1200	0.62
2	78	80	130	1300	0.605
3	64	67	110	1100	0.62
4	-	62	80	800	0.29
5	-	51	64	640	0.33
6	-	26	34	340	0.31

Test 1: Wire tie-down points to composite panels. Top panel (wires 1, 2, 3) with screws in every other place.

Test 2: Top panel with all screws in place.

Test 3: Wire tie-down points to metal ring members.

The data shown is generally what was to be expected as discussed in the prediction section (Section 6). As a gross check on the effects of the metal in the area, (test wire #6) the voltage has a marked reduction near the metal strake on the right hand side where flux (and current) densities are the highest in the region.

7.4.2 Loop Voltage Test Results

Single wire loops were next installed in various area of the aft section in order to measure average flux density (see Figure 58). Table 9 is a list of data taken with these loops and indexes peak loop voltages and magnetic flux densities. Flux was calculated from time integrations of the proportioned $\frac{d\phi_D}{dt}$ waveforms (see Figure 59). Loops 1 and 2 (7.5 inch vertical separation) have large areas and the induced voltages in these loops measure a combination of flux vectors as distributed throughout that area in a vertical plane.

The smaller loops (3, 4, and 5) in the top of the bay demonstrate flux coupling in the same locale and in a horizontal plane but were constructed to demonstrate diffusion flux distribution in the aft bay. Loops 3 and 4 are identical in size and are located in the same vertical plane. Loop 5 is twice the area of loop 3 and is located in the same vertical plane. As can be seen from Table 9, the peak flux density remains the same since the (i.e., loops 3, 4 compared to loop 5) 2 times loop area to the 2 times integration ratio divides out to yield identical average flux densities. The 2 times loop area factor was directly observed because the peak voltage readings in loop 5, Figure 59, were twice the amplitude of loop 3 and 4, but the general waveshape of all loops was identical.

Loops on the left side were used to show the effects of different structural members on diffusion flux. Loop #8 was placed under a small composite access door (composite to composite interface) and compared to loop #6 which is under a solid composite panel. The general waveshapes of both voltages were the same except for a slightly longer zero-crossover time from loop #8. The flux densities have a 1.8:1 ratio but this is due to different diffusion flux densities at the respective positions. The important fact here is that the waveshapes were identical which shows that the access door interface did not introduce external fields into the bay. Loop #6 can also be

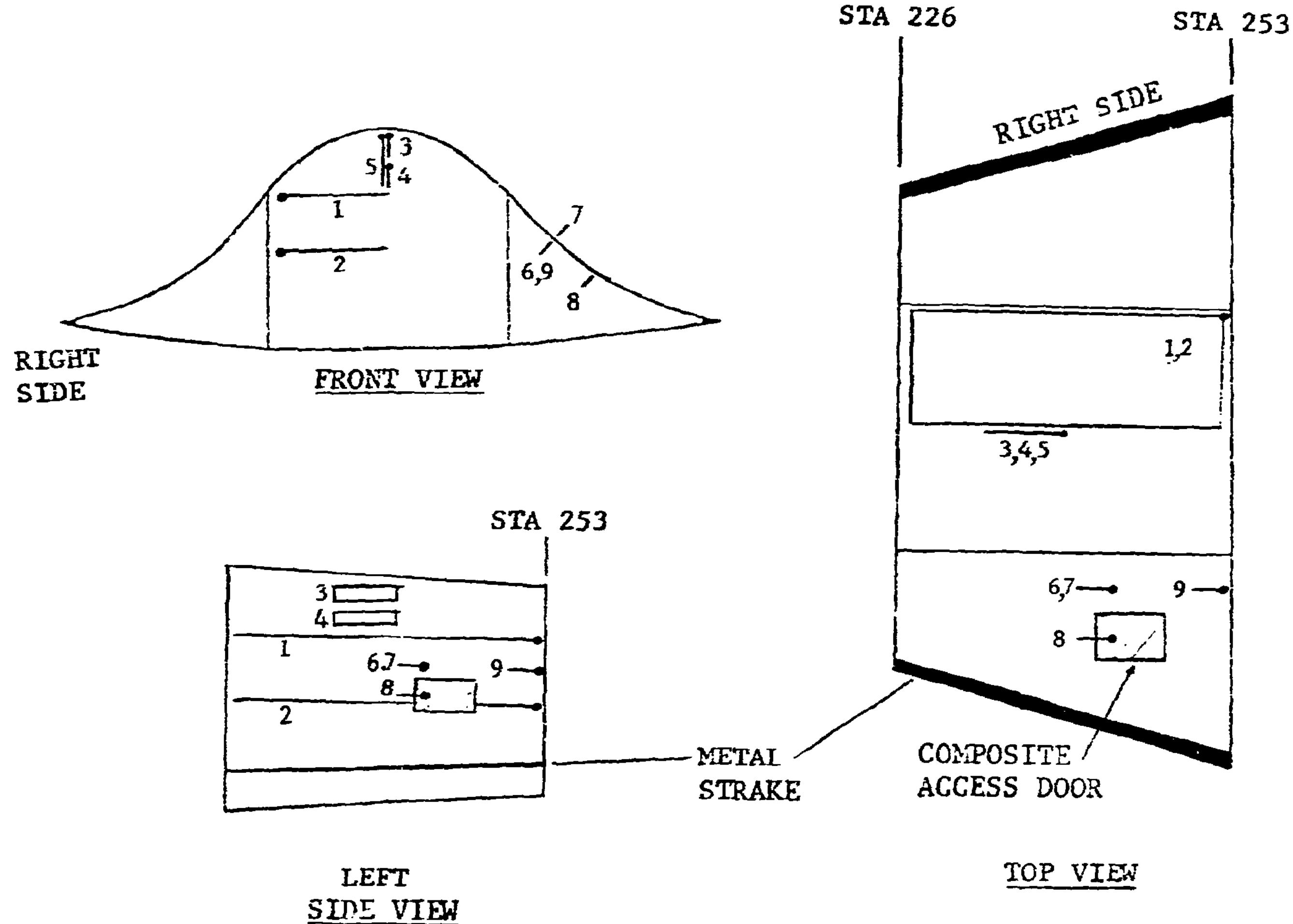

Figure 58: Loop Placement in the Aft Section

Table 9: Loop Measurements in the Aft Section and Equivalent Magnetic Flux Density

LOOP NO.	LOOP VOLTAGE		PEAK MAGNETIC FLUX DENSITY (10^{-4} W/m^2)		Loop Area (10^{-3} m^2)
	Peak (Volts)	Zero-Crossover (usecond)	@20kAmps	@200kAmps	
1	85	8	16.4	95.9	319.0
2	51	8	9.3	54.4	319.0
3	2.9	11	12.1	70.8	13.5
4	2.6	10	12.0	70.2	13.5
5	5.9	10.3	12.1	70.8	27.0
6	1.5	6.2	31.2	182.5	1.7
7	7.0	3.2	49.1	287.2	1.7
8	0.9	6.6	17.4	101.8	1.7
9	1.6	5.9	30.6	179.0	1.7

NOTE: Loop voltage zero-crossover is flux density peak time.

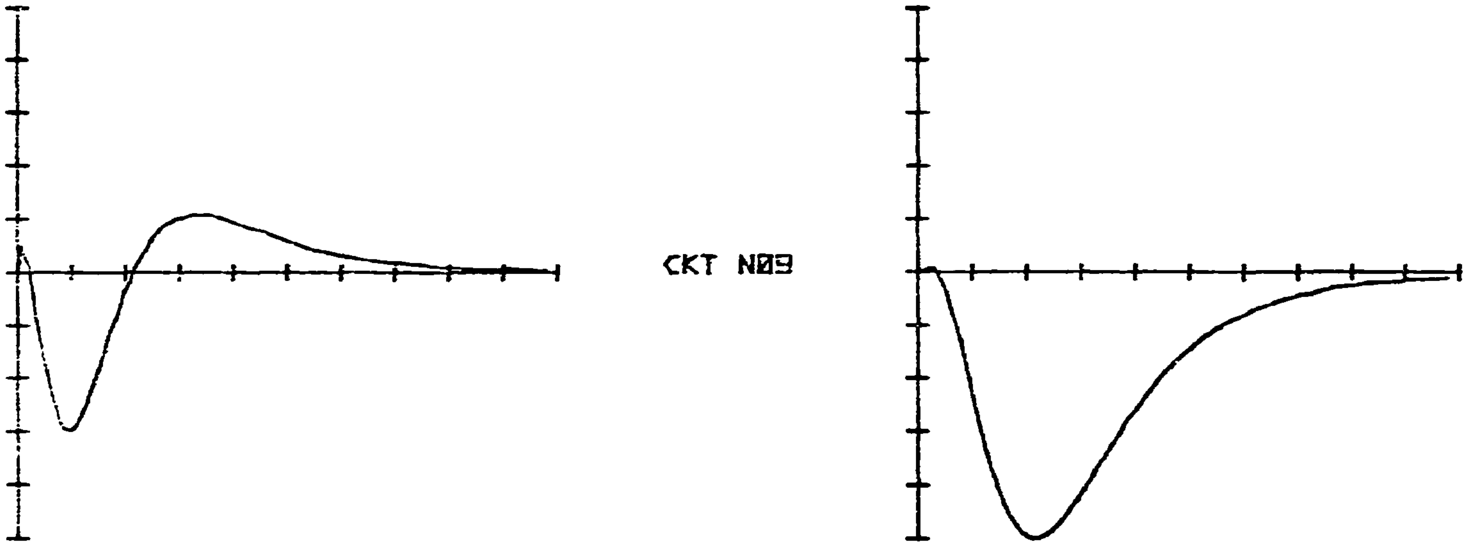

Figure 59 Time Integration of Loop #5 Voltage Measured in the Aft Section

compared to loop #9 which is situated next to the aft metal bulkhead, station 253. Here again, the waveshapes were similar with peak amplitude practically identical. Even though loop #9 is by a metal ring member, it would be parallel to extra flux vectors introduced by current flow along the member which would not be detectable.

The final test was set up with loop #7 placed external to the fuselage and in-line with loop #6. A comparison of the measured voltages are given in Figures 60 and 61 which shows waveshapes of diffusion flux, Loop #6, and a di/dt external flux, Loop #7. Peak values should not be misconstrued as a measure of transfer loss from the outside to inside for a composite panel but are an illustration of diffusion and di/dt flux patterns at those two points. The transfer loss in a configuration such as this also is tied to the sectional geometry as well as material properties such as resistivity and thickness.

One of the more important aspects which can be obtained from the loop data is that internal voltages will be a sub-set in amplitude and frequency content to the voltages which exist along the surface (IR or $J\rho$). This is discussed in more detail in the theory section of Appendix I.

A. Loop #6 voltages.
Vertical: 1 Volt/Div.
Horizontal: 2 usec/Div.

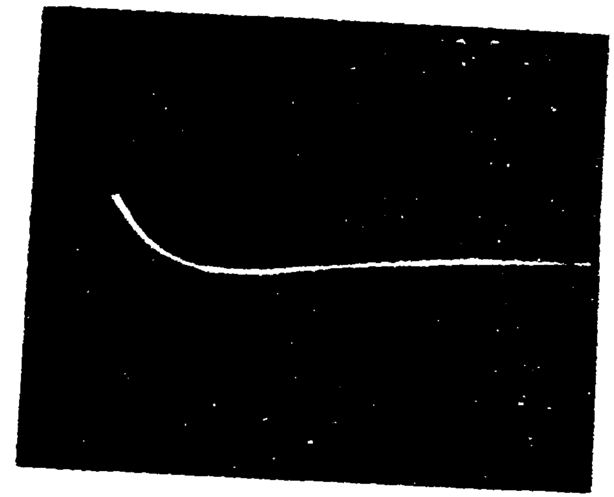

B. Loop #7 voltages.
Vertical: 2 Volts/Div.
Horizontal: 2 usec/Div.

Figure 60 Voltage Measurements From Loops #6 and #7 in the Aft Section (Expansion photographs in Figure 61)

A. Loop #6 initial rise.
Vertical: 0.5 Volts/Div.
Horizontal: 200 nsec/Div.

B. Loop #7 initial rise.
Vertical: 2 Volts/Div.
Horizontal: 200 nsec/Div.

Figure 61 Initial Rise Voltages From Loops #6 and #7 in the Aft Section

SECTION VIII

CONCLUSIONS

For the graphite-epoxy fuselage, there are a number of conclusions or generalizations which may be drawn from the tests reported herein. Some of these conclusions also have ramifications regarding lightning effects on metal airframes.

- There are three primary mechanisms of energy transfer from a lightning strike to electrical/electronic equipment. These primary transfer mechanisms assume that design precautions are taken to prevent direct transfer of energy to the interior of a fuselage shell such as conduction of a lightning stroke down a pitot line or pitot heater wiring. The three are:

  a. IR ($J\rho$ voltage per unit length)
  b. Diffusion Flux
  c. Aperture Flux

- The IR and diffusion flux voltages are low frequency signals (below 50kHz) and will impact only those circuits which form significant loop areas and/or have multiple airframe reference points.

- The aperture flux is a function of geometry and construction techniques and is approximately the same whether the fuselage is graphite or aluminum.

- High frequency effects are primarily aperture dominated. However, due to the short diffusion time through graphite, HF effects can appear inside a fuselage and be distributed by the E field developed along graphite shell surfaces. These distributed HF effects are basically displacement currents and are proportional to the rate-of-change of the $J\rho$ voltage along the interior of the fuselage.

- The IR voltages appearing inside the fuselage will be approximately 3×10^3 higher than they would be in an aluminum fuselage.

- Induced effects due to diffusion flux can never be higher than the highest $J\rho$ voltage which exists along the surface of the fuselage.

- The fuselage response behaves in a manner predictable from transmission line theory and is independent of fuselage material.

- Linear scaling of induced effects in a graphite fuselage is not always permissible. If system response is desired at high levels of I and di/dt, testing must be done at high levels to determine if non-linear conditions exist. Once appropriate scaling factors are determined, IR voltages scale by I and loop voltages scale by di/dt.

APPENDIX

THEORY OF INDUCED MECHANISMS

1. Aperture Coupled Voltages

With an aperture created by an electrically transparent opening e.g., within the cockpit, or within bays having glass fiber, Kevlar or other insulating covers, direct coupling of magnetic flux occurs to wiring and circuits. This flux changes as fast as the external flux, hence the induced voltage per meter V_M in a wire to airframe configuration is given by

$$V_M = \frac{d\phi}{dt} = c\,\frac{di}{dt} \qquad \text{V/m} \qquad \text{(A1)}$$

ϕ = instantaneous flux which links circuits via aperture/meter

i = total instantaneous lightning current

The constant of proportionality c for any particular circuit using an airframe return is the fast flux transfer inductance, M_{TF} given by

$$M_{TF} = L' - M \qquad \text{H/m} \qquad \text{(A2)}$$

L' = fuselage inductance at aperture region in H/m

M = mutual inductance, fuselage to circuit in question

Hence

$$V_M = M_{TF}\,\frac{di}{dt} \qquad \text{V/m} \qquad \text{(A3)}$$

MTF can be calculated by a variety of techniques including field plotting, (Reference 6) filamentary techniques and others.

Thus, voltages are proportional to the instantaneous rate of

PRECEDING PAGE BLANK

change of the externally applied current. The current waveform and the corresponding di/dt aperture coupled voltage are illustrated in Figures A1(a) and A1(b). Often HF resonances produce significant amplitudes of hash as in Figure A1(b) which adds to the basic di/dt waveform.

Electric field coupling ($\propto dE/dt$) may also occur in some circuits within apertures and will also be more apparent at higher frequencies. Quantitative statistics are not available for dE/dt of natural lightning and no attempt was made to simulate it in the test. Nevertheless, electric fields would have been produced in the testing by both the inductive effect of the load assembly at L.F. and through the standing wave electric field patterns at H.F.. Thus, these electric fields could have contributed to the measured results. When a better understanding is available of the magnitude of E-fields in a natural lightning strike, the accuracy of the simulation in this test can be assessed.

2. Resistive/Diffusion Voltages in Homogeneous Tubes

If we consider a long circular tube, diameter D, of homogeneous resistive material, resistivity ρ, of wall thickness h ($<< D$), the resistance per meter length is given by equation (A4) and the voltage V_R for a d.c. current I is given by equation (A5).

$$R = \frac{\rho}{\pi D h} \quad \Omega/\mathrm{m} \qquad \text{(A4)}$$

$$V_R = \frac{I \rho}{\pi D h} \quad \mathrm{V/m} \qquad \text{(A5)}$$

If a step function pulse $\overline{I}$, is applied to this tube at $t = 0$ which has an external and remote current return, and V_R is sensed internally as in Figure A3, the voltage V_R as a function of time will be given by equation (A6) (Reference 8).

$$V_R(t) = \frac{\overline{I}\rho}{\pi D h} \left\{ 1 + 2 \sum_{n=1}^{\infty} (-1)^n \exp\left(\frac{-n^2 t}{T_M} \right) \right\} \mathrm{V/m} \qquad \text{(A6)}$$

$$T_M = \frac{\mu_0 h^2}{\pi^2 \rho} \quad \mathrm{sec} \qquad \text{(A7)}$$

$$= \frac{0.127 h^2}{\rho} \quad \mu\mathrm{sec} \quad (\text{for } \mu_r = 1) \qquad \text{(A8)}$$

where T_M is the characteristic diffusion time.

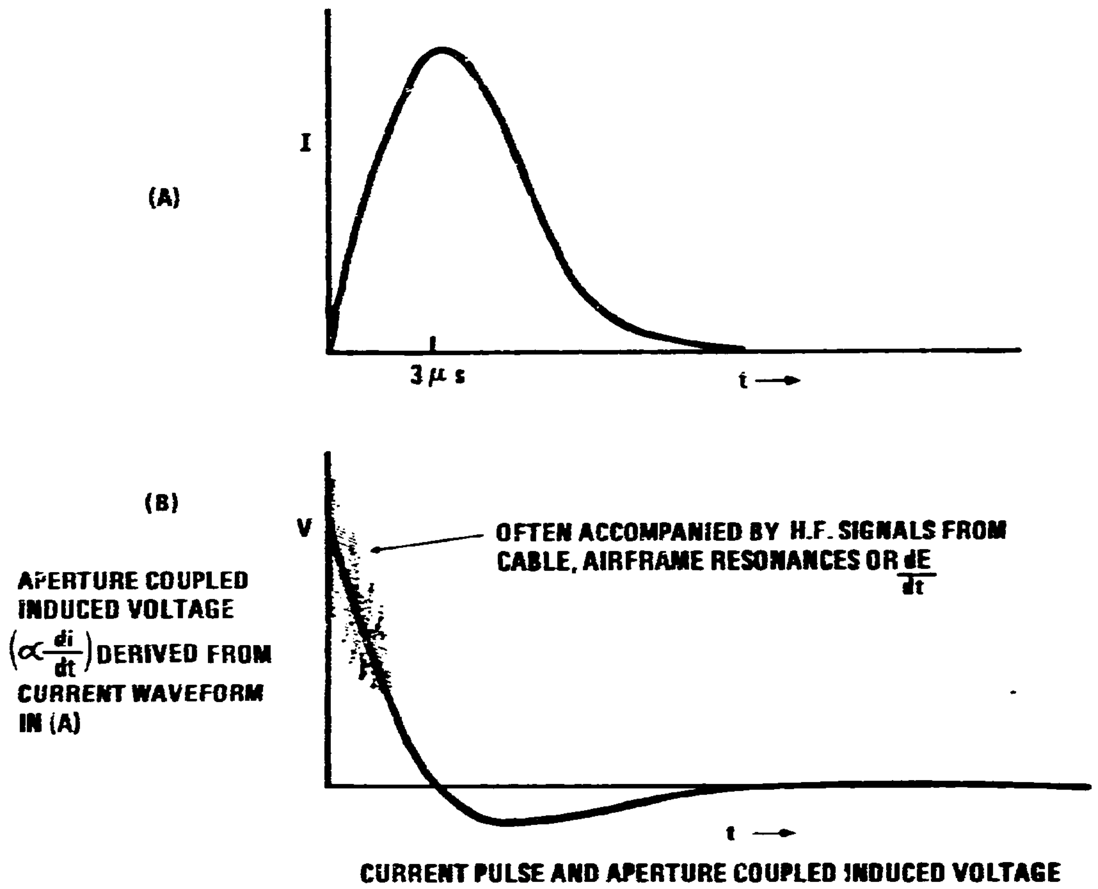

Figure A1 Current Pulse and Aperture Coupled Induced Voltages

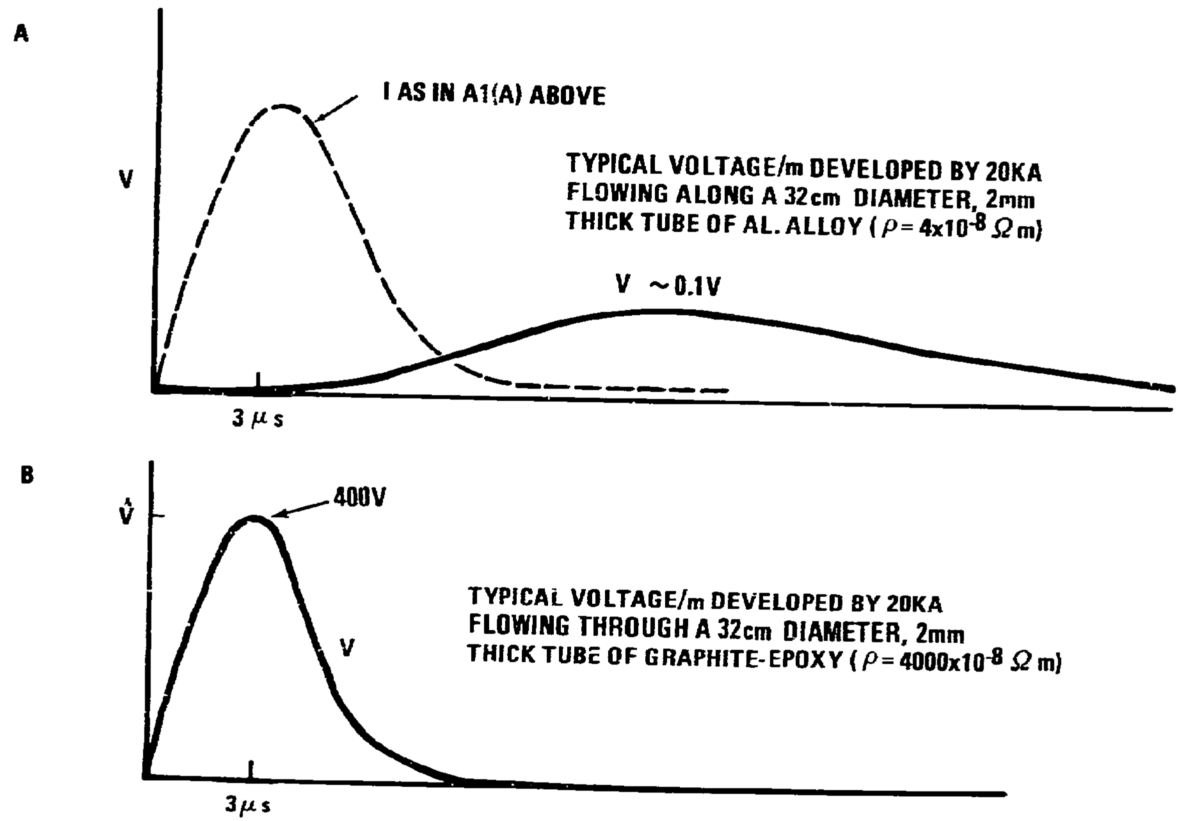

Figure A2 IR Voltage in (a) All Metal and (b) All Graphite Structures

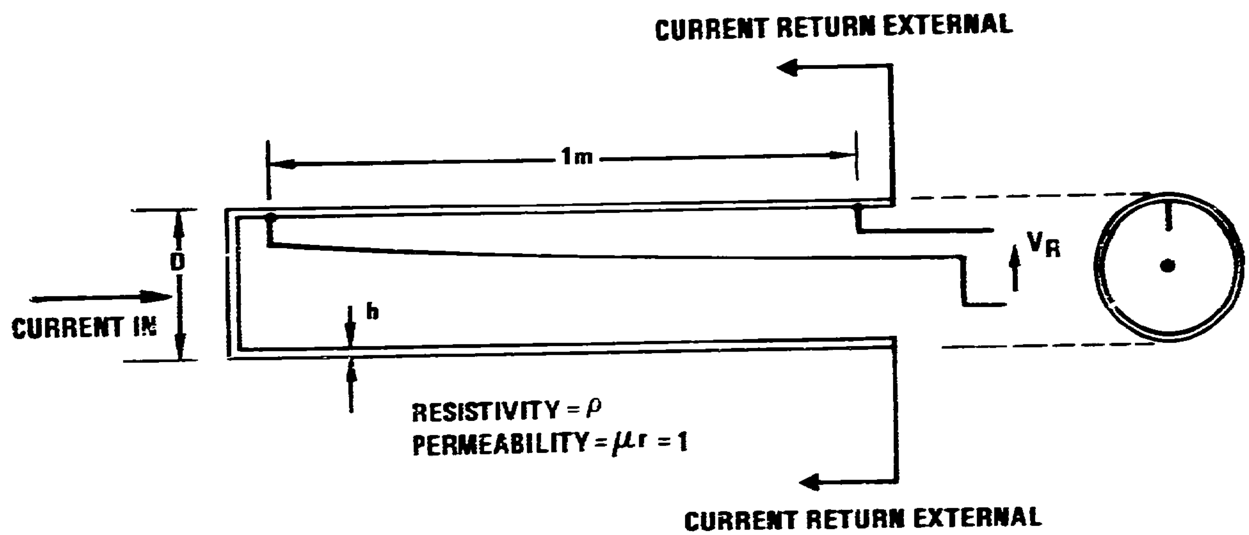

Figure A3 Cylindrical Model for Diffusion Flux Effects Evaluation

The bracketed term in equation (A6) is a lacunary function and cannot be summed analytically. It can, however, be summed numerically very easily. It is a universal function and its shape is shown in Figure A4 as a function of t/T_M. Its value always lies in the range 0 to 1. This function is somewhat similar to the complementary error function and both have a slope of 0 at $t = 0$. Figure A4 exhibits a dead time (i.e., function = 0) until $t = \frac{1}{2}T_M$. Values of T_M for 2mm aluminum alloy ($\rho = 4 \times 10^{-8}\ \Omega$-m) and graphite ($\rho = 4000 \times 10^{-8}\ \Omega$-m) are as follows:

T_M (Al) = 12.7 microsecs ; T_M(gr) = 12.7 nanosecs

T_M (Al) is comparatively long compared to times of interest in lightning pulses (e.g., the current pulse of Figure A1(a)) but T_M (gr) is very short indeed. The waveforms of voltages which would be measured in the tube of Figure A3 for the current pulse of Figure A1(a) would be as in Figure A2(a) and (b) for aluminum and graphite. A large T_M appreciably changes the pulse shape, especially near $t = 0+$. The maximum rate of change of Figure A4 occurs at $t = 0.9T_M$.

Alternatively, in the frequency domain, the bandwidth to the -3dB point, f_c, is given by

$$f_c = \frac{0.35}{t_r} = \frac{0.35}{2.35T_M} \quad \text{Hz} \qquad \text{(A9)}$$

$$= \frac{1.17\rho}{h^2} \quad \text{MHz (for } \mu_r = 1) \qquad \text{(A10)}$$

Equation (A10) gives 12 MHz for graphite and 12 kHz for aluminum alloy with ρ and h as above. Thus, the aluminum tube severely attenuates all components of the lightning pulse above 12 kHz whereas the graphite panel attenuates only those frequencies above 12 MHz and so gives a very accurate voltage proportional to the current pulse waveform. (cf Figure 5, I spectrum)

Although a graphite fiber panel is not electrically homogeneous, the results of Reference 7 (page 82) have shown that skin effect does exist in a predictable manner (although better agreement is achieved in the example quoted in Reference 7 if a lower value of resistivity is used for the graphite; $3750 \times 10^{-8}\ \Omega$-m instead of $10{,}000 \times 10^{-8}\ \Omega$-m as suggested in this report.).

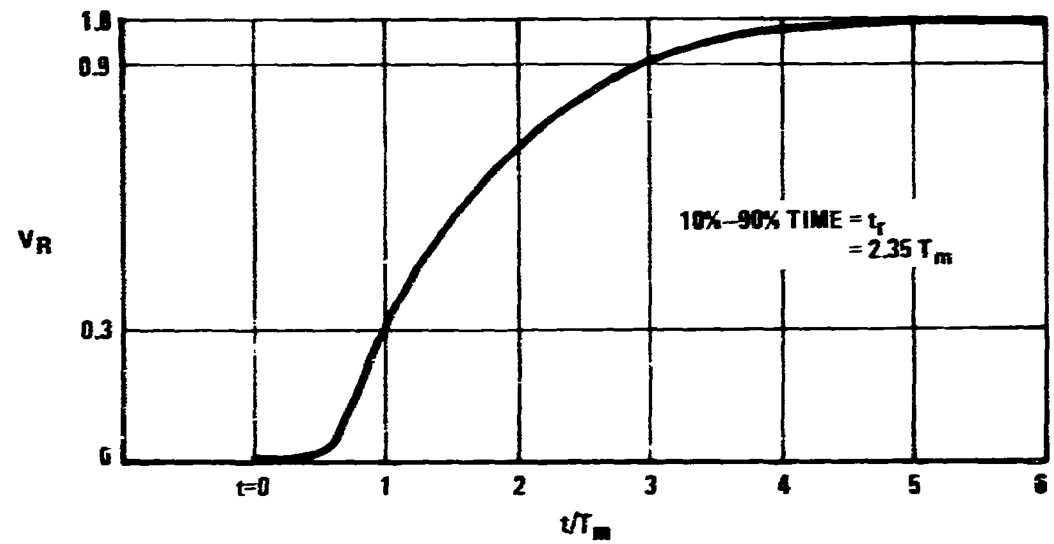

Figure A4 Graph of $1 + 2 \sum_{n=1}^{\infty} (-1)^n \exp\left(\frac{-n^2 t}{T_m}\right)$

3. Resistive/Diffusion Voltages in Complex Electrical Geometry

The general case of a two material system is shown in Figure A5(a), in a circular tube made of dissimilar resistivity materials ρ_1 and ρ_2. Looking at the inside surface of the tube wall, as in Figure A5(b), this analysis examines the total potential drops around a surface path ABCD and ABC'D'. If the narrow center strip is graphite and the remainder aluminum (i.e., $\rho_2 = 1000 \times \rho_1$) then $T_{M1} = 1000 \times T_{M2}$. There are three important regimes to note:

1) In very short times, $t < \frac{1}{2}T_{M2}$ (i.e., within the deadtime for the graphite) V_{AB} 0; V_{DC} 0; therefore, potential drops around the path = 0.

2) DC case, $t \rightarrow \infty$ and current sharing between the materials is resistively controlled, therefore $V_{AB} = V_{DC}$, and $V_{AB} - V_{DC} = 0$. Therefore, potential drops = 0.

3) Intermediate* case t $\frac{1}{2} T_{M2}$; $V_{AB} \neq V_{DC}$, (and $V_{AB} \neq V_{D'C'}$).

In the intermediate case, which commences in nanosec times for graphite and extends for tens of microseconds typically, current redistribution occurs from the inductive sharing case 1, to the DC case 2, and potential drop balance around the close paths ABCD and ABC'D' must be maintained by a diffusion flux which links the paths and hence:

$$V_{AB} - V_{DC} = \frac{d\phi_D}{dt} \qquad \text{(A11)}$$

where $\frac{d\phi_D}{dt}$ is the rate of change of diffusion flux. This flux enters and leaves the interior via the graphite so linking both paths equally as in Figure A5(b). Thus the diffusion flux appears as soon as there is a potential drop along AB which is not balanced by an equal potential drop along DC (clearly in the case of the homogeneous tube considered in para. 2 above, everywhere within the tube:

$$V_{AB} = V_{DC} \quad \text{and} \quad \frac{d\phi_D}{dt} = 0.)$$

*There is a long period intermediate case involving current diffusion into the metal which is not important in this description.

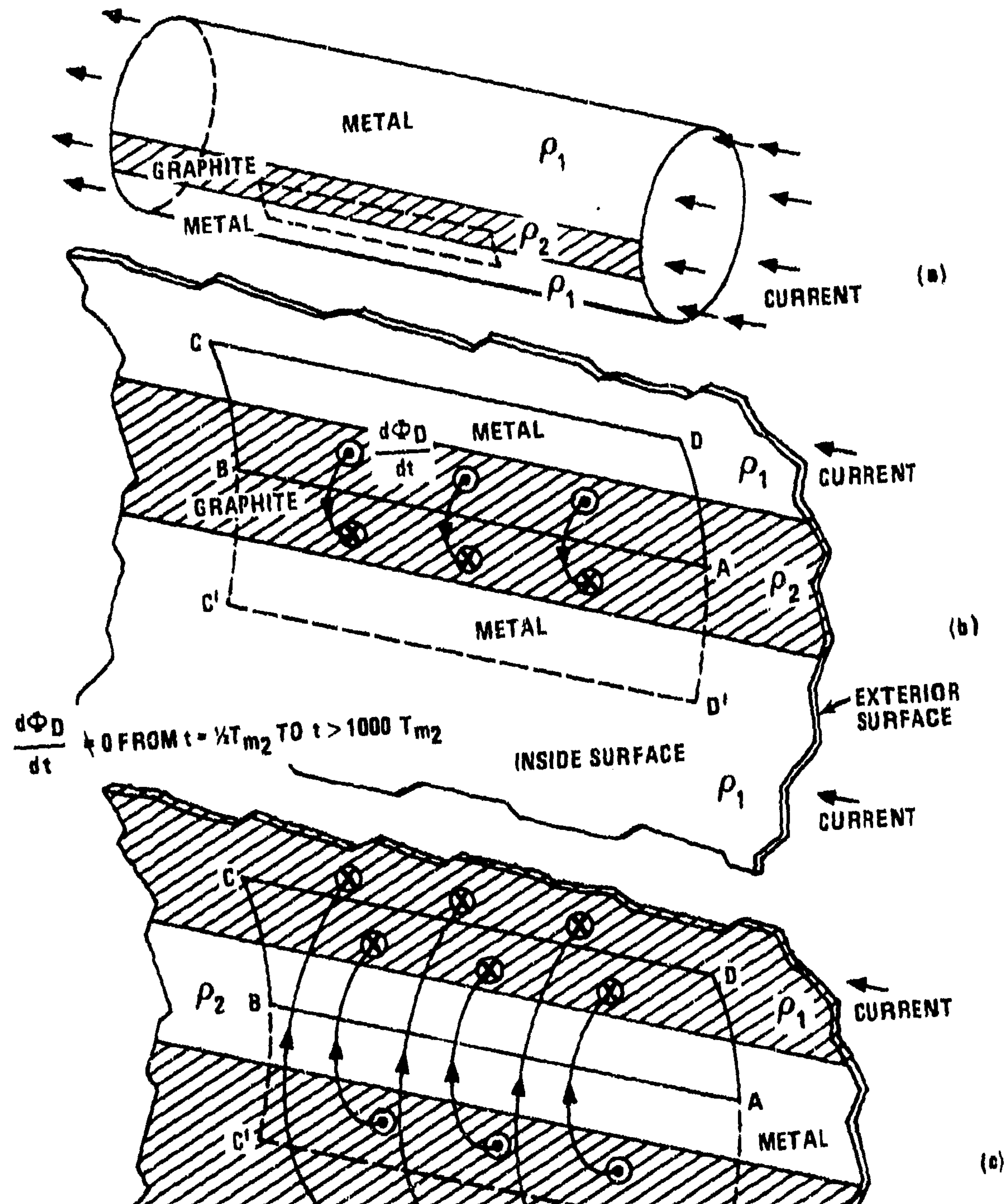

Figure A5 Interior Flux Distributions for a Cylindrical Model (a) $\rho_1 < \rho_2$ (b) $\rho_1 < \rho_2$ (c) $\rho_1 > \rho_2$

Thus, in cross section, the field shown in Figure A5(b), will be as in Figure A6(a). The pattern of flux within the tube is very similar to the aperture flux field which would occur in the tube if the graphite strip were removed. However, the diffusion flux in Figure A6(a) is not related in time to the external flux. However, use can be made for the prediction of diffusion voltages of the similar geometric pattern within. Prediction of diffusion flux voltages is given below.

If we reverse the resistivities in Figure A5(b), let $\rho_1 = 1000\,\rho_2$ (i.e., graphite tube and narrow metal strip) the situation is reversed. $V_{DC} > V_{AB}$ and hence $\frac{d\phi_D}{dt}$ links the paths as shown in Figure A5(c) and A6(b).

Induced Voltage Corollaries

From equation (A11) and the configuration of Figure A5(b) if ρ_1 is very small such that $V_{DC} \to 0$;

$$\frac{d\phi_D}{dt} = V_{AB}\,(t) \qquad \text{(A12)}$$

Corollary 1

Diffusion flux induced voltages have the same form and spectrum as the dominant resistive voltage within an enclosure.

Starting at points D and C, V_{DC} (via the direct route) = 0, but V_{DC} (via A and B) = V_{AB} hence:

Corollary 2

It is the circuit route which determines the induced voltage, not the reference points at each end.

Referring to Figure A6(a), diffusion flux within the tube is clearly weaker toward the bottom than near the top, (where $\frac{d\phi_D}{dt} = V_{AB}$) hence:

Corollary 3

Diffusion flux induced voltages within an enclosure, induced in single loops, are always less than - or in the limit, equal to the largest resistive potential drop which occurs on the surface of the enclosure, and will be smaller with increasing distance from that surface.

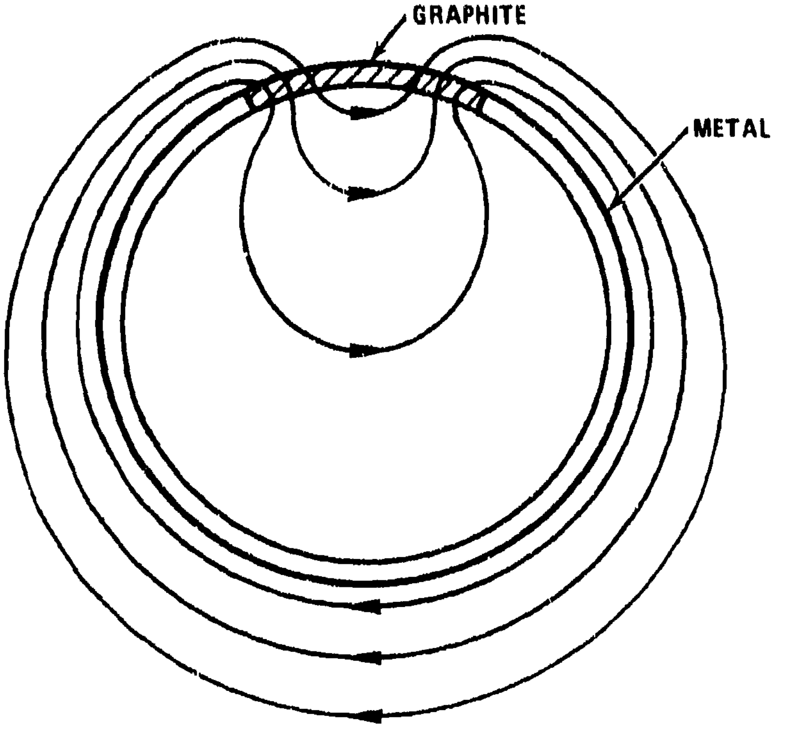

a) Diffusion Flux into Tube Interior through Small Graphite Section

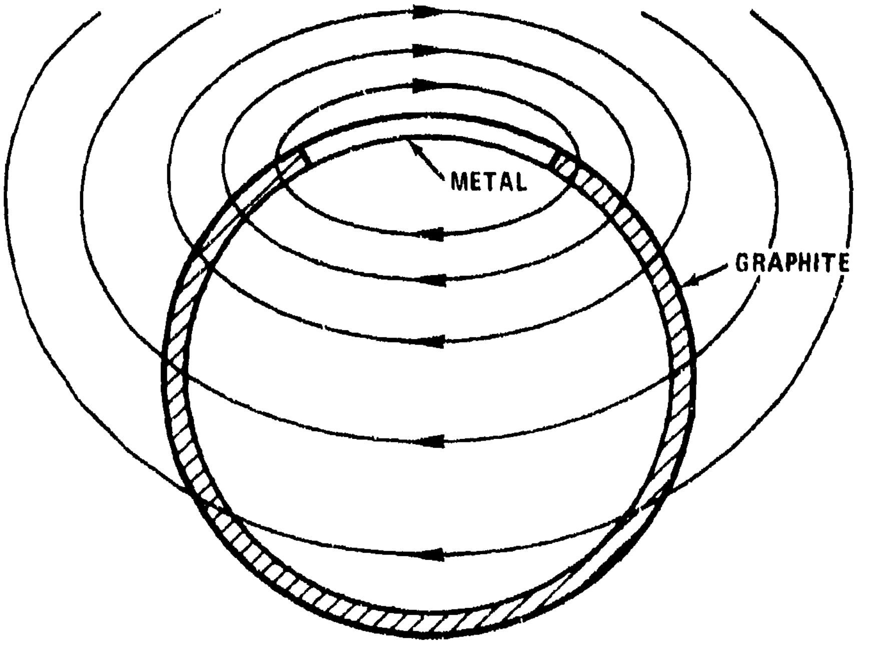

b) Diffusion Flux into Tube Interior through Large Graphite Section

Figure A6 Diffusion Flux in Complex Tubes (Current into paper)

An approximate technique of estimating the voltage on a loop within an enclosure is to use the field mapping technique for an aperture in the place of the graphite and then to scale the voltage as follows:

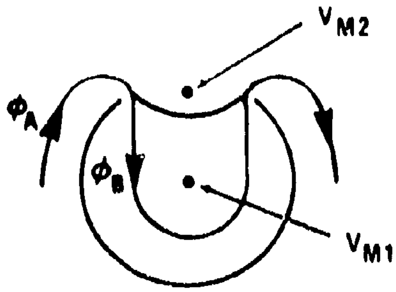

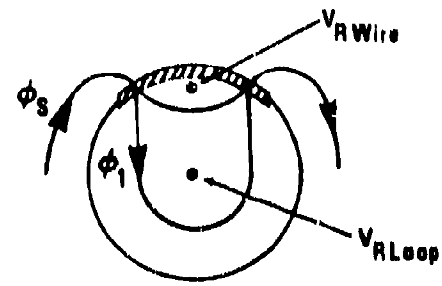

$$\frac{V_{M1}}{V_{M2}} \qquad \frac{\phi_B}{\phi_A} \qquad\qquad \frac{V_R \text{ loop}}{V_R \text{ wire}} \qquad \frac{\phi_1}{\phi_S} \qquad \text{(A13)}$$

$$\text{Therefore, } V_R \text{ loop} = V_R \text{ wire} \times \frac{\phi_1}{\phi_S} = V_R \text{ wire} \times \frac{\phi_B}{\phi_A}$$

ϕ_A and ϕ_B are obtained from a POTENT aperture plot to give the ϕ_1/ϕ_S for a wire within the bay with a graphite cover panel.

In all cases, the voltages here are loop voltages comprising a wire in the position shown connected back to the inside metal surface, where "V_{DC}" = 0.

The worst case value for V_R on any graphite panel can be calculated by assuming that the current is inductively shared around the whole conductor periphery and is then calculated from J and ρ. In practice, owing to current redistribution V_R will generally be somewhat less, since current redistribution may take place before peak current is reached.

DEMONSTRATIONS OF 'COROLLARIES'

Corollary 1

All the measurements on diffusion flux generated voltages within graphite skin bays have shown the close relationship to IR voltages and therefore to the current waveform. Scaling of diffusion flux voltages, for fixed di/dt has been shown to be only amplitude dependent.

Corollary 2

Note that it is the wire route rather than the end connections which determine the type and amplitude of induced voltages. A specific test was run to demonstrate this in the cockpit floor illustrated in Figure A7. The three measurements and the reference points are shown in the figure, and all wires were run close to the graphite skin, but circuit B was routed from 2 across to near 1 and alongside wire C to 4 and across to 3. No contact was made between wire B and points 1 and 4. The measurements clearly show the equivalence of B and C thus illustrating the importance of the wire route. This corollary is of great practical significance in routing wires in a graphite fuselage.

Corollary 3

Demonstrated by many tests - for example the aft bay test with IR wire #1 (Figure 56) and loop #1 in Figure 58. The IR wire gave 120 volts when measured metal-to-metal across the graphite panel compared with 85 volts on the loop below. The corollary was used in this case to help measurements since the first measurement on the panel did not include the joint resistances and gave only 74V which is less than the loop voltage within. Hence, in calculating diffusion flux loop voltages within structures the total of panel IR and joint voltages should be used to calculate the loop voltage.

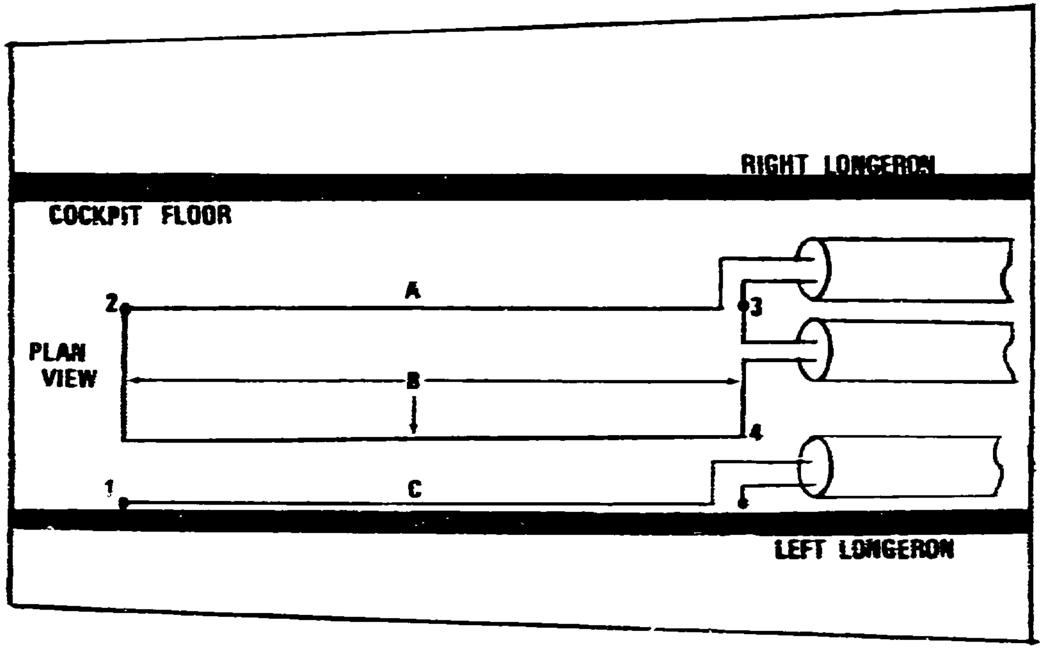

CIRCUIT	REFERENCE POINTS	MEASURED VOLTAGES (VOLTS)
A	2-3	150
B	2-3	89
C	1-4	87

Figure A7 Corollary 2 Demonstration

R E F E R E N C E S

1. Lightning Test Waveforms And Techniques For Aerospace Vehicles And Hardware - Report of SAE Committee AE-4, Special Task F, 5 May 1976.

2. Berger, Anderson, and Kroniger, Parameters of Lightning Flashes.

3. B.J.C. Burrows, C. Luther, and P. Pownall, Induced Voltages in Full Scale Aircraft at 10" A/S, Culham Laboratory, UKAEA, Abingdon, Oxfordshire, England, 1977, IEEE International Symposium on Electromagnetic Compatibility.

4. ASTP-Simulated Lightning Test Report, JSC 09221, Prepared by R. L. Blount, R. D. Gadbois, D. L. Suiter, and J. A. Zill, N.A.S.A., Lyndon B. Johnson Space Center, Houston, Texas, November 1974.

5. Electromagnetic Pulse Handbook for Missiles and Aircraft in Flight, SC-M-71-0346, Sandia Laboratories, Albuquerque, September 1972.

6. Thomas, C. Ll., A Package for the Numerical Solution of Potential Problems in General 2 - Dimensional Regions, Culham Laboratory Report CLM P339.

7. Boeing Final Report - D180-20186-4, Investigation of Effects of Electromagnetic Environment on Advanced Composite Aircraft Structures and their Associated Avionic/Electrical Equipment, Phase II, Vol. I, September 1977.

8. R. H. Evans, Penetration of Current and Magnetic Flux into the Wall of a Long Thin-Walled Cylinder, Royal Aircraft Establishment, UK Ministry of Defense (PE) Farnborough, Hampshire, U.K., December 1975.

9. Lightning Effects Analysis of F-16 Nonmetallic Structures, GE-CR&D Report SRD-76-068, J. A. Plumer, June 1976.

☆U.S.Government Printing Office: 1979 -- 657-002/429